MARTIN MARIETTA ENERGY SYSTEMS LIBRARIES
3 4456 0250018 5

CENTRAL RESEARCH LIBRARY
DOCUMENT COLLECTION

ORNL-2505
Revised cy. 3

THE ORNL GAS-COOLED REACTOR

MATERIALS AND HAZARDS

LIBRARY
REFERENCE COPY

OAK RIDGE NATIONAL LABORATORY
operated by
UNION CARBIDE CORPORATION
for the
U.S. ATOMIC ENERGY COMMISSION

CENTRAL RESEARCH LIBRARY
DOCUMENT COLLECTION
LIBRARY LOAN COPY
DO NOT TRANSFER TO ANOTHER PERSON
If you wish someone else to see this document, send in name with document and the library will arrange a loan.

ORNL-2505
Revised
C-81

Contract No. W-7405-eng-26

THE ORNL GAS-COOLED REACTOR MATERIALS AND HAZARDS

By the Staff

of the

Oak Ridge National Laboratory

DATE ISSUED

May 22, 1958

OAK RIDGE NATIONAL LABORATORY
Oak Ridge, Tennessee
operated by
UNION CARBIDE CORPORATION
for the
U. S. ATOMIC ENERGY COMMISSION

MARTIN MARIETTA ENERGY SYSTEMS LIBRARIES

3 4456 0250018 5

SECTION 12

EXPERIMENTAL MATERIALS PROGRAM

12. EXPERIMENTAL MATERIALS PROGRAM

CONTENTS

12.1 Introduction 12.1

12.2 Fuel 12.1

12.2.1 Development of Fabrication Methods for UO_2 ..... 12.1

12.2.2 Radiation Damage Studies 12.3

12.2.3 In-Pile Loop Test of Fuel Assemblies 12.9

12.3 Capsule Material Development 12.9

12.3.1 Effects of Contaminants in the Helium 12.11

12.3.2 Effects of Aging Reaction 12.13

12.3.3 Buckling of the Capsule Wall 12.14

12.3.4 Effects of Section Size and Bending Moments 12.20

12.4 Fuel Element Assembly 12.21

12.4.1 Development of Closure Welds 12.21

12.4.2 Methods of Fabricating Fuel Element Components 12.22

12.4.3 Methods of Inspection 12.25

12.4.4 Manufacture of Test Samples 12.26

12.5 Contamination of the Coolant 12.26

12.5.1 Studies of the Rates of Adsorption and of Evolution of Gases by Graphite 12.27

12.5.2 Reactions of Contaminants with Graphite 12.29

12.5.3 Large-Scale Out-of-Pile Loop Experiments 12.33

12.5.4 Large-Scale In-Pile Loop Tests 12.42

12.6 Aerodynamic and Heat Transfer Tests 12.43

12.6.1 Pressure-Drop Studies 12.43

12.6.2 Heat Transfer Studies 12.46

12.6.3 Hydrodynamic Studies 12.49

12.6.4 Finned-Tube Studies 12.50

12.7 Pressure Vessel 12.50

12.7.1 Effects of Radiation on Mechanical Properties 12.50

12.7.2 Welding Studies 12.54

12.7.3 Inspection Methods 12.55

12.8 Other Reactor Material Components 12.56

12.8.1 Shielding Materials 12.56

12.8.2 Control Rod 12.57

12.8.3 Ductwork 12.57

12. EXPERIMENTAL MATERIALS PROGRAM

12.1 Introduction

In Part 2, Section 3 of this report, the various problems in materials selection were discussed and optimum choices of materials were made for the given design parameters. In most cases, however, it will be necessary to develop the technology of these materials before final design specifications can be established. This section of the report will outline and explain the experimental program proposed for advancing the technology of bulk oxide fuel, coolant, and the various structural materials to a stage sufficient for use in such a reactor.

Component tests of heat transfer systems will be operated to give a better understanding of the aerodynamics and heat transfer characteristics of the reactor system.

The proper gas-handling techniques for the reactor system will be developed as an outgrowth of both in- and out-of-pile experiments with large-scale loops.

The single largest developmental undertaking is the correlation of the manufacturing method for the UO_2 with its radiation damage characteristics. Statistical radiation damage testing will be conducted, with the variables being manufacturing methods of the oxide, density of the body, temperature, burn-up and stress on the element.

12.2 Fuel

12.2.1 Development of Fabrication Methods for UO_2: The use of encapsulated UO_2 slugs as fuel for the GCR-2 necessitates an extensive development program to produce such slugs more inexpensively. The elimination of granulation, pre-firing and grinding operations and the use of a short high-temperature sintering cycle are the means whereby such economies may be achieved. However, a particular type of UO_2 is required, and careful control must be maintained during manufacture, as explained in Part 2, Section 3.

An extensive amount of well-advanced technology is available from the processes used in producing normal fuel pellets for the Pressurized Water Reactor. Additional development work on slightly enriched UO_2 is being carried out by the General Electric Company on the fabrication of pellets

for the Dresden Station Reactor. However, in both cases the procedures for manufacturing fuel utilize milled ceramic grades of oxide, granulated with organic additives, compacted at high pressures, pre-fired and finally sintered in hydrogen at moderate temperatures for long periods. As stated above, the use of carefully refined oxide should enable the elimination of several of the more costly operations of the manufacturing process.

The present experimental program is a cooperative effort on the part of the Chemical Division of Y-12 and the Oak Ridge National Laboratory Ceramic Section, directed toward producing a suitable oxide and establishing final manufacturing specifications. The use of enriched fuel necessitates the production of oxide directly from UF_6, but the complexing action of fluoride ions complicates the procedure. Many other factors in the chemical processing also affect the properties of the UO_2. The characteristics which have the greatest effect on the fabricability are the crystallite size and perfection and the surface-to-volume ratio. The present study consists essentially in correlating data from the chemical processing with information obtained from differential thermal analysis (DTA) studies[1] and observations on fabricability.

It is proposed to expand the present program to include surface area determinations, microscopic examination and complete chemical analysis of the various batches of oxides studied. Correlation of these data with the above information should establish firm specifications for the desired type of oxide .

Production of large batches of oxide would be necessary to secure final specifications. This oxide will then be used to develop the granulation technique and to establish procedures for compacting the granulated powder. Production of a large number of compacted slugs will then be carried out on an automatic press, and sintering of these slugs to the required density should give a statistical summary of the dimensional control and density tolerances obtainable. Sintering would be carried out in an induction-heated atomosphere furnace for minimum sintering time as well as in a standard hydrogen furnace.

Extrusion will also be investigated as an alternate fabrication method. Extruded slugs could be quite long compared to their diameter, and may

---

[1] R. E. Grim, Clay Mineralogy (New York: Mc-Graw-Hill, 1953) p. 194.

possibly be produced with the desired density and dimensional control. In general, extruded parts do not sinter as well as cold-compacted or isostatically pressed pieces since additions of water, plasticizers, and binders are required. However, by the proper selection of oxide, or blend of oxides, it may be possible to extrude UO_2 slugs which can be dried and sintered without cracking or warping.

Physical properties of the sintered UO_2 will also be determined. Of particular interest is the open porosity and the surface-to-volume ratio of sintered slugs since these properties directly affect the fission gas release. The influence of sintering conditions on the purity and the uranium-to-oxygen ratio will be determined by chemical analysis.

Data from the program as outlined should yield the following specific information concerning the GCR-2 fuel:

(1) the degree of control over the manufacturing variables necessary for production of slugs of the desired tolerances,

(2) a close estimate of the most economical manufacturing tolerances,

(3) an evaluation of the fuel slugs by comparison with physical and chemical properties of PWR pellets with known fractional fission gas release, and

(4) the suitability of the extrusion process for production of UO_2 fuel slugs.

12.2.2 Radiation Damage Studies: The proposed use of bulk oxide fuel in a gas-cooled design at the reference design temperature will necessitate extensive radiation tests on the fuel selected. The fission-gas-release data from prior work are quite encouraging,[2,3] but must be confirmed with tests on other types of oxide. Indications are that at moderate surface temperatures the fission gas release is small, but that it is strongly dependent on temperature and bulk density. Other factors which may affect the rate of gas release are the method of manufacture, sample geometry, and rate of fuel burnup.

---

[2] B. Lustman, Release of Fission Gases from UO_2, WAPD-173 (March, 1957).

[3] J. D. Eichenberg, P. W. Frank, T. J. Kisiel, B. Lustman, and K. H. Vogel, Effects of Irradiation on Bulk UO_2, WAPD-183 (October, 1957).

Previous work has shown that cracking of the UO_2 will occur very early in the radiation cycle.[4,5] However, in nearly all cases the UO_2 bodies retained their shape, and spalling or fragmentation of the UO_2 was not reported to be a serious problem. Nevertheless, there is disagreement concerning the actual core temperatures and center melting of fuel pellets.[6] Work at Chalk River has indicated that sublimation rather than melting of the fuel is responsible for the voids found in exposed samples.

Since the release of fission gases may cause pressure build-up in the capsule and an increase in UO_2 temperature, due to dilution of the helium, the study of the rate of gas release has been given a high priority. The first series of experiments will also serve to study the dimensional stability of the UO_2, as well as fission gas retention. By increasing the enrichment of these samples, the atomic burn-up can be accelerated to match that of actual GCR-2 conditions. The dimensions of these samples will be reduced in order to achieve realistic temperature and thermal stress conditions. The samples will be sealed under helium in a stainless steel container and maintained at temperature by forced air cooling. The in-pile capsule assembly is illustrated in Fig. 12.1.

The encapsulated samples are assembled with an annulus that permits cooling air to pass over the outside of the capsule. This assembly is inserted into a dry tube facility that extends into a beryllium block in the lattice of the LITR. The temperatures of the samples are monitored by thermocouples welded to the outside of the capsule and by one thermocouple extending through a seal into a hole drilled through the UO_2. The temperature of the UO_2 is controlled by varying the air velocity over the capsule. After irradiation, the capsule will be pierced in the hot cell and the fission gases will be pumped out and analyzed.

---

[4] Ibid.

[5] J. Belle and L. J. Jones, Resume of Uranium Oxide Data - No. X, WAPD-TM-73 (August 15, 1957).

[6] A. M. Perry, Notes on Visit to Chalk River (January, 1958).

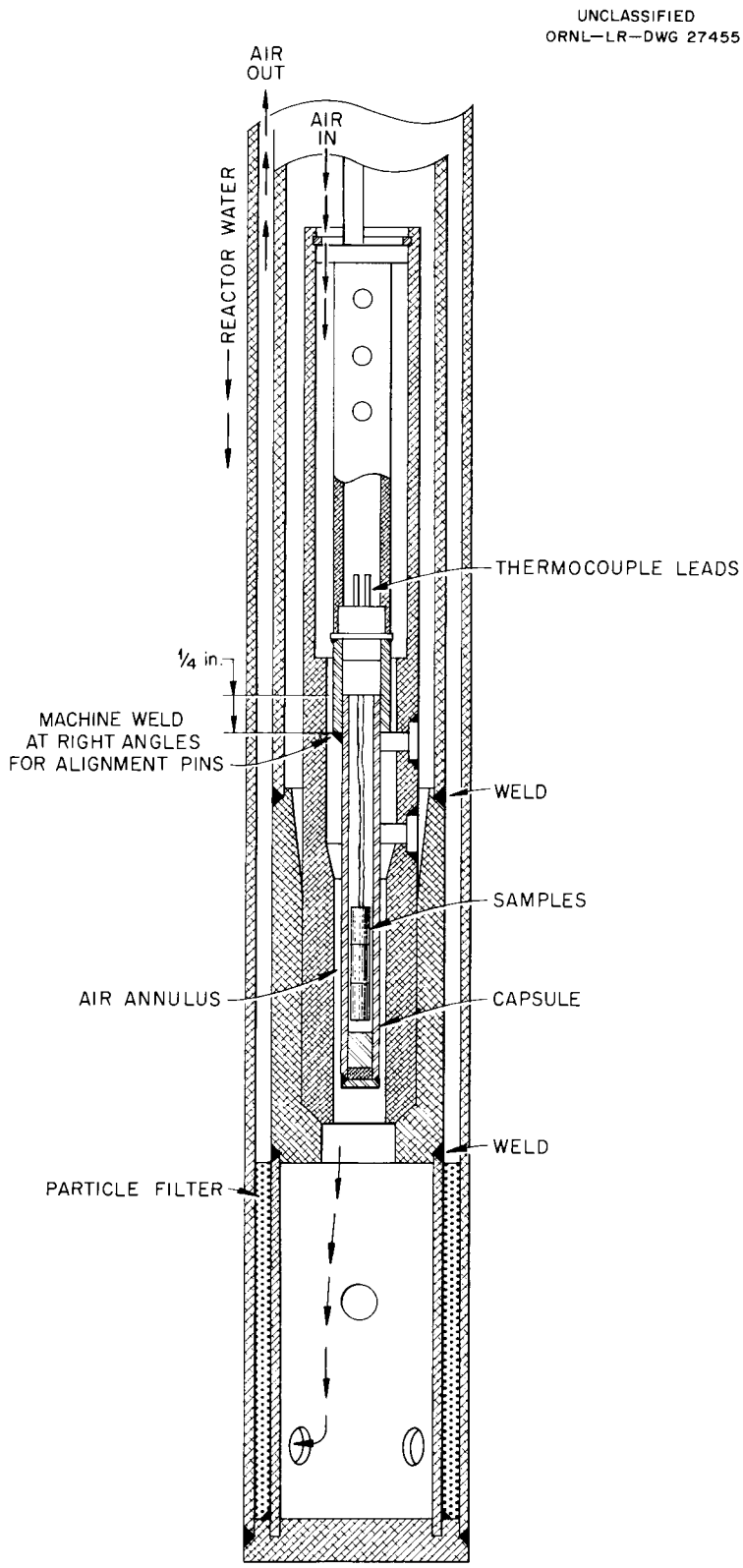

Fig. 12.1. Capsule for UO_2 Irradiation Experiment.

In another series of experiments, which will duplicate the actual operating conditions, a fueled capsule will be subjected to the same external pressure, axial tensile force on the capsule wall, and compressive force on the UO_2 as will be experienced by the GCR-2 fuel element. Figure 12.2 shows the in-pile assembly.

A compression spring mounted at the bottom of the stainless steel-UO_2 fuel element provides a compressive force on the UO_2 equivalent to that of an actual full-length element. This also results in a tensile force on the capsule wall. Helium pressure around the outside of the capsule duplicates the external pressure in the proposed reactor. Heat generated by this experiment is dissipated to the LITR coolant water. Both the capsule temperature and the inside UO_2 temperature are monitored by thermocouples, and the temperature of the fuel element is controlled through a positioning device at the top of the reactor. The entire assembly may be raised or lowered into the high-flux region to maintain a constant temperature. A disassembly release allows the apparatus to be disengaged easily for transfer to the hot-cell area.

The capsule dimensions and fission gas evolution will be measured immediately after irradiation. Because of the low enrichment of the UO_2, a hot cell capable of handling plutonium is required to examine and test the actual UO_2 slugs. Such a cell is being designed in order to allow metallographic examination of the irradiated fuel elements and to measure physical property changes of the UO_2.

This same type of experiment will be modified to allow irradiation testing of a fuel capsule containing a deliberate defect in the capsule wall.

A comparison of the proposed GCR-2 fuel element parameters with the first two irradiation test conditions is given in Table 12.1. These experiments should prove quite versatile in that the heat flux and UO_2 temperature may be varied somewhat and should be readily controlled. Thus, an extensive series of similar experiments should give a good statistical survey of the fission gas release and cracking from thermal stresses for UO_2 bodies manufactured by various methods. These data will then establish the type of UO_2 to be used and confirm the design parameters for the fuel capsules. The use or need for cores or supporting rods and end spacers in the fuel capsules

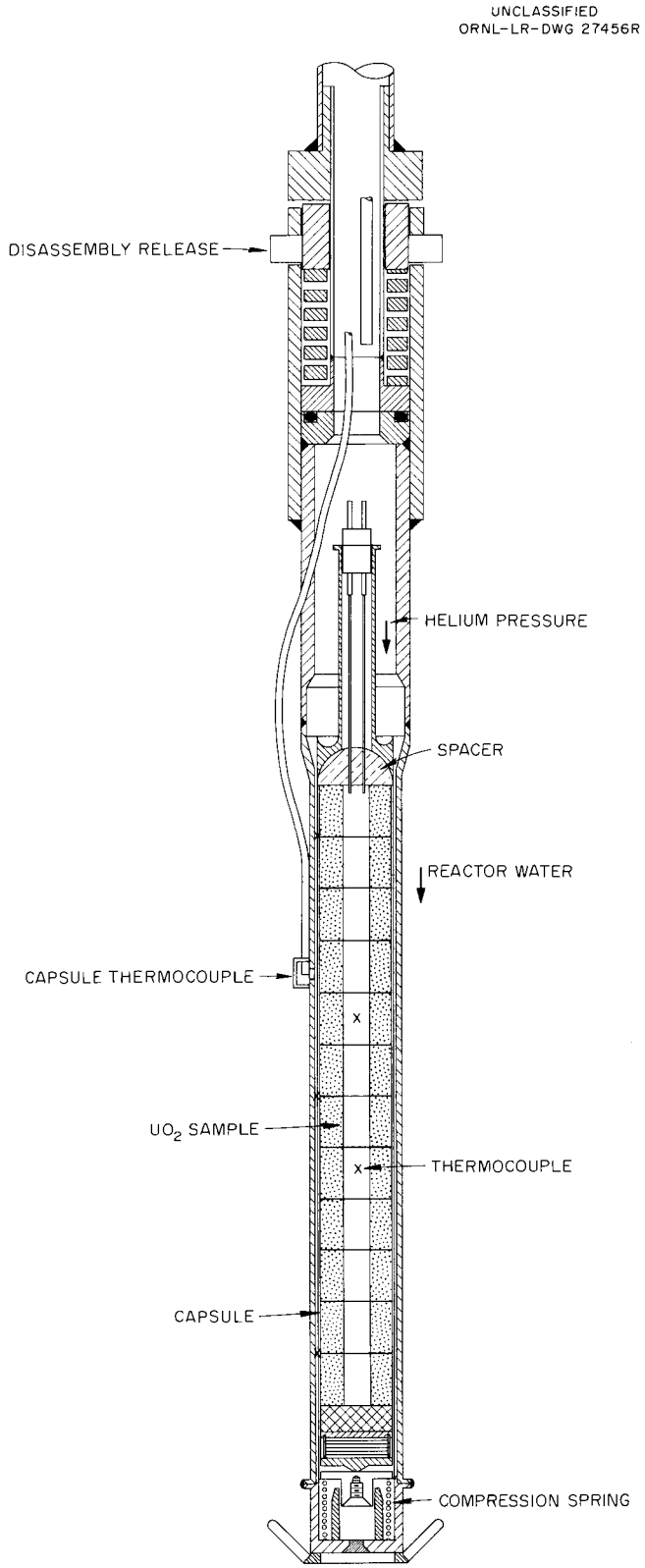

Fig. 12.2. Assembly for GCR-2 Fuel Element Irradiation Experiment.

TABLE 12.1

COMPARISON OF FUEL ELEMENT TESTS

		Units	GCR-2	Experiment 1	Experiment 2
Fuel Element:	OD	Inches	0.75	0.156	0.70
	ID	Inches	0.32	0.078	0.25
Fuel Capsule:	OD	Inches	0.80	0.266	0.75
	ID	Inches	0.76	0.158	0.71
Power Density:	Maximum	Watts/cm^3	106		
	Average		53	730	85
	Minimum		12		
Heat Flux:	Maximum	BTU/hr-ft^2	110,000	40,000	120,000
	Average		55,000		
UO_2 Center Temperature, at Maximum Power, at beginning of run		°F	2,480	1,770	2,750
UO_2 Perimeter Temperature, at Maximum Power, at beginning of run		°F	1,470	1,470	1,550
Capsule Surface Temperature		°F	1,300	1,100	1,300
Thermal Stress		Psi	140,000	40,000	140,000
Total Burn-up		Mwd/t	7500 – 15000	5000 – 15000	500 – 1500
Time in Reactor		Weeks	90 – 300	10 – 30	10 – 30
Fuel Enrichment		% U^{235}	2.0	15.0	1.8

will also be established. Severe cracking in hollow fuel slugs could result in collapse and failure of the fuel capsule. More moderate cracking may result in the collection of fragments at the bottom of the hollow core, with possible overheating. A solid fuel slug or core of MgO or graphite to support the slugs is not as attractive as the hollow slugs used in the reference design and may not be required.

12.2.3 In-Pile Loop Test of Fuel Assemblies: The final performance testing of the fuel elements will require an in-pile, pressurized, gas-cooled loop experiment. The flow diagram for the proposed experiment is shown in Fig. 12.3. This experiment, in addition to final testing of fuel slugs, will enable a study of the thermal ratcheting problem. This phenomenon may occur from stresses arising from differential expansion of the UO_2 and the capsule wall during temperature cycling. It has not been found to be a problem in the design of elements fueled with bulk UO_2 and cooled with pressurized water. However, longer elements operating at higher temperatures and with larger temperature cycles will necessitate an investigation of the phenomenon.

The final design and operating parameters would depend on the results of the first two series of radiation damage experiments. The data from operation of such a loop will confirm the design criteria and help to establish final design specifications for the fuel slugs, fuel capsules, spacers, and hangers.

12.3 Capsule Material Development

The research and development program is required to establish the stress and environmental conditions which will permit the life of the type 304 stainless steel capsule material to exceed the life of the fuel. The program will determine the effect of four basic phenomena on the mechanical properties of the type 304 stainless steel. The problems associated with these phenomena and the experimental work necessary to overcome these problems are described, as follows:

12.3.1 Effects of Contaminants in the Helium

12.3.2 Effects of Aging Reactions

12.3.3 Buckling of Capsule Wall

12.3.4 Effects of Section Size and Bending Moments

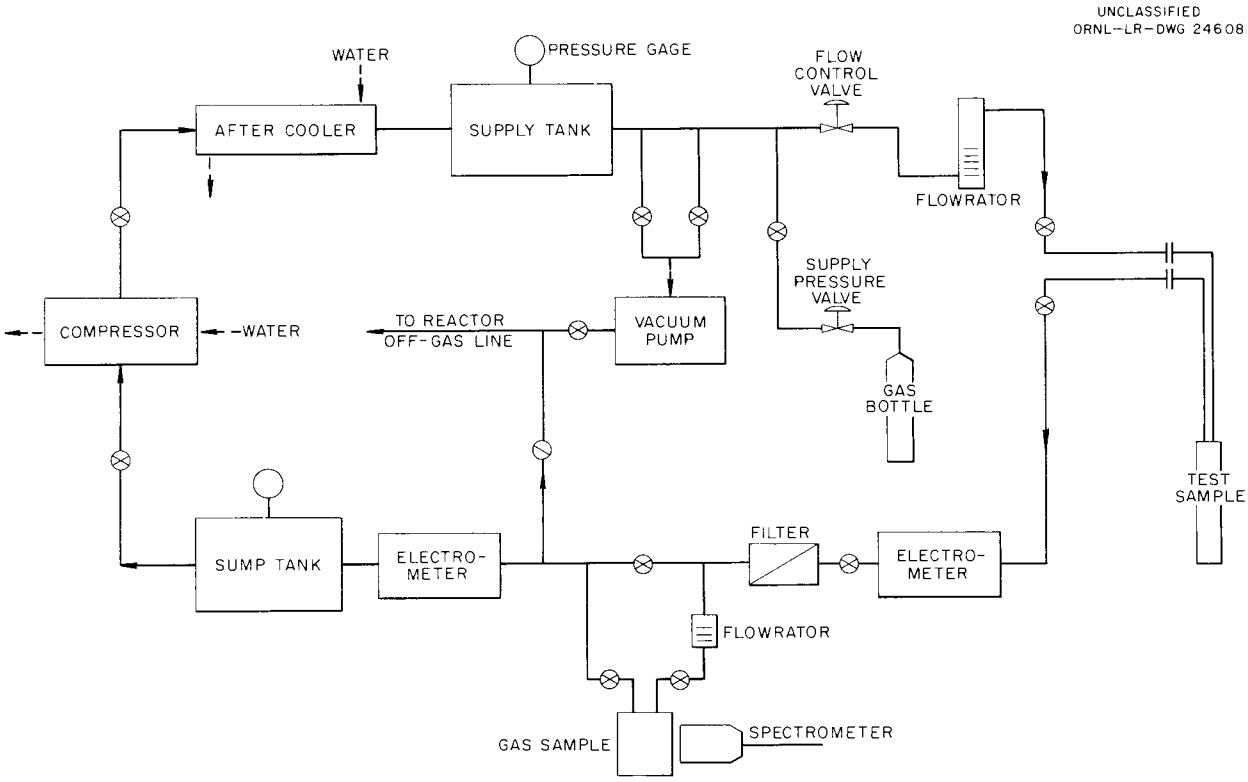

Fig. 12.3. Flow Diagram of Ceramic-Fuels Forced-Cooling Experiment.

12.3.1 Effects of Contaminants in the Helium: Although the behavior of type 304 stainless steel in air and in steam is well understood over the temperature range of interest to the GCR-2 (450–1500°F), its behavior in helium containing modest amounts of CO, CO_2, and steam cannot be predicted with certainty. Therefore, an experimental program must be carried out to determine if type 304 stainless steel will survive for five to seven years in the complex environment of the gas-cooled reactor.

When type 304 stainless steel is exposed in an environment of air or steam, an oxide film quickly forms which is adherent and is nearly impervious to the passage of more oxygen or metal atoms. Because of its properties, this oxide film produces an extraordinary resistance to attack. In the absence of strongly oxidizing conditions the adherent film may not form or may be reduced so that no protection is provided for the metal. Although none of the probable contaminants in the helium would be expected to react violently with unprotected steel, without the film small amounts of oxygen from CO_2 or water could selectively oxidize the chromium in the steel internally, by the diffusion of oxygen into the metal, and produce a serious loss in strength over a long period of time. In order to maintain an impervious oxide film, an oxidizing atmosphere is provided in most applications of the stainless steels. In the GCR-2, however, graphite is also present and would react with oxygen additions to produce carbon monoxide, which will reduce iron and nickel oxide. Any large oxygen additions would also produce carbon mass transfer as discussed previously in Part 2, Section 3.

Carburization of the type 304 stainless steel could also occur in the contaminated helium atmosphere by the reaction: $2\ CO \rightleftarrows C$ (dissolved in the steel) + CO_2. Carburization of type 304 stainless steel has both a beneficial and a detrimental effect. The beneficial effect is the improved creep strength that is derived from the formation of chromium carbide ($Cr_{23}C_6$) in the grain boundaries. The detrimental effect is that this formation also results in a decreased ductility, particularly notch ductility. The room temperature Izod impact strength in type 302 stainless steel, which has a higher carbon content than type 304, but is otherwise similar, is reduced from about 120 ft-lb to 30 ft-lb when annealed material is reheated 3000 hr

at 1200°F.[7] This loss in ductility is a result of a carbide precipitation at the grain boundaries. In the GCR-2 carburization could result in a much more serious decrease in the notch ductility, because by carburization even higher carbon contents might be achieved than the 0.20 wt % maximum found in type 302. A high notch ductility would be desirable because impact stresses are certain to be imposed on the fuel element by the vibration they will experience during the loading, unloading, or moving of the fuel element assemblies.

Relocation of the fuel elements to achieve more uniform burn-up of the fuel introduces an additional problem. Upon moving, an element which has experienced thousands of hours at one temperature will find itself in a new higher or lower temperature region. Due to the nature of the CO_2/CO equilibrium, the steady-state composition found in the reactor may be oxidizing at one temperature level and reducing at another. This alteration of conditions could have serious consequences with regard to the mechanical properties of the type 304 stainless steel. In addition to this type of alteration, cyclic changes in the oxidizing potential of the atmosphere would also be expected to occur during start-up, during reloading, and when leaks develop. These cyclic changes could also have serious consequences.

In order to evaluate the effects and tendencies for carburization and internal oxidation, long-time studies should be carried out on type 304 stainless steel in a series of carefully controlled atmospheres which would scan the range of conditions likely to occur in the GCR-2. In these studies, samples of type 304 stainless steels would be held in constant-temperature furnaces ranging in temperature from 450 to 1500°F and exposed to the controlled atmospheres for periods up to one year. These samples would then be examined metallographically to determine what structural changes had occurred. Additional tests would be made in those environments which produced significant effects to determine the changes in creep strength and stress-rupture life as well as the notch ductility. Similar studies would be made under conditions of alternating oxidizing and reducing atmospheres. From these studies the range of conditions which would produce carburization, be inert,

---

[7] R. M. Brick and A. Phillips, Structure and Properties of Alloys (New York: McGraw-Hill, 1949) p. 425.

and cause oxidation would be determined as well as the effects of extensive carburization or oxidation on the mechanical properties. From the results, recommendations could be made with respect to the degree of gas purification required to give the desired service life for the capsule materials.

12.3.2 Effects of Aging Reactions: In addition to the possibilities of carburization and internal oxidation, the long-time stability of type 304 stainless steel at the operating temperatures of the GCR-2 must be considered. Annealed, wrought type 304 stainless steel has a structure which consists only of austenite (the face-centered-cubic form of iron) and carbides. Upon prolonged aging in the range 1000 to 1300°F, some ferrite (the body-centered-cubic form of iron) is nucleated and grows so that the equilibrium structure consists of a mixture of austenite and ferrite. As a result the stress-rupture life of the material is reduced.[8,9] Prolonged aging of type 304 may also produce some sigma phase, the brittle, complex, intermallic compound Fe-Cr. Indirect evidence has been given for such a precipitation,[10] with indications that it further reduces the stress-rupture life of type 304 stainless steel. Even with these transformations, the stress-rupture life of the type 304 stainless steel capsules should exceed seven years with the stress computed for the reference design. Since thinner sections than 0.020 in. (the reference design thickness) would be desirable from the standpoint of neutron economy, the in-influence of these aging reactions on the serviceability of the type 304 stainless steels under higher stresses should also be evaluated.

For the aging studies, creep tests would be made on samples of type 304 stainless steel at a constant temperature in an inert atmosphere for periods in excess of a year under the conditions of stress likely to occur in the GCR-2. Significant changes in the microstructure would be manifested by a difference in the creep rate and thus would be detected. The samples would also be studied metallographically and the notch ductility after prolonged aging would be determined. The results would be used to re-evaluate the applicability of type 304 stainless steel for the particular application.

---

[8] J. K. Y. Hum and N. J. Grant, "Austenite Stability and Creep-Rupture Properties of 18-8 Stainless Steels," Trans. ASM, 45, 105 (1953).

[9] F. C. Monkman, P. E. Price and N. J. Grant, "The Effect of Composition and Structure on the Creep-Rupture Properties of 18-8 Stainless Steels," Trans. ASM, 48, 418 (1956).

[10] Ibid.

12.3.3 Buckling of Capsule Wall: The major stress on the capsule material arises from the pressure exerted by the coolant. There must be some initial clearance between the capsule and the slugs to facilitate assembly and to maintain reasonable dimensional tolerances. Since commercial tolerances are desirable for the sake of economy, the clearance between capsule wall and slugs may be as large as 0.015 in. Thus, under operating conditions the capsule will have a tendency to collapse. This buckling may aggravate the hot-spot problem, as the resulting wrinkling leads to dimensional changes in the metal and between the slug and the wall.

A program was initiated to determine the optimum gap and to examine the structural behavior and integrity of the capsule material. Specimens for these tests had an outside diameter of 0.750 in. and a wall thickness of 0.020 in. with a gage length of 4.0 in. Inserts of the same material, to simulate the slugs, were placed inside the tubes before the end caps were welded in place.

Two buckling tests, performed by the Mechanical Engineering Department of the University of Tennessee, were made at room temperature on Inconel specimens to determine the buckling mode and the associated elastic stresses. The diametral clearances between the shell and the inserts were 0.100 and 0.020 in., respectively. The specimens were subjected to a slowly increasing external pressure. Buckling occurred in both specimens at 2000 psi as indicated by strain gages mounted on the specimens. Table 12.2 indicates the strain that occurred as the pressure was increased. The one-lobe mode of creep buckling is evident from the photograph, Fig. 12.4, of the specimen with the 0.100-in. diametral clearance. A cross-sectional view of this specimen is shown in Fig. 12.5. Rupture of the tube did not occur even with this severe deformation.

In the elevated-temperature test program it was assumed that the maximum hot-spot temperature would be 1500°F. Service conditions could be only approximated since it would be exposed to many different environments during the life of the capsule. Also in order to accelerate the test program, higher temperatures and pressures were used which could roughly be related to long service under less severe conditions. Thus, the initial tests were conducted at 1675°F for 500 hr at a pressure of 525 psi. Type 316

TABLE 12.2

BUCKLING TESTS OF INCONEL TUBING AT ROOM TEMPERATURE

Pressure (psi)	Strain			
	Spec. No. 1* micro-inches/inch	%	Spec. No. 2** micro-inches/inch	%
200	63	0.0063	51	0.0051
400	93	0.0093	101	0.0101
600	135	0.0135	152	0.0152
800	160	0.0160	211	0.0211
1000	203	0.0203	271	0.0271
1200	232	0.0232	330	0.0330
1400	406	0.0406	389	0.0389
1600	524	0.0524	448	0.0448
1800	1015	0.1015	609	0.0609
2000			2013	0.2013

* Diametral clearance - 0.020 in.
** Diametral clearance - 0.100 in.

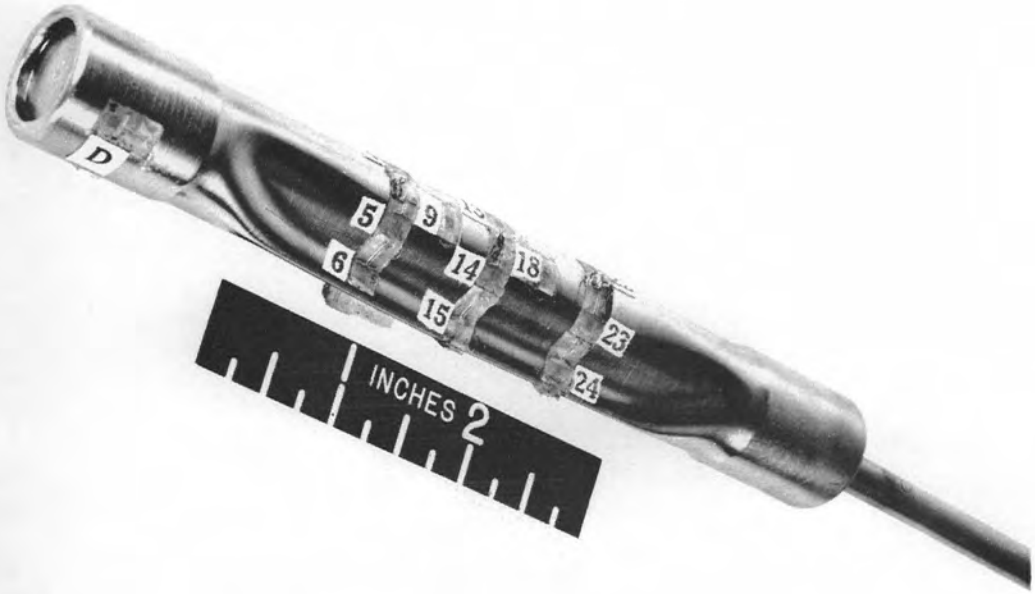

Fig. 12.4. Inconel Buckling Specimen Tested at Room Temperature Under an External Pressure of 2000 psi. Diametral clearance of 0.100 in. between capsule wall and slugs.

UNCLASSIFIED
Y-25066

Fig. 12.5. Cross Section of Inconel Buckling Specimen Tested at Room Temperature Under an External Pressure of 2000 psi. Diametral clearance of 0.100 in. between capsule wall and slugs.

stainless steel specimens were tested under these conditions with various diametral clearances between the inserts and the tube wall. No ruptures occurred in the wall of these specimens but all collapsed around the inserts as shown in Fig. 12.6. Figure 12.7 is a photograph of the specimen with 0.020-in.-diametral clearance. The force exerted on the metal by the pressure is evident from the outline of the inserts which are discernible through the tube wall. Measurements of the specimens after test indicated that deformation occurred evenly in all specimens. A cross section of the above specimen, Fig. 12.8, shows that no buckling occurred, in contrast to that which occurred in room temperature tests. The thermocouple protection tubes also collapsed during the 500 hr test, as is shown in Fig. 12.9, even though the stress on the walls of these tubes was only one-fifth of that on the specimen.

In another test four 3/4-in.-dia Inconel specimens with a 0.020-in. wall were subjected to a pressure of 300 psi at 1675°F for 500 hr. Diametral clearances of 0.004, 0.010, 0.020 and 0.100 in. between the capsule and inserts were used. Uniform collapse of the tube wall around the inserts occurred in the specimens with diametral clearances of 0.004 and 0.010 in. Specimens with diametral clearances of 0.020 and 0.100 in. buckled in a one-lobe mode as shown by Fig. 12.10, indicating that the tube wall-to-gap ratio as a function of temperature is important.

As a result of the preliminary investigation, it appears that the capsule cannot survive an extended period of time without collapsing. Therefore, deformation will have to be controlled by the UO_2 slugs so that once the capsule has collapsed around the slugs, subsequent deformation will be negligible.

The results obtained indicate several areas of investigation which should be explored.

(1) Determination of the buckling behavior of type 304 stainless steel tubes with 0.020-in. wall as a function of temperature and diametral clearance.

Fig. 12.6. Type 316 Stainless Steel Buckling Specimens Tested at 1700°F for 500 hr with an External Pressure of 525 psi.

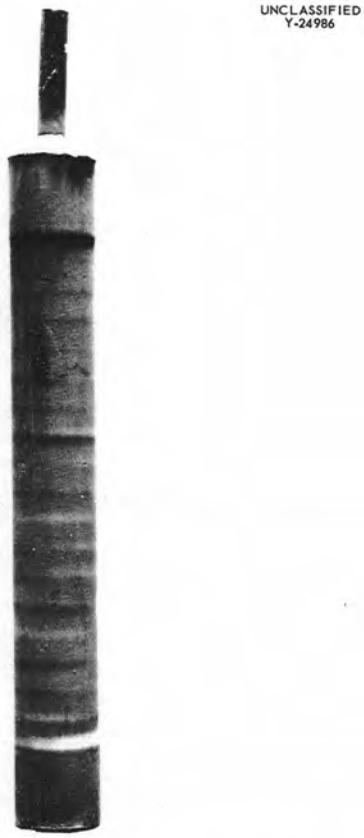

Fig. 12.7. Type 316 Stainless Steel Buckling Specimen with a Diametral Clearance of 0.020 in. Tested at 1700°F for 500 hr at an External Pressure of 525 psi. Note outline of slugs revealed when capsule collapsed.

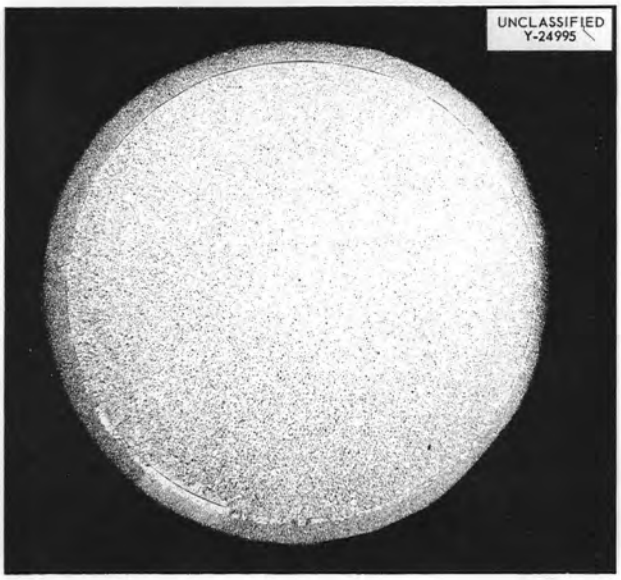

Fig. 12.8. Cross Section of Type 316 Stainless Steel Buckling Specimen with 0.020-in. Diametral Clearance. Note the pressure bond achieved between capsule wall and slug. 5X. Reduced 23.5%.

UNCLASSIFIED
Y-24988

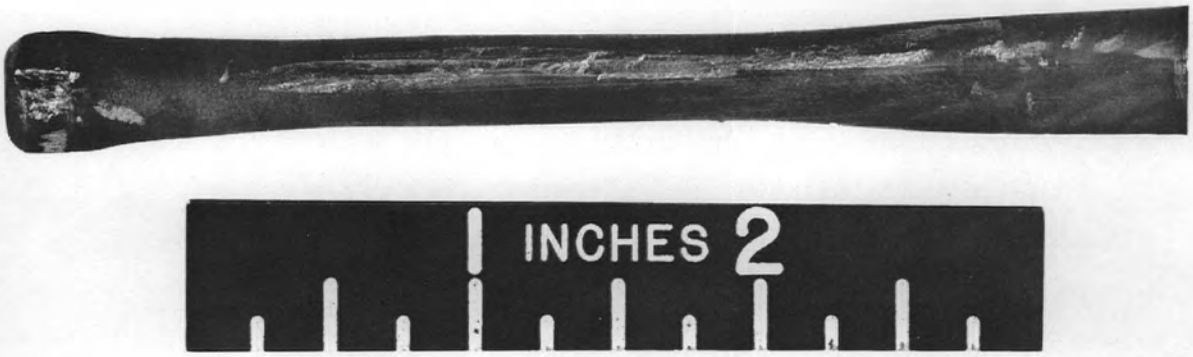

Fig. 12.9. Collapsed Thermocouple Tube of a 500-hr Buckling Test Performed at 1700°F and 525 psi.

UNCLASSIFIED
Y-25090

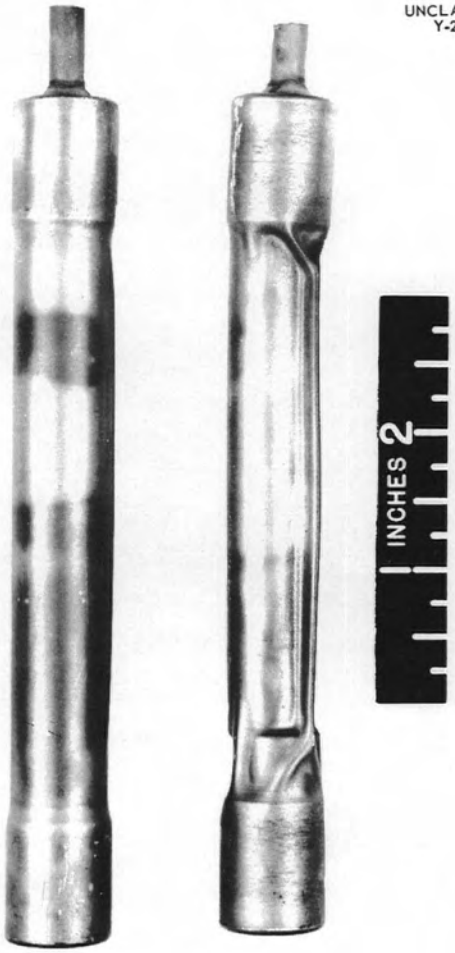

1
0.020 IN.

2
0.100 IN.

DIAMETRAL CLEARANCE BETWEEN CAPSULE WALL AND SLUGS

Fig. 12.10. Inconel Buckling Specimens Tested at 1675°F for 500 hr with an External Pressure of 300 psi.

(2) Determination of the relationship of wall thickness to the buckling behavior as a function of temperature and diametral clearance.

(3) Determination of the effect of repeated cyclic temperature fluctuations on the integrity of the tube wall as a function of the wall thickness and diametral gap.

In addition, tests will be run to explore the effect of collapse of the tube wall where the area of collapse is rigidly confined. The possibility exists that under thermal stresses the UO_2 slugs will crack and disintegrate in certain areas. This material would tend to fall through the center hole of the slug, thus removing support from the tube wall over a small area. Under such conditions deformation of the wall induced by further collapse may exceed the ductility of the metal and cause failure through the wall.

Another possible cause of failure of the capsules is the prolonged exposure to gaseous environments which are sometimes oxidizing, sometimes partially oxidizing and sometimes carburizing. Creep tests of type 304 stainless steel will be conducted in environments simulating these conditions to determine if they produce adverse effects on the mechanical properties or produce such intergranular oxidation as to allow a free path for fission gases to escape.

12.3.4 Effects of Section Size and Bending Moments: The fuel element hangers have been designed to act as cantilever beams loaded in simple bending. The creep-rupture lives of beams in bending have been predicted by Platus within a fair degree of accuracy using tensile creep data of lead at room temperature.[11] Results have indicated that the maximum fiber stress probably diminishes and is re-distributed as plastic deformation occurs. This reduction is approximately 20 to 25% of the maximum fiber stress.

For a maximum fiber stress of 2500 psi (the predicted stress in the fuel element hangers) the reduced stress would be about 2000 psi. It can be seen from Fig. 3.5, Part 2, Section 3, using the 1000°F curve rather than 950°F as an additional safety factor, that the strain resulting from this stress will be of a conservative value. The strain in seven years, approximately 62,000 hr, would be less than one per cent.

---

[11] D. L. Platus and B. Y. Cotton, Prediction of Creep Failures of Lead in Bending from Tensile Data, ORNL-CF-57-7-58 (July 17, 1957).

There are, however, several uncertainties in this method of using lower stresses obtained from creep theory as compared to elastic calculation. Most of the available data are based on constant load and not constant stress. Variations in strain over the cross section just after loading may have an appreciable effect on the stress distributions. These short-time stresses and strains in turn may markedly effect the stress-rupture life of the beam. Also the "third stage" creep displayed in most tensile creep specimens would be absent from bend tests, because the outer fibers in a beam would be restrained from such an acceleration. This would lead to an increase in life over that predicted by tensile data.

As a result of the room temperature work by Platus, an investigation of the creep properties of Inconel under bending at elevated temperatures was initiated. Data from several tests at 1500°F lend some support to the correlation predicted by Platus. However, further exploration of the high-temperature bending creep tests is necessary.

Bend-creep tests then will be conducted on type 304 stainless steel from 800 to 1200°F and over a sufficient range of stress to permit extrapolation of relatively short-time tests to the expected life of the fuel assembly.

12.4 Fuel Element Assembly

The experimental program necessary to achieve a dependable, low-cost fuel element involves the development of a good joint design and a good joining procedure, the determination of the most inexpensive methods of fabricating end caps, hangers, and spacers, and the development of inexpensive but reliable inspection techniques. This section summarizes the initial program to be carried out at Oak Ridge National Laboratory to attain optimum fuel element specifications. Further modifications within the specifications to achieve the minimum costs will be expected from the vendors of these components.

12.4.1 Development of Closure Welds: In assembly of the fuel element capsule, the closure for one end of the capsule is less complicated than the other in that no fuel is in place at the time of welding. This weld may be inspected more easily and may be repaired. The weld to be made after loading of the fuel is more difficult as it is close to the fuel and may be contaminated during the welding process. Repairs on the final weld will be restricted and any need for removal of the weld will reject the element due to length tolerances.

The inert-gas-shielded tungsten-electrode process has been selected for the automatic welding of the caps to the tubes. This process has been proven for high-quality welds on thin-section materials. In the automatic process, variables of welding are most easily controlled and it is adaptable for atmosphere chamber techniques. Although it is a widely used method of joining metals, certain tests are required to develop this technique for the specific application. These tests will be designed primarily to determine the optimum welding variables necessary to produce sound welds, such as arc length, power input, rate of travel, etc. Additional data such as shrinkage and strength of the joint will also be determined.

Two types of joints are being considered as illustrated in Fig. 12.11. The butt-fusion type is favorable due to ease of inspection and high joint efficiency from the strength standpoint. However, repair of faulty welds of this type is difficult, and the strength is highly sensitive to alignment.

The other type joint which is considered is the edge-fusion joint. The advantage of this joint is that the weld area is removed from the fuel and may not require dry-box welding. In addition, this weld is not as sensitive to alignment as the butt-fusion type. Difficulties encountered in this type of joint are that inspection is difficult and joint efficiency is low. For these reasons it might be necessary to depend on the cap design or spot welding for joint strength and use the fusion weld only for sealing.

12.4.2 Methods of Fabricating Fuel Element Components: The most economical method of fabrication for each of the end cap designs shown in Fig. 12.12 is by automatic screw machine. The stock used to manufacture the parts will be forging quality bar stock which will have been previously inspected using ultrasound techniques.

To select the optimum design for end caps, it will be necessary to manufacture several specimens of each type and perform tests to determine the design having minimum cost and maximum reliability. Merits and handicaps of the two joint designs from the welding standpoint have been discussed previously. However, in addition to selecting the proper weld design, a design having the maximum strength with a minimum amount of metal must be considered to increase the fuel-to-poison ratio.

UNCLASSIFIED
ORNL-LR-DWG 27101

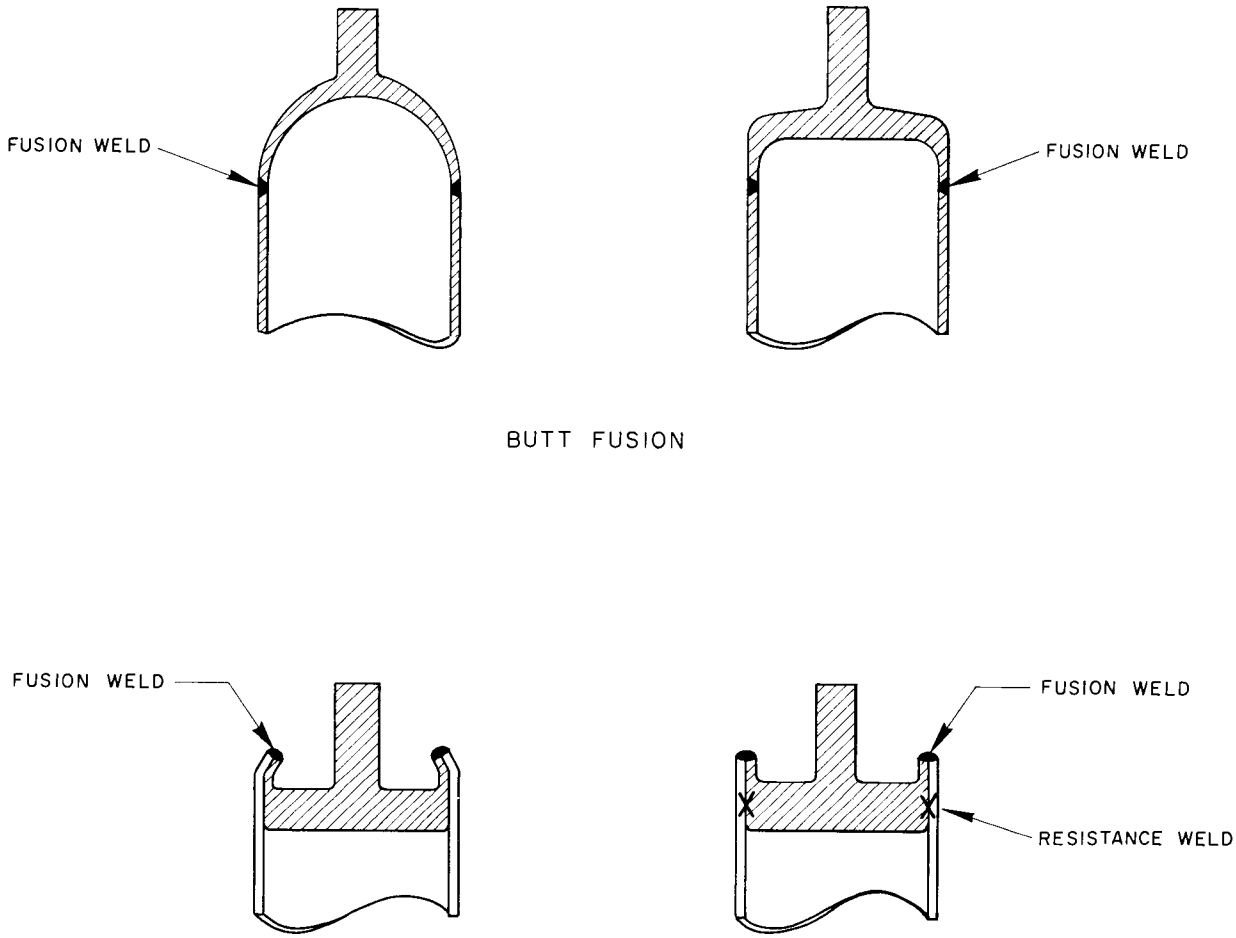

Fig. 12.11. Alternate Joint Designs.

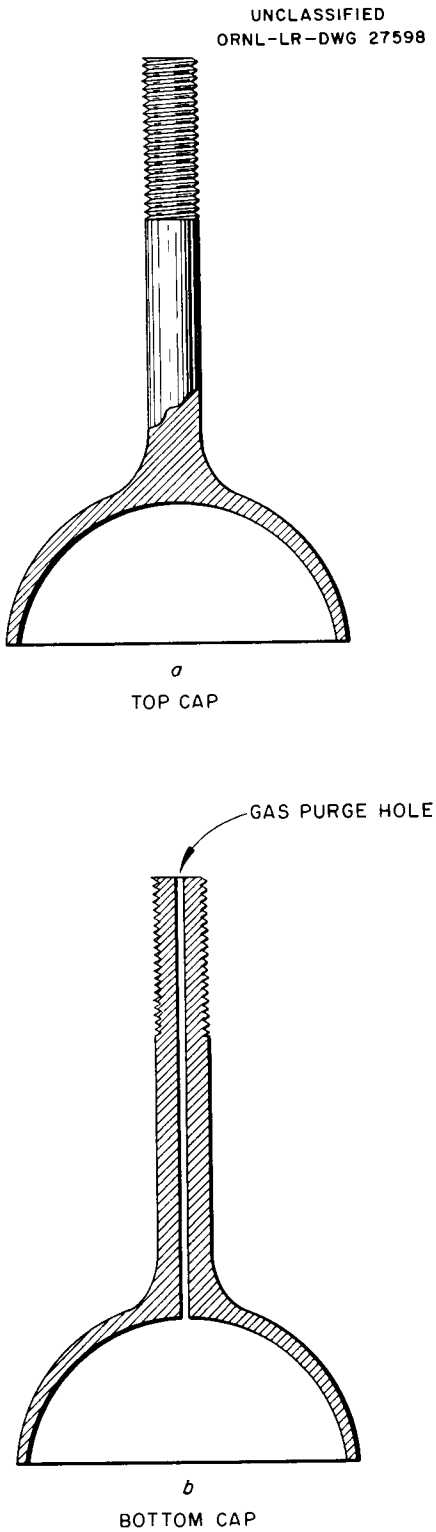

Fig. 12.12. Fuel Capsule End Caps.

Alternate designs and fabricating techniques for hangers and spacers were discussed in Part 2, Section 4.3.3. Further work will be needed to develop hangers and spacers which are more economical and have better nuclear properties. Both stamped and precision-cast components will be exposed to the reactor operating conditions and evaluated on the basis of creep deflection.

12.4.3 Methods of Inspection: End caps, spacers, and hangers may be inspected using conventional techniques such as ultrasound and dye-penetrant inspection. Suitable fixtures for handling the individual parts on a production basis will have to be designed and certain modifications to existing commercial inspection equipment will be necessary.

Inspection of the tubing for fabricating capsules will pose a more difficult problem. Presently, tubing is being inspected in industry both by radiographic and electronic techniques. The electronic methods of inspection appear to be more economical, since manpower and time requirements are high for radiographic inspection. The eddy-current method is the most applicable of the available electronic techniques for inspecting tubing of this particular size.

However, in applying eddy-current inspection techniques to austenitic stainless steels, the variation of magnetic permeability introduced by segregation and cold work in the metal presents a troublesome inspection problem. Additional development work in the field of eddy-current inspection is warranted not only for the Gas-Cooled Reactor Program but for all of the reactor programs utilizing thin-walled tubing fabricated from austenitic stainless steels, as this method of inspection lends itself to processing large quantities of material at a lower cost than other available techniques. It is proposed that some effort be expended to modify both coil design and instrument design to minimize the spurious signals coming from the variations of magnetic permeability without the sacrifice of test information. Several avenues of approach are anticipated: among these are the use of very thin and very closely spaced differential coils and the use of phase-sensitive detectors in the test instrument.

The radiographic inspection of the weld closure joining each end cap to the tube forming the fuel capsule is the most expensive single inspection to be performed on the fuel capsule. It is proposed that the application of

fluorscopic methods or of x-ray-sensitive closed-circuit television systems be thoroughly explored and evaluated as methods of inspecting this type of joint. Radiographic inspection is fairly expensive because nearly half of the cost is used up in manpower to read and interpret the films. The use of mechanized scanning and direct-visual presentation of the x-ray image can cut the manpower requirements by at least a factor of two. Preliminary studies of closed-circuit television systems have indicated a strong possibility of success in using such a technique on weld closures in thin-walled small-diameter tubing.

12.4.4 Manufacture of Test Samples: The several proposed designs for the capsule and element must be evaluated in regard to known production technique and reliability when exposed to the reactor environment. This evaluation may be accomplished most expeditiously by manufacturing samples of each design and correlating the variables involved. These samples will serve a two-fold purpose in that assemblies for flow testing, thermal cycling and radiation damage testing will be needed. Each of the test assemblies will have certain modifications to suit the conditions of test but should maintain sufficient identity to provide the information needed on fabrication variables. The ideal assembly for each of the above tests would be a full-scale model of the fuel element. In cases where this is not practical, small assemblies or components of the assembly will be tested.

12.5 Contamination of the Coolant

The compatibility of helium with the reactor components was given special consideration in its selection as the coolant. In practice, however, contamination of the helium by small quantities of CO_2, CO, H_2, O_2, H_2O, and hydrocarbons will occur, and the effect of the contaminants on the reactor components, principally the graphite and the metal capsules, should be established through experimental studies.

The proposed experimental work includes:

12.5.1 Studies of the Rates of Adsorption and of Evolution of Gases by Graphite. - The degree and type of contamination of the helium could be estimated from the data obtained in these studies.

12.5.2 Reactions of Contaminants with Graphite. - Reaction rates for the graphite-CO_2 interaction and decomposition of CO

will be included as will some work on the effect of radiation.

12.5.3 Large-Scale Out-of-Pile Loop Experiments. - These will be out-of-pile engineering-scale studies of the effect of contaminants in the helium on the reactor components under conditions simulating those that will prevail in the reactor. Large-scale loops will also be used to study the flow and heat transfer characteristics of the GCR-2 reference design fuel elements.

12.5.4 Large-Scale In-Pile Loop Tests. - These tests will be designed to show the effect of radiation when contaminated helium is circulated over graphite and type 304 stainless steel surfaces.

These proposed studies are discussed in more detail in the following paragraphs.

12.5.1 Studies of the Rates of Adsorption and of Evolution of Gases by Graphite: It is anticipated that the gases evolved from the graphite, especially during start-up and the early stages of operation at power, will result in serious contamination of the helium. Data are required from which the quantity and the composition of the evolved gases as well as the rate of evolution may be predicted for the GCR-2. Such information is necessary in deciding whether or not a gas-purification system will be required in the proposed plant design.

The graphite will be exposed to ambient atmosphere for six months or longer during the construction of the reactor; in spite of all precautions that may be taken to protect the graphite from gas pickup during manufacture, significant gas adsorption is expected. Accordingly, data are required on the rate of adsorption of gases by graphite from ambient atmospheres as a function of relative humidity, geometry of specimens and the time of exposure. Although the results of these studies will permit reasonably reliable estimates of the quantity of adsorbed gases present on the graphite, the rates at which these gases may be evolved during start-up and operation of the reactor are even of greater importance. Therefore, studies of the rate of evolution of gases from graphite as a function of the temperature, pressure, time, and geometry of the specimen also should be carried out. Supplementary data related to the composition of the gases evolved could be obtained through analyses of the gases with the mass spectrometer.

A survey of previous studies related to the gas-evolution problem has been presented in Part 2, Section 3.3.2 of this report. It is evident that very little information is available having any direct bearing on the problems associated with the GCR-2.

The rate of gas pickup by graphite will be determined by exposing suitable specimens to air containing various amounts of water vapor for known periods of time, followed by degassing of the samples. The volume of the evolved gases will be measured and in some cases the composition determined by gas analyses or by means of a mass spectrometer. It is planned to collect data related to the rate of gas pickup for graphite specimens, of dimensions approximating those of the reactor graphite, exposed to air with relative humidities in the range of 15 – 50% for periods of time ranging from a few weeks to several months. This information will be useful in calculating the gas content of the stacked graphite in the moderator and in combination with data for the evolution of gases will be used to predict the degree of contamination of the helium.

The other phase of the experimental work involves the determination of the rates at which the gases are evolved from the graphite. This will be accomplished by heating the graphite at the desired temperature in a quartz tube, pumping off the evolved gases and collecting these gases in a suitable collection apparatus. The volume of the evolved gases will be measured and the composition determined by gas analyses or in a mass spectrometer.

The rate of evolution will be measured primarily as a function of the temperature and the geometry of the specimens. Most studies of the effect of temperature will be made over the temperature range of 90° – 1100°F that the graphite matrix will experience, and particularly over the range of the GCR-2 design temperature of 460 – 1050°F. Collection of the gases will be made at 200° intervals in this range. The rates of evolution at these temperatures will determine whether or not most of the adsorbed gases may be removed during the start-up of the reactor before the graphite attains its maximum temperature. Some studies also will be made at temperatures well above 1100°F to measure the residual gases which may come off very slowly at 1020 – 1110°F. It is known that the rate of evolution increases quite rapidly at high temperatures. Additional studies will be made of the effect of pressure on the rate of evolution at temperatures of 210 – 570°F. The

pressures to be studied will range from the start-up pressure to the reference design pressure.

The rate at which the gases are evolved at some definite temperature is mainly dependent on the rate of diffusion of the gases through the pore structure of the graphite. In general, the diffusion rate increases with temperature. In addition to studying the effect of temperature changes, experiments will be performed in which the gases will be collected for extended periods of time at some definite temperature. Information on the diffusion rate will also be obtained by measuring the rate of evolution of gases at some fixed temperature and varying the dimensions of the graphite specimens. The data obtained from these studies of the effect of temperature and geometry of the specimens will be useful in predicting the rate of evolution of gases from the graphite matrix and thereby estimating the degree of contamination of the helium.

12.5.2 Reactions of Contaminants with Graphite: It is believed that the reaction $C + CO_2 \rightleftarrows 2\ CO$ is most important when graphite is exposed to the contaminated helium. Other impurities such as O_2 and H_2O may burn out small amounts of graphite. However, it is expected that the concentration of CO_2 will be considerably higher than the concentrations of the other contaminants, and furthermore that temperature gradients present in the reactor may lead to deposition of soot in the cooler regions by a shift in the chemical equilibrium of the reaction.

The reaction rate for the graphite-CO_2 reaction at low partial pressures of CO_2 should be measured at temperatures of 930 – 1110°F. Small-scale circulating systems operating at various flow rates and having appropriate gas-to-graphite relationships will yield useful data even if carried out in the absence of radiation. However, the decomposition of CO is known to be induced by radiation, so the quantity of useful data supplied by small-scale out-of-pile experiments will necessarily be limited. Large-scale experimental work will provide additional data but it probably will be necessary to operate a large-scale in-pile loop to obtain the necessary data. The proposal for such a loop is presented in 12.5.4.

A. Survey of Prior Work. Extensive information is available on the reaction rates of CO_2 with graphite, decomposition of CO and the effects of radiation on these processes. However, very little of the data is directly applicable to the GCR-2.

The rate of graphite burnout has been shown to be 21% per 1000 days at 1300°F and by extrapolation to be 3.0×10^{-5}% per 1000 days at 750°F with a CO_2 pressure of one atmosphere in the absence of radiation.[12] Considerably lower reaction rates at comparable temperatures would be expected at the CO_2 pressures likely to be present in the GCR-2, since the reaction rate is dependent on the CO_2 pressure. However, the intense radiation present in the reactor will promote chemical reactions at temperatures well below those required in the absence of radiation. For instance, studies[13] by Hanford have shown that the burnout rate of graphite is ~ 0.06% per 1000 days at room temperature under irradiation. This rate requires a temperature of about 1150°F in the absence of radiation. British work indicates that the increase in the rate of reaction for the CO_2-graphite system is roughly proportional to the radiation intensity.[14] However, the temperature coefficient of the radiation-induced reaction is quite small. It is postulated that the thermal reaction probably masks the radiation effect on the CO_2-graphite reaction at temperatures above 900°F due to this small temperature coefficient. Similarly, it has been observed that pressure changes are not as important as might be anticipated. For example, a seven-fold increase in the pressure of CO_2 was found to

---

[12] P. C. Davidge and W. R. Marsh, The Effect of Pile Radiation on the Carbon Dioxide-Graphite Reaction, AERE-C/R-1374 (1955). Declassified with deletions September 3, 1957.

[13] R. E. Woodley, Promotion of Chemical Reaction in Gas-Graphite Systems by Gamma Radiation, HW-31929 (May 24, 1954).

[14] Davidge and Marsh, loc. cit.

increase the reaction rate by less than a factor of three at 660°F.[15] British studies[16] of the effect of flow rate indicate a maximum reaction rate at intermediate flow rates, the location of the maximum with respect to flow rate being a function of the geometry of the system and the lifetime of the intermediates postulated for the radiation induced reactions.

The above data indicate that although the reaction rate is low at 1050°F, a significant amount of graphite reacts with CO_2 yielding a measurable quantity of CO. It would be expected that eventually a steady-state condition would be reached in the reactor despite the low reaction rate. The time required to reach this state would depend not only on the reaction rate of CO_2 with graphite but also on the leak rate of the system and the rate of evolution of gases from the graphite. The concentration of CO present would depend not only on the CO_2 concentration and temperature but also on the degree to which the decomposition of the CO is catalyzed by radiation and metallic surfaces. The steady-state conditions would very likely be quite different from any that might be calculated using thermodynamic equilibrium constants.

Hanford studies[17] have shown that the CO_2-graphite reaction occurs at room temperature under pile irradiation yielding gaseous CO and carbon sub-oxide polymers as $(C_4O_3)_x$ and $(C_3O_2)_x$. In addition, the decomposition of CO is promoted by radiation in the absence of graphite, resulting in production of the same polymers. Upon prolonged exposure these polymers are degraded by energetic neutrons until the solid phase may consist mainly of elemental carbon. There also is evidence which suggests that the decomposition of CO may occur in the gas phase at a distance from any surface. Any solid formed in this manner would be free to circulate with the coolant.

---

[15] Ibid.

[16] Ibid.

[17] R. E. Woodley, The Promotion of Chemical Reaction by Pile Radiation, HW-40142 (November 22, 1954).

Accordingly, contamination of the gas stream as well as the metal surfaces by solids may result from the decomposition of CO.

Sufficient data are not available to predict what quantities of soot may result during reactor operation. British experience indicates that it is not a serious problem under the operating conditions at Calder Hall,[18] namely a maximum graphite temperature of 660°F and a CO_2 pressure of 8 atm. The reaction rate for the CO_2-graphite reaction is somewhat higher at 1050°F than at 660°F for comparable CO_2 pressures. The increase in temperature also results in a shift of the equilibrium to give an increase in the CO pressure. However, the low partial pressure of CO_2 in the GCR-2 coolant should prevent the reaction from becoming a problem. It is likely that the steady-state conditions will be less favorable for the transport of carbon than any estimate that might be made from available reaction rates and equilibrium data for the CO_2-graphite system.

B. Description of Proposed Work. The reaction rates for the interaction of CO_2 with graphite in the absence of radiation will be measured in a small-scale dynamic system in which the gas will flow over the graphite and either be removed from the system after a single pass or be re-circulated. The gas will be sampled and changes in the CO concentration will be used to evaluate the reaction rate. The studies will be performed at low partial pressures of CO_2 in helium as well as with varying ratios of CO_2 to CO in helium. Results from initial experiments at 930–1100°F will dictate what other temperature ranges might be used. In addition to studying the effect of temperature and partial pressures of CO_2 and CO, such factors as total pressure and flow rates will be investigated. Data collected from these studies should enable one to establish the reaction rate as a function of these variables.

Studies in which the gas will be re-circulated as well as those in which CO will be added will utilize a temperature gradient. These investigations will yield some information on the rate of soot deposition through the decomposition of CO. However, to study this phase of the problem, it will be necessary to operate circulating systems under radiation. These could be operated after the out-of-pile studies have demonstrated desirable design and operating procedures. Data from the small-scale in-pile systems should also prove helpful in the design and operation of the projected large-scale in-pile loops.

---

[18] R. V. Moore and B. L. Goodlet, "The 1951–1953 Harwell Design Study," J. British Nuclear Energy Conf., 2, No. 2, 50 (April, 1957).

12.5.3 Large-Scale Out-of-Pile Loop Experiments: An important consideration in the selection of capsule materials for a helium-cooled graphite-moderated reactor is the type and amount of gases which are evolved from the graphite at the reactor operating temperatures. The gaseous impurities contained in graphite, as discussed previously, may result in carburization and/or oxidation of structural components. Further, since CO_2 will represent a large fraction of the impurities outgassed from the graphite, the back reaction of CO_2 to form soot may cause a serious problem in colder regions of the circulating helium stream.

Accordingly, engineering scale tests have been designed to determine the effects of the graphite and its impurities on structural and cladding materials under conditions simulating those of the proposed reactor. Graphite logs and blocks having dimensions comparable or equal to those in the reactor are utilized and exposures of the graphite and metal test specimens are made in an inert-gas atmosphere at elevated temperatures. The metal test pieces include those materials which have been considered for fuel element support structures and capsules.

Three types of experiments are planned. The first and simplest is a pot-type static-gas materials-compatibility test now underway in which random-size metal specimens and graphite blocks are assembled in a convenient structure and exposed to helium at 1400°F. The second is a refinement including a temperature differential, circulation of the helium by thermal convection and a complete fuel element assembly mock-up. This is now in fabrication and assembly. The third is a forced-convection test in which gas velocities and momentum will be matched to those of the reactor to simulate erosion effects by particles of graphite or other materials which may be carried by the high-velocity gas streams. A temperature differential equivalent to that for the reactor is to be maintained. This experiment is now in the design stage.

Gas samples will be removed periodically from each experiment to determine the amount and composition of impurities. Initial test periods will be short (1000 hr) to determine the magnitude of the problems. If a need is indicated, much longer test periods will be considered for later experiments. A 1400°F temperature has been chosen for the initial tests since this approximates the hot-spot temperatures for the reactor.

Later tests may be run at other temperatures, if necessary. The tests are to be conducted at a nominal pressure of 30 psig for convenience. Argon will be used instead of helium in the forced-convection erosion test to provide an equivalent density since this will affect the erosion characteristics.

A quantity of TSF graphite having a known history has been obtained for the initial experiments. Later tests may include types GBF and AGOT, if warranted by the over-all program. Extreme care is exercised in all graphite handling to minimize contamination and a record is maintained of all exposure to air during graphite fabrication and assembly of the experiments. Deliberate exposure to air may be made in later experiments to simulate reactor assembly conditions. Samples of all graphite used will be submitted for laboratory degassing and results will be correlated with data from experiments.

A primary objective of the test program is to determine the need, if any, for gas purification equipment for the reactor and, if required, the testing of its features and operation. The program can be extended to include such equipment, if necessary, and this could become a primary function of either or both the thermal-convection and forced-convection test units.

A. Static-Gas Materials - Compatability Test. An assembly of graphite blocks and test specimens for the pot test is shown in Fig. 12.13. As can be noted, the specimens are bound to the blocks so that approximately one-half of the surface of each is in contact with the graphite with the remainder exposed to the gas. The samples supported on the rack are included to determine corrosion effects for materials exposed only to the gas atmosphere. After arranging the graphite and samples inside the pot shown in Fig. 12.14, the top seal weld closure is made and the pot is purged with helium until the effluent gas has a total impurity composition less than 10 ppm.

Following the purge, the experiment is ready to proceed to elevated temperatures. First the gas pressure is reduced to 11.7 psia to accommodate expansion and achieve an ultimate pressure of 45 psia when hot. The pot is then heated at a rate of 50–100°F/hr to 500°F and held at that temperature for 100 hr. Gas samples are removed periodically for analysis during this period. The pot is next heated at the previous rate to 1400°F

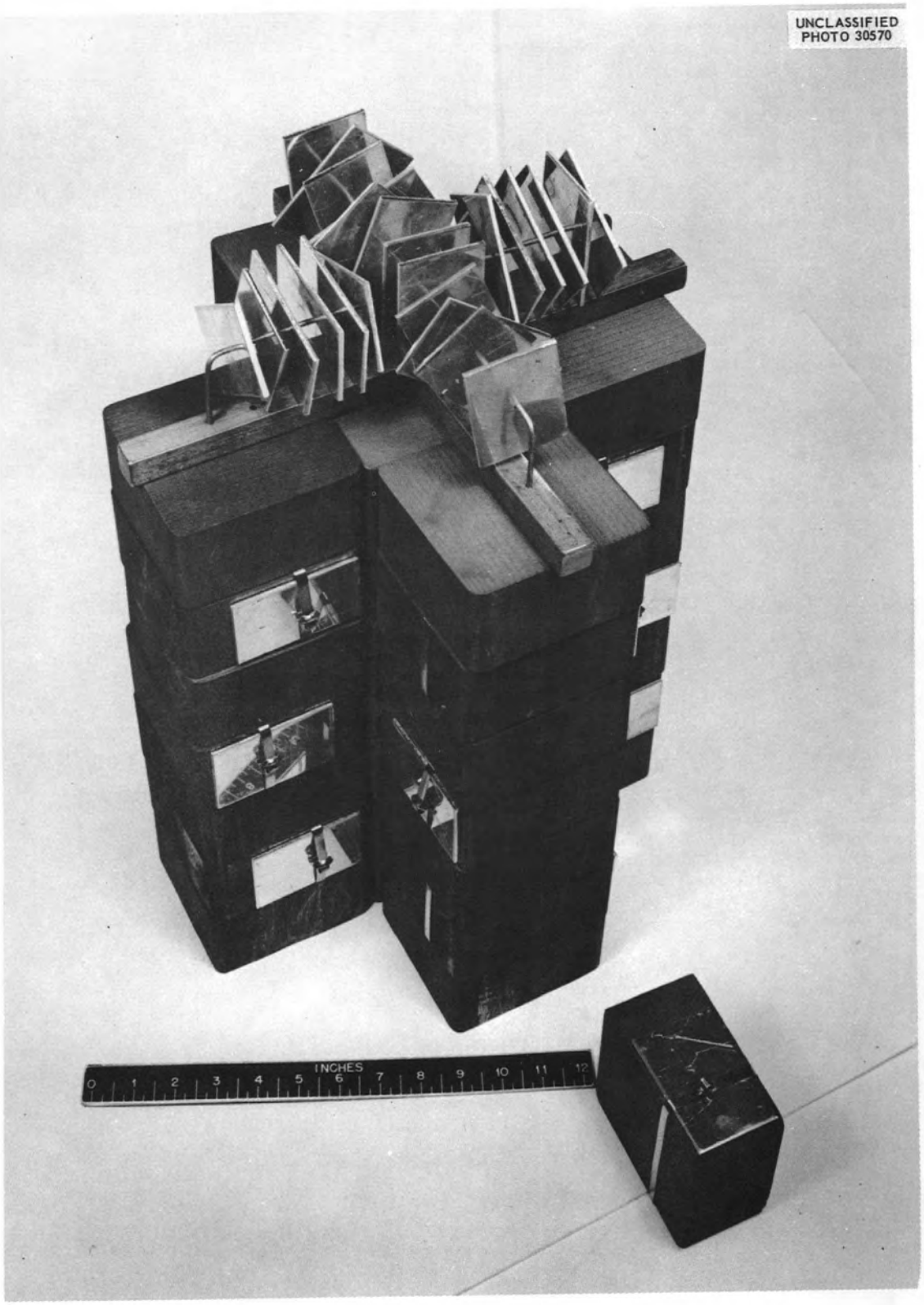

Fig. 12.13. Assembly of Graphite Blocks and Test Specimens for Static Test.

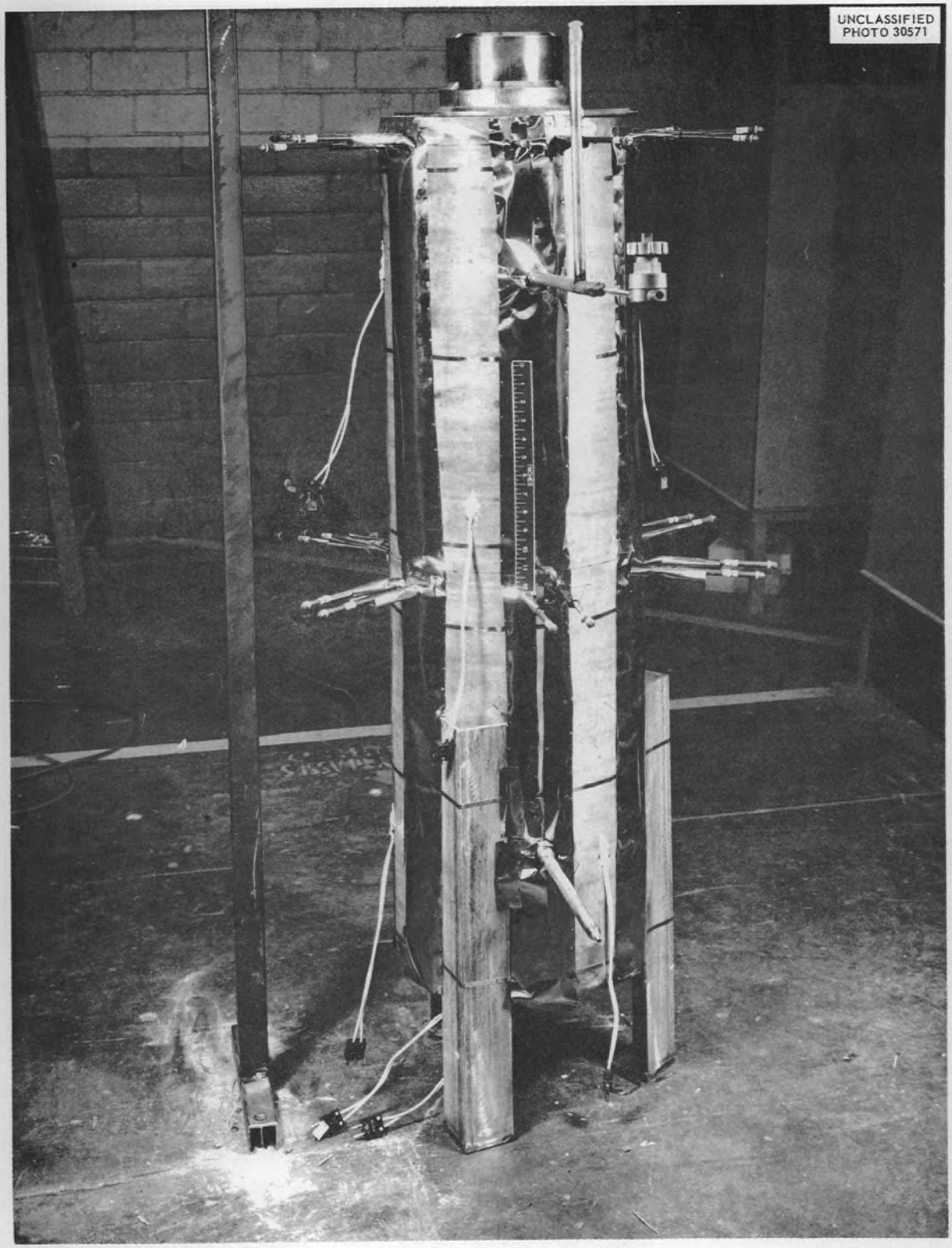

Fig. 12.14. Vessel for Static Compatibility Test.

and the temperature held constant for the duration of the experiment. Gas sampling is continued throughout the test period. After cooling, the vessel is opened and inspected; the samples and graphite are removed and examined.

The assembled equipment is shown in Fig. 12.15. This experiment was designed to provide engineering data prior to submission of this report and hence is somewhat rudimentary. Preliminary results from gas sampling indicate that no serious problems exist, but it is too early to draw conclusions regarding the need for gas purification equipment in a reactor installation.

B. Thermal-Convection Test. The thermal-convection loop design is shown schematically in Fig. 12.16. One fuel element passage is included in a graphite assembly having an 8 in. x 8 in. cross section. A uniform temperature of 1400°F will be maintained in the graphite to simplify evaluation of results and to provide a maximum head differential to motivate the thermal-convection flow. The side arm is to be cooled to a temperature of 500°F providing a maximum thermal driving force both for gas circulation and for mass transfer reactions while maintaining water, if it is present, in the vapor phase. A fuel element assembly is mocked up, as shown in the detail of Fig. 12.17, to simulate gravity-induced stresses and to provide the design load contact on the graphite. The heating and sampling schedule for this test is to be similar to that for the pot experiment. Two test facilities are being provided to accelerate the program. The relative simplicity of the thermal-convection test makes it particularly attractive for long-term test exposures if these are warranted.

C. Forced-Convection Test. Since relatively high gas velocities are employed to obtain good heat transfer in the reactor core, erosion of the graphite passages appears possible from action of suspended particles. It is proposed to evaluate this problem experimentally in a test facility of moderate size shown schematically in Fig. 12.18 and which is capable of achieving the reactor gas velocities. A portion of a single fuel element passage complete with a fuel element will be subjected to test. If appreciable erosion is observed in the test piece, side-stream filtering of the gas may be required for the reactor installation. Evaluation of equipment for this purpose will be conducted in this test stand.

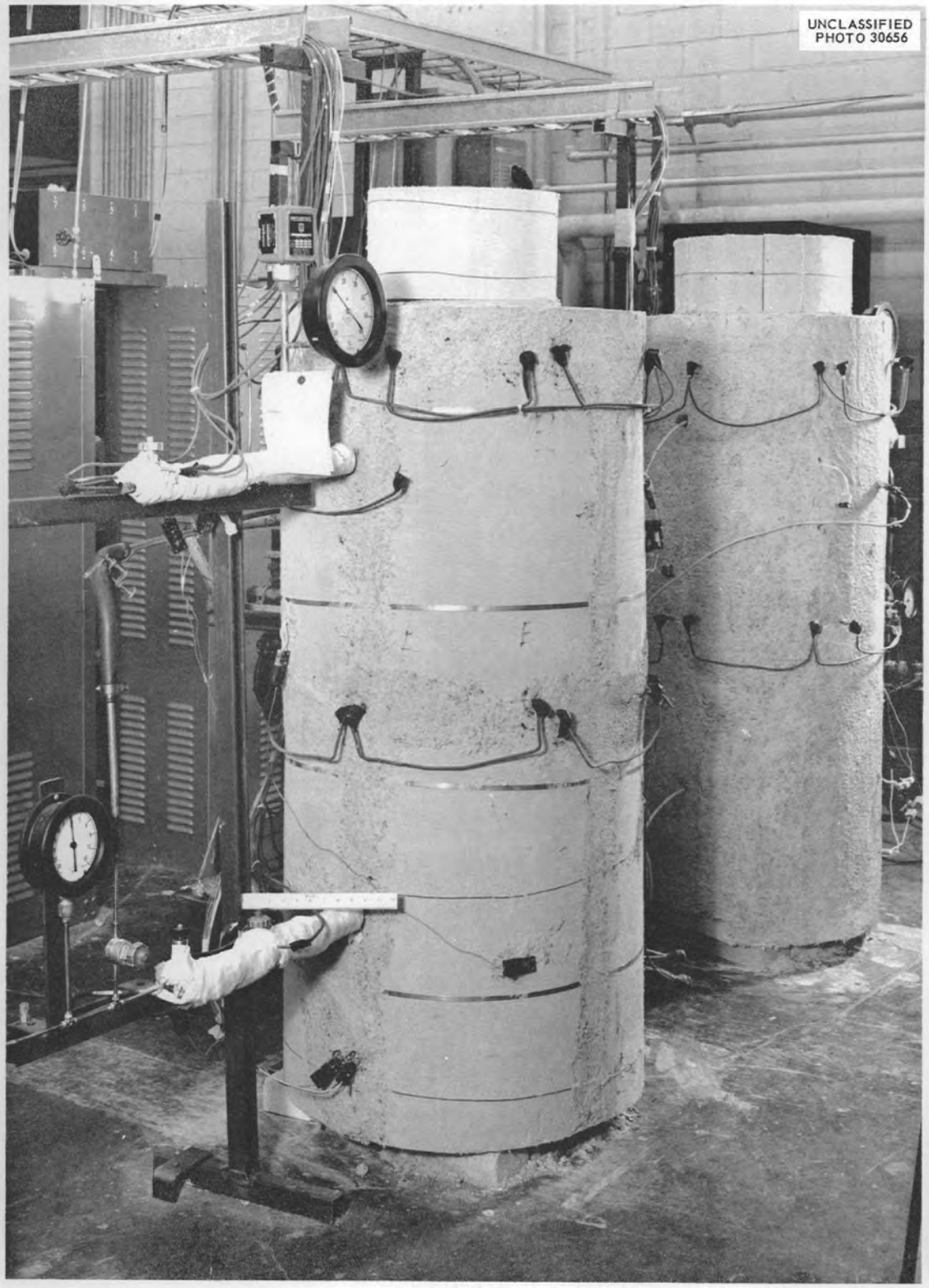

Fig. 12.15. GCR-2 Materials-Compatibility Tests Assembled and Ready to be Heated.

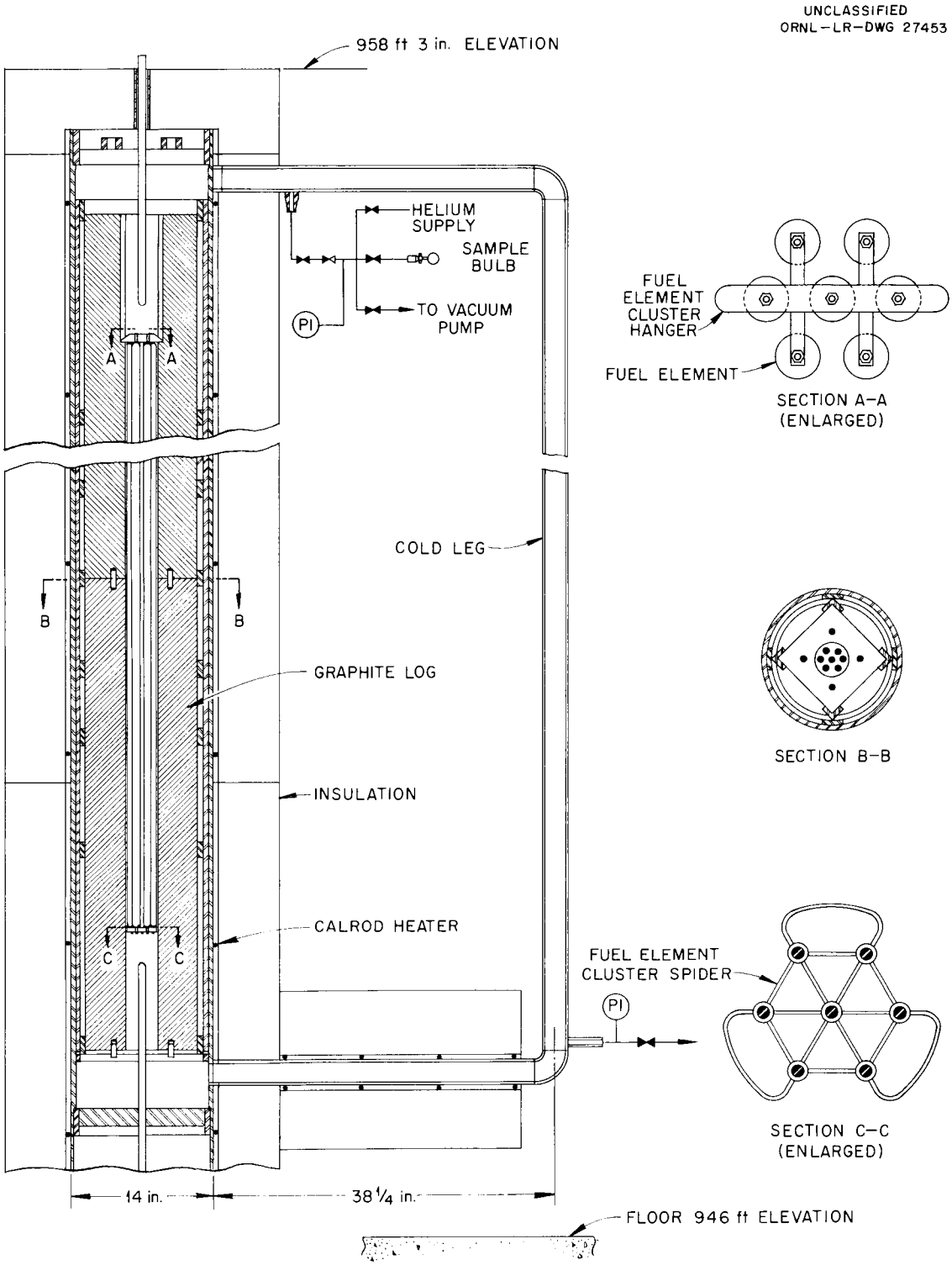

Fig. 12.16. GCR-2 Natural Convection Test.

UNCLASSIFIED
PHOTO 30660

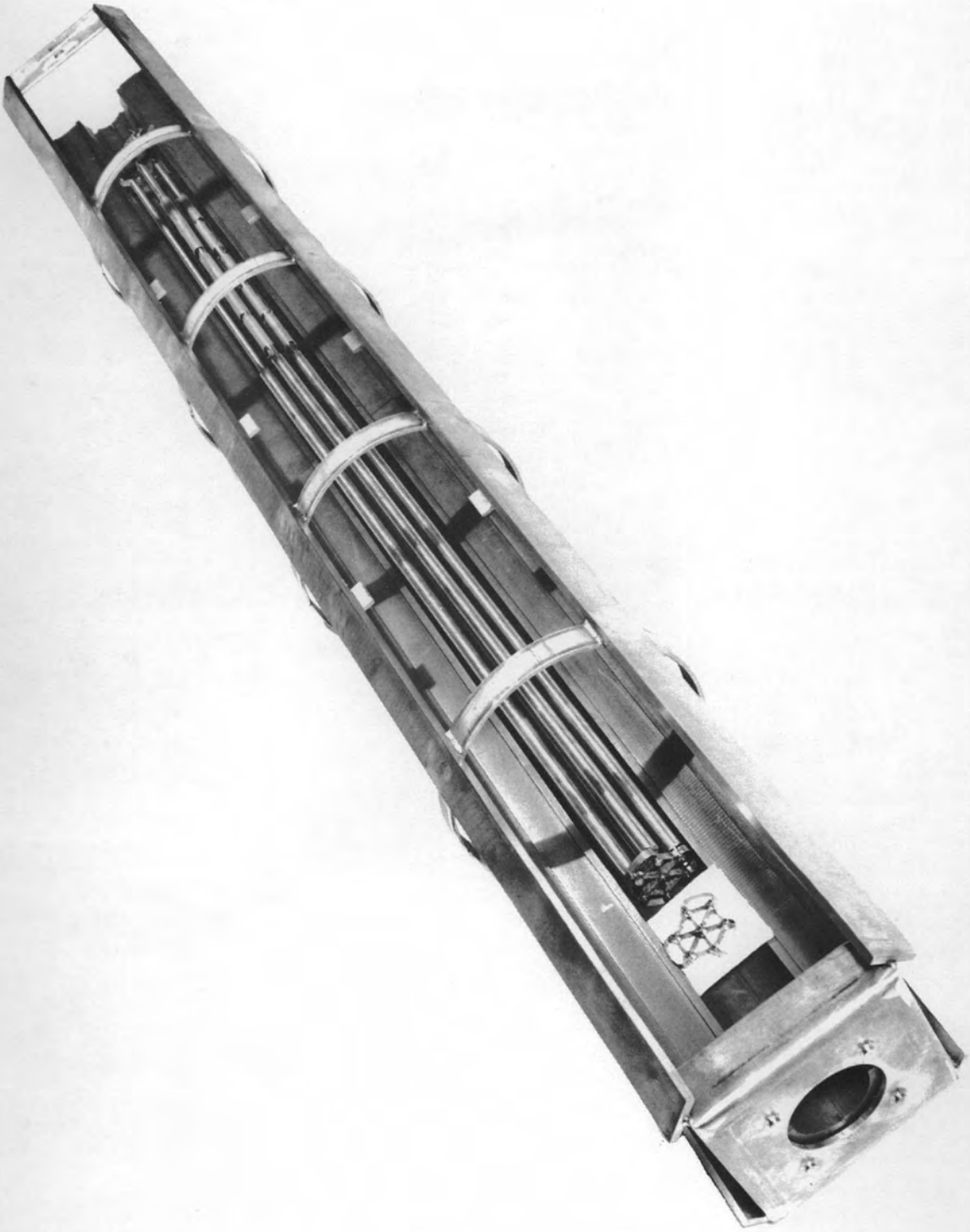

Fig. 12.17. GCR-2 Natural Convection Test Cutaway View Showing Mockup of Fuel Element Assembly in Graphite Block.

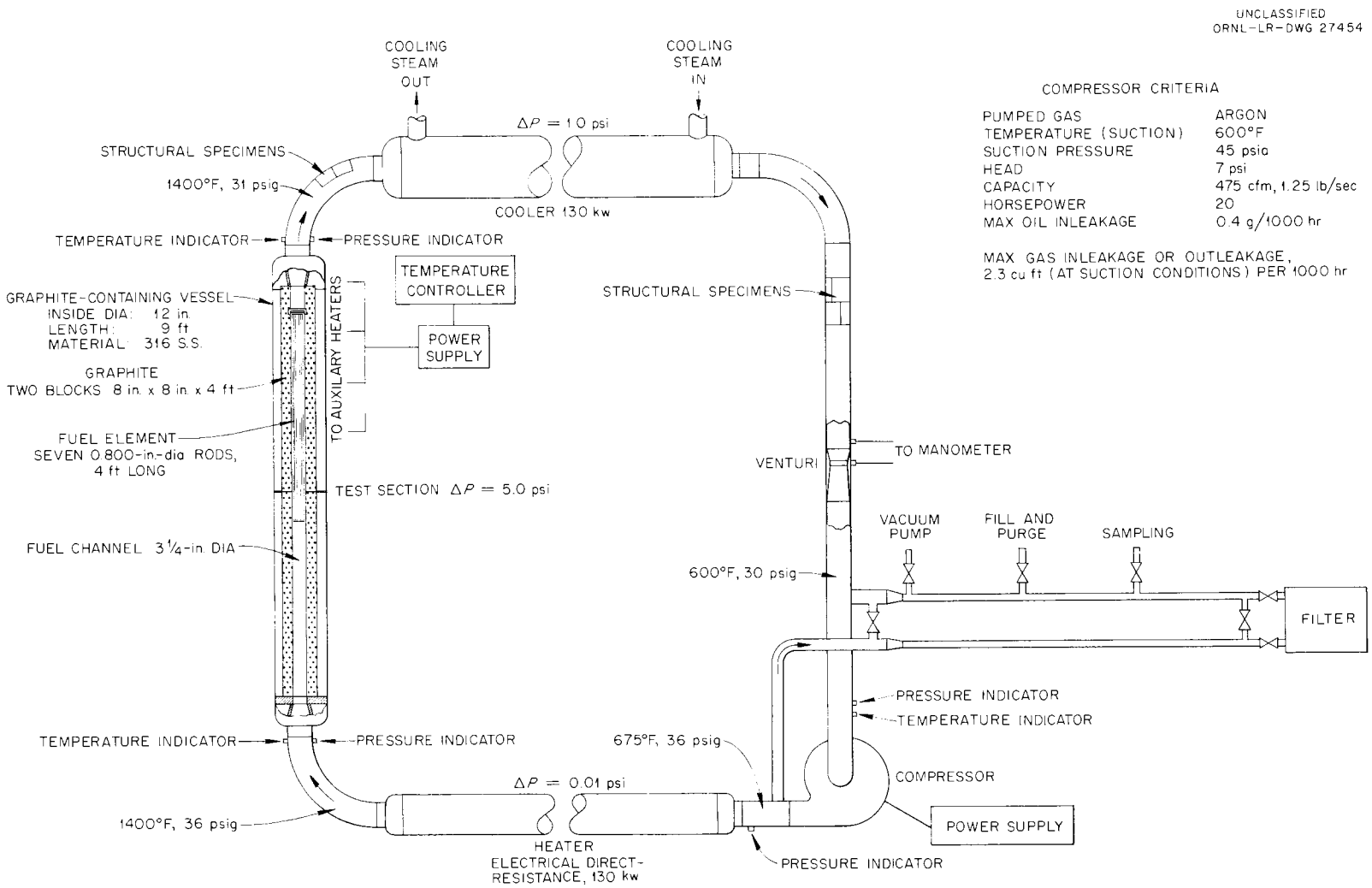

Fig. 12.18. GCR-2 Forced-Convection Loop.

Although the erosion effects can be observed in an isothermal system, no suitable circulator is available without extensive development to operate for extended periods at the maximum reactor temperature. Therefore, it seems expedient to design a system in which temperature differentials of the same magnitude are employed to permit the use of a low-temperature compressor (ca. 400–600°F suction temperature) of conventional design. This has the added advantage of introducing all of the materials-compatibility test conditions affecting the reactor except nuclear radiation in a single system. The disadvantages are in the heat transfer equipment needed and the increased energy requirements, about 130 kw.

Since this will be a relatively large test loop simulating several basic features of the reactor design, it should provide valuable experience on the retention and handling of helium in high-temperature equipment. Sampling for gaseous impurities will be conducted as a confirmation of results from the single static-pot and thermal-convection tests.

12.5.4 Large-Scale In-Pile Loop Tests: The previous experiments will supply data related to (1) the burnout rate of graphite by CO_2, (2) the decomposition of CO and resulting soot formation, and (3) the effect of radiation on the reactions of CO_2-CO-graphite. Variables such as temperature, partial pressures of CO and CO_2 and flow rates will be studied in these programs. However, it probably will be necessary to operate a large-scale in-pile loop under conditions simulating the GCR-2 to obtain all necessary data. The simulation of the graphite fuel channels and the type 304 stainless steel fuel elements can be effected only through a large-scale assembly and the radiation effects best determined by in-pile operation. Experience obtained from the other experimental programs will facilitate the design and operation of this large-scale in-pile loop test.

It is proposed that a large-scale loop be operated in the Oak Ridge Research Reactor. This loop will be designed to operate at a helium pressure of at least 300 psi and at temperatures up to 1300°F. Provision will be made for introducing contaminants such as CO_2, CO, and H_2O into the helium and for monitoring the helium for these contaminants. Temperature gradients, flow velocities and geometry will be such as to simulate the

proposed reactor. A graphite structure and fuel element assembly similar to that proposed for the GCR-2 will be incorporated in the loop. Fuel elements of type 304 stainless steel will be used.

Operation of such a loop will provide information on the rate of graphite burnout both from gas analyses and loss in weight of graphite specimens. The deposition of soot in the cooler regions of the loop will be studied as functions of CO concentration, temperature gradient, and flow velocity, establishing the conditions under which the deposition of soot might occur in the reactor. The rate and degree of contamination of the helium by gases evolved from the graphite will be measured. The effect of the contaminants in the helium on the type 304 stainless steel will be observed as will the compatibility of other materials with the contaminated helium. Finally, data will be obtained related to the steady-state condition in the loop which will prove helpful in predicting the steady-state conditions in the reactor.

12.6 Aerodynamic and Heat Transfer Tests

In the design of the GCR-2, it has been necessary to use heat transfer and pressure-drop data derived from experiments on geometries other than those herein conceived. It is believed that the correlations used are sufficient for such preliminary design. However, since optimization toward maximum heat transfer with minimum energy expenditure is of vital importance in a reactor intended for commercial power production, it becomes necessary to perform experiments on the proposed geometries both to check the validity of the original assumptions and to obtain the desired optimization. In addition, such data are needed to determine whether, due to flow maldistribution or fuel element misalignments, hot spots exist in a given design which could seriously shorten the reactor lifetime projected on the basis of nuclear considerations.

12.6.1 Pressure-Drop Studies: An experimental study will be made of the fluid friction characteristics of the fuel element intended for use in the GCR-2. This element (described in greater detail in Part 2, Section 4) consists of a central capsule surrounded by six symmetrically positioned capsules of similar design. In the reference design these elements consist of 3/4-in.-dia capsules with a ligament, or clearance between capsules,

of 0.402 in. The element is supported and positioned within the fuel channel by a hanger at the upper end of the 38-in.-long assembly. A spacer is used at the bottom of this assembly to eliminate vibration of the fuel capsules in the high velocity gas stream. The several facets of this pressure-drop study will cover the determination of the skin friction contribution to the over-all pressure drop, the effects of capsule misalignment and bending and the effect of varying the ligament. This information will be used in evaluating the experimental results of a pressure-drop study on a full-scale model of a flow channel embodying the final design configuration.

Figure 12.19 shows the experimental system constructed for the pressure-drop studies. Air rather than helium is used as the working fluid. Because of the low estimated pressure loss (of the order of 1 psi), a full-scale channel is being studied. The air flow is provided by a rotary positive-displacement blower manufactured by the Sutorbilt Corporation. This blower has a variable speed drive and can provide approximately 1000 cfm of air at 3 psig pressure. The air flows from the blower to a 30-ft^3 surge tank, and thence to the test section through a 9-ft run of 4-in. pipe containing an orifice for flow measurement. The test section is mounted vertically with flow upward through the unit. With this design, test sections can be quickly changed.

The test section for the determination of the skin friction loss was fabricated from a 3-1/4-in. ID aluminum tube having a 1/8-in. wall thickness. This tube contains a cluster of seven 3/4-in.-dia aluminum rods approximately 20 ft long supported at each end and aligned by three small spacers positioned at 5-ft intervals. The inlet support is located approximately 3 ft from the tube entrance to allow re-establishment of the velocity profile following the inlet elbow. Pressure taps are located 18 in. downstream from the cluster entrance and 5 in. before the exit. At each position six circumferentially spaced static taps are provided. For future experiments, these can be easily altered to allow the insertion of pitot tubes or hot wires for velocity traverses. Provisions have been embodied in the design of this flow channel to allow radial movement of the six circumferential rods to determine the effect of cluster geometry on the pressure drop. Also it will be possible to study the effects of fuel rod misalignment or warpage.

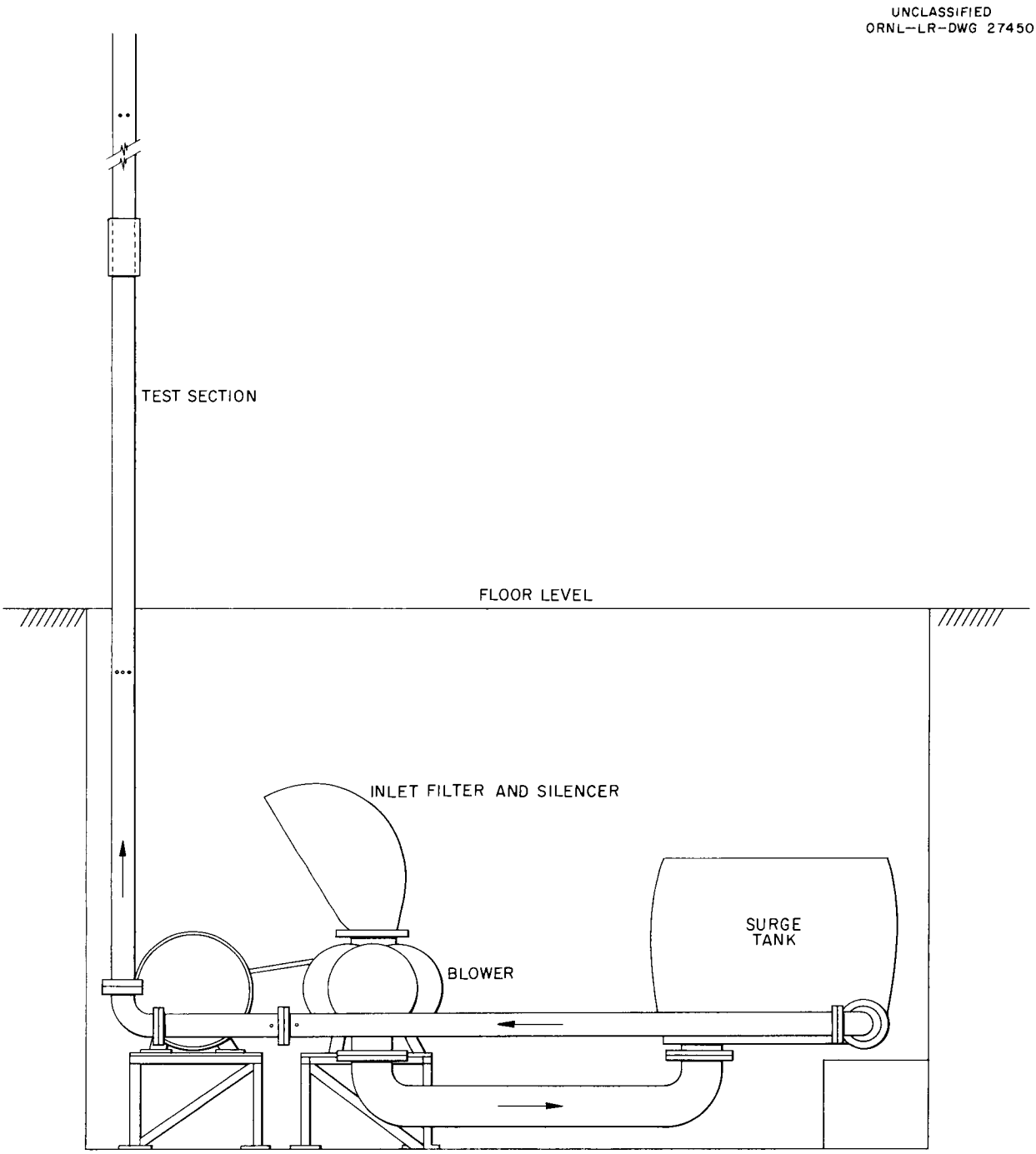

Fig. 12.19. Apparatus for GCR-2 Flow Studies.

Preliminary results obtained in this initial study are given in Fig. 12.20. The data lie approximately 5% above the correlation for flow within circular tubes over a Reynolds modulus range from 10,000 to 60,000.

12.6.2 Heat Transfer Studies: The experimental unit intended for the determination of the heat transfer characteristics of this type of system is currently being designed. The test loop will remain essentially unchanged with the new test section replacing the units used in the pressure-drop studies. A preheater may be installed between the orifice and the test section to obtain the desired inlet datum temperature. This preheater will probably consist of a stack of resistance-heated wire screens fitted into the inlet end of the test section. It will also be necessary to include a gas cooler at the exit end of the test section, or to use a closed loop, because of the large amounts of heated air involved.

Figure 12.21 shows a few details of a proposed test section. The unit is not drawn to scale and shows only one of the seven identical capsules of the fuel element. The test section will be heated by the passage of alternating current through the thin-walled stainless steel tube. The power will be distributed uniformly to the seven tubes through specially designed copper support brackets at the ends of the cluster. Heat generation in these electrodes should be negligible. The length of the heated section will be between two and four feet and will be dictated by the available electrical capacity and the maximum allowable tube surface temperature. It is hoped to approximate the anticipated heat generation of the reactor. Electric self-heating of the tube was chosen since it does lead to high volumetric heat generation and at the same time allows the use of a technique for accurate measurement of surface temperatures. A movable thermocouple will be inserted into the central region of the tube as is shown in Fig. 12.21. The thermocouple junction will be shielded and oriented such that it will view only a small area of the inside tube surface. With a small mass, the junction should rapidly reach thermal equilibrium with the viewed surface, and the surface temperature may then be calculated allowing for the heat generation in the tube. This thermocouple thus allows circumferential and axial traversing of tube surface temperatures. It will be necessary to use an insulating insert to reduce radiant heat transfer within each tube which would tend to

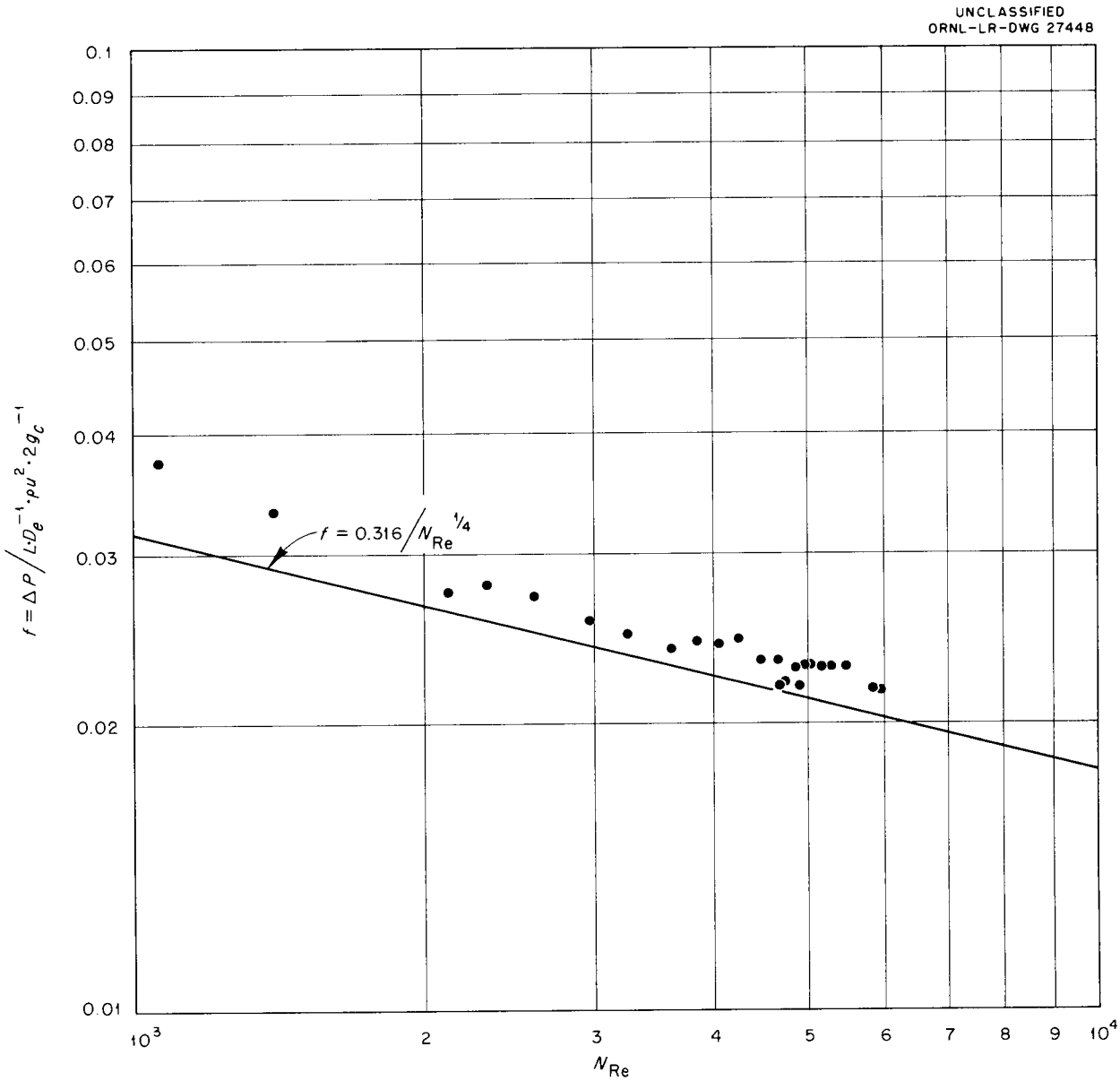

Fig. 12.20. Preliminary Experimental Friction Characteristics for ORNL Gas-Cooled Reactor Fuel Channel Without Spacers.

UNCLASSIFIED
ORNL-LR-DWG 27451

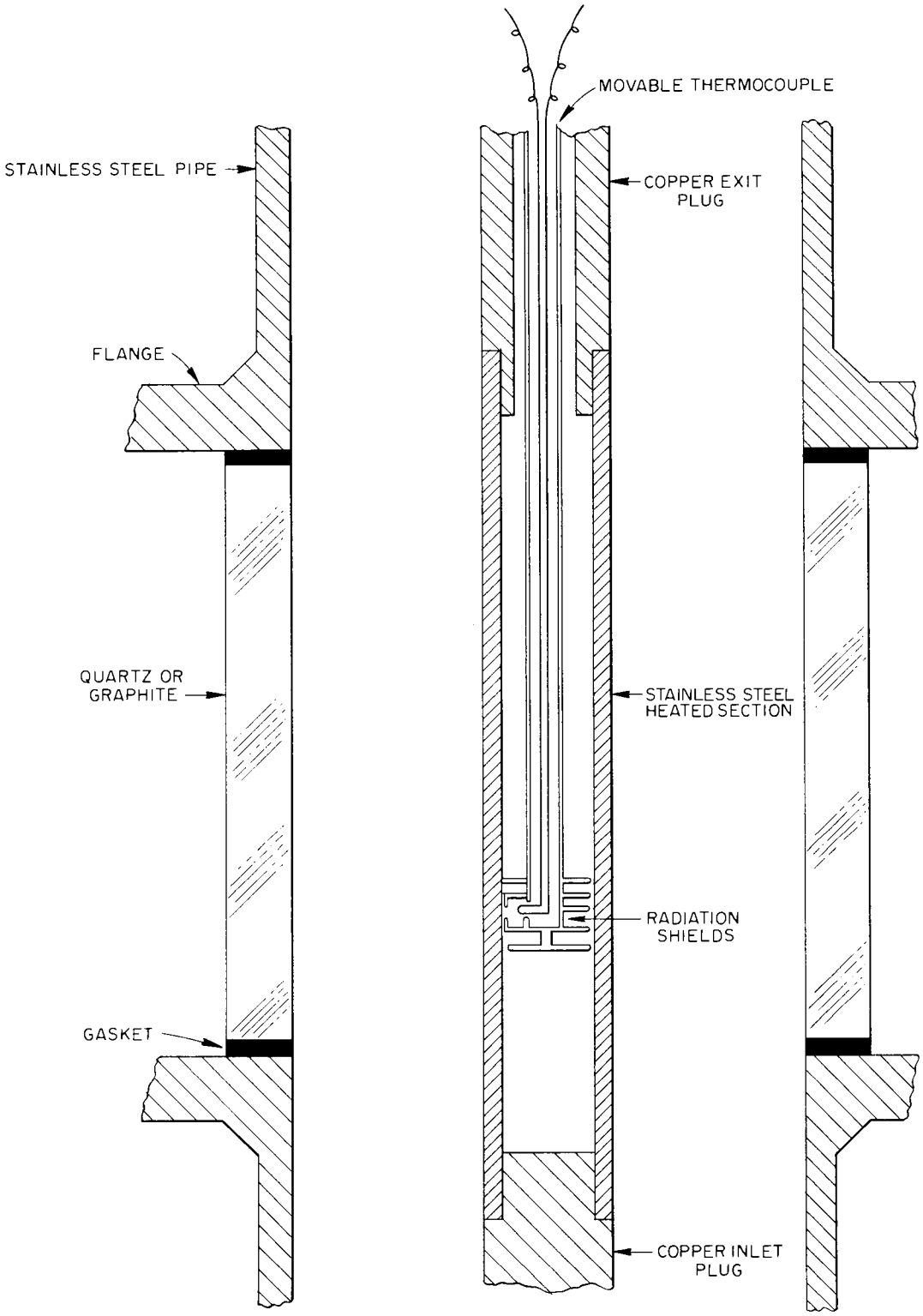

Fig. 12.21. Proposed Test Unit for GCR Heat-Transfer Studies.

alleviate hot spots caused by unequal flow distribution around the tubes.

Should unexpected difficulties arise in this measurement a second technique is being considered. For this purpose a quartz section is included in the flow channel shown in Fig. 12.21. It is proposed to make use of infra-red photography and/or optical methods to measure the outside-wall temperatures. This removable wall section will also allow the inclusion of a graphite channel to ascertain the effect of the difference in radiation emissivities between graphite and stainless steel on the heat transfer.

The effect of varying the ratio of the fuel capsule diameter to the channel diameter as well as varying the spacing of the peripheral ring of capsules will constitute further studies with this system. Also proposed are experiments to determine the effect of bowing or canting of the capsules on the heat transferred and on the surface temperatures. By proper design, it should be possible to produce the condition in which the heat generation is not equal in the seven capsules.

The possibility of designing a heat transfer section to include the fuel element hangers and spacers in order to study the surface temperature distribution in this region is being investigated.

12.6.3 Hydrodynamic Studies: If it is hoped to understand and eventually to predict the heat transfer in a proposed system in lieu of performing an almost endless series of experiments on specific geometries, detailed knowledge of the flow patterns in such systems is needed. It is not to be inferred that after a few relatively simple hydrodynamic experiments it will be possible to estimate with reasonable accuracy the heat transfer characteristics of all similar systems, since the solution to the problem involves not only quantitative data on the velocity distribution in the channel, but also knowledge of the heat and momentum eddy diffusivities. However, a better qualitative understanding of the heat transfer mechanism will enable a more intelligent choice of succeeding designs. Phosphorescent-particle, dye-injection, and hot-wire techniques will be used for studies of flow parallel to tubes as in the GCR-2 fuel element. In general, the test sections will be transparent plastic models, full-scale or larger, of the actual systems.

12.6.4 Finned-Tube Studies: Concurrent with the investigations for the GCR-2, heat transfer and pressure-drop studies of the Kaiser-ACF finned-tube fuel channel will be conducted. The specific fuel elements to be tested will be designed and fabricated by Kaiser-ACF for inclusion in the test loop. Provision can be made for operating with the proposed reactor fluid. The technique for heating the finned rods has not yet been specified. However, one feasible method involves centering a heating element, such as a Globar, within a finned tube. By proper choice of fin cross section-to-tube cross section ratio, it may even be possible to use resistance heating. The parameters to be studied include fin height-to-fin thickness ratios, fin pitch and perhaps fin cross section geometry, ratio of fin height to tube diameter and channel diameter, and the effect of noncentering or canting of the finned tube within the fuel channel.

12.7 Pressure Vessel

A failure of the GCR-2 pressure vessel obviously has alarming implications. It is evident that there is a need for some experimental work in the field of nuclear pressure vessel technology to supply a measure of insurance and confidence that such a failure will not occur.

In a number of areas pressure vessel technology is rather well developed. Some of this material has been surveyed in Part 2, Section 3. It is proposed that in those areas where outside work is already well advanced no experimental studies be performed by Oak Ridge National Laboratory, but merely that the outside work be closely followed. A suitable approach to such a goal would be to encourage, sponsor, and participate in the activities of the Pressure Vessel Research Committee of the Welding Research Council, whose studies to date have been of great use in the advancement of pressure vessel technology. In addition, such work as that of the Naval Research Laboratory on high-yield-strength steels should be followed.

The fields in which studies at the Oak Ridge National Laboratory will be most useful are radiation damage, welding and inspection. This work will effectively supplement the pressure vessel information which is received from outside the Laboratory.

12.7.1 Effects of Radiation on Mechanical Properties: Neutron irradiation is capable of causing embrittlement of pressure vessel steels and

welds. The magnitude and seriousness of the effects depend upon fast neutron dosage, the temperature of irradiation, and a number of poorly understood metallurgical variables. Fast neutron doses greater than 10^{18} nvt cause noticeable property changes; doses of 10^{19} nvt and greater may cause large and even unsafe property changes. A typical integrated, fast neutron dose for the GCR-2 reactor vessel should be 10^{18}–10^{19} nvt as shown by measurements on the Calder Hall Reactor.[19] The general effects of irradiation on pressure vessel steels are as follows:

1. The ductile-to-brittle transition temperature is increased.
2. The energy level at which nominally ductile fractures occur is reduced.
3. The deformation characteristics in the tensile tests are modified so that the uniform elongation tends to be rapidly reduced.

Figure 12.22 shows how the notch-impact results of a typical pressure vessel steel is changed by irradiation. Figure 12.23 illustrates the rapid decrease in uniform elongation with increased dose in a weld material.[20] The effects of irradiation may be reduced by exposure at elevated temperatures, although some properties may show greater changes at high, rather than low, irradiation temperatures. However, the temperature dependence of the radiation effects is not yet well understood. In addition, there appears to be a strong dependence of sensitivity to radiation effects on the structure and possibly the composition of steels.

Apparently, one of the materials that is most sensitive to deleterious irradiation effects is weld metal. It is only recently that studies on irradiated weld metals have begun, and it is imperative that a strong program be carried out for the GCR-2. This is particularly necessary because of the many variables in weld-metal composition and structure.

---

[19] T. J. Heal, Irradiation of Steels, IGR-TN/C-651 (August, 1957).

[20] R. G. Berggren and J. C. Wilson, Recent Data of the Effects of Neutron Irradiation on Structural Metals and Alloys, ORNL-CF-56-11-1 (January 30, 1957).

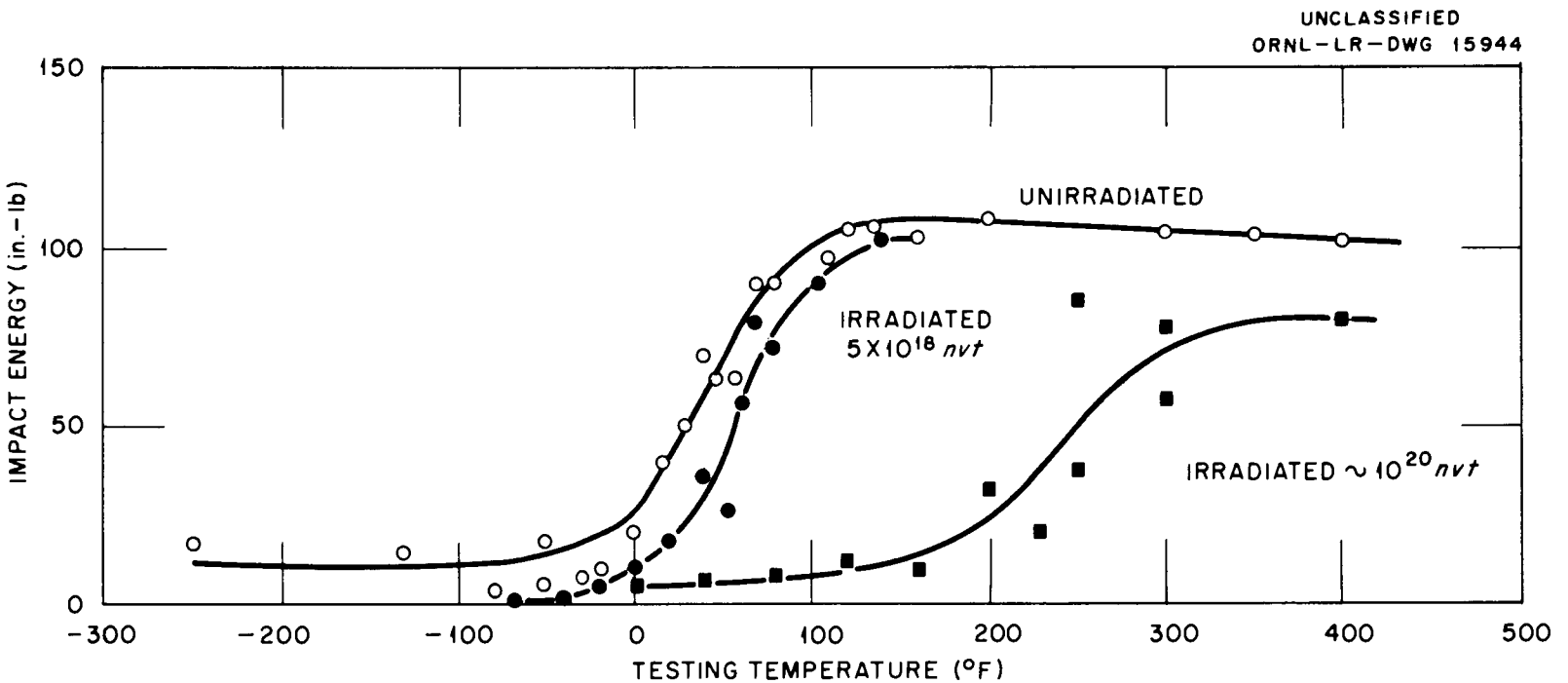

Fig. 12.22. The Effect of Fast Neutron Irradiation on the Notch-Impact Properties of a Carbon Steel.

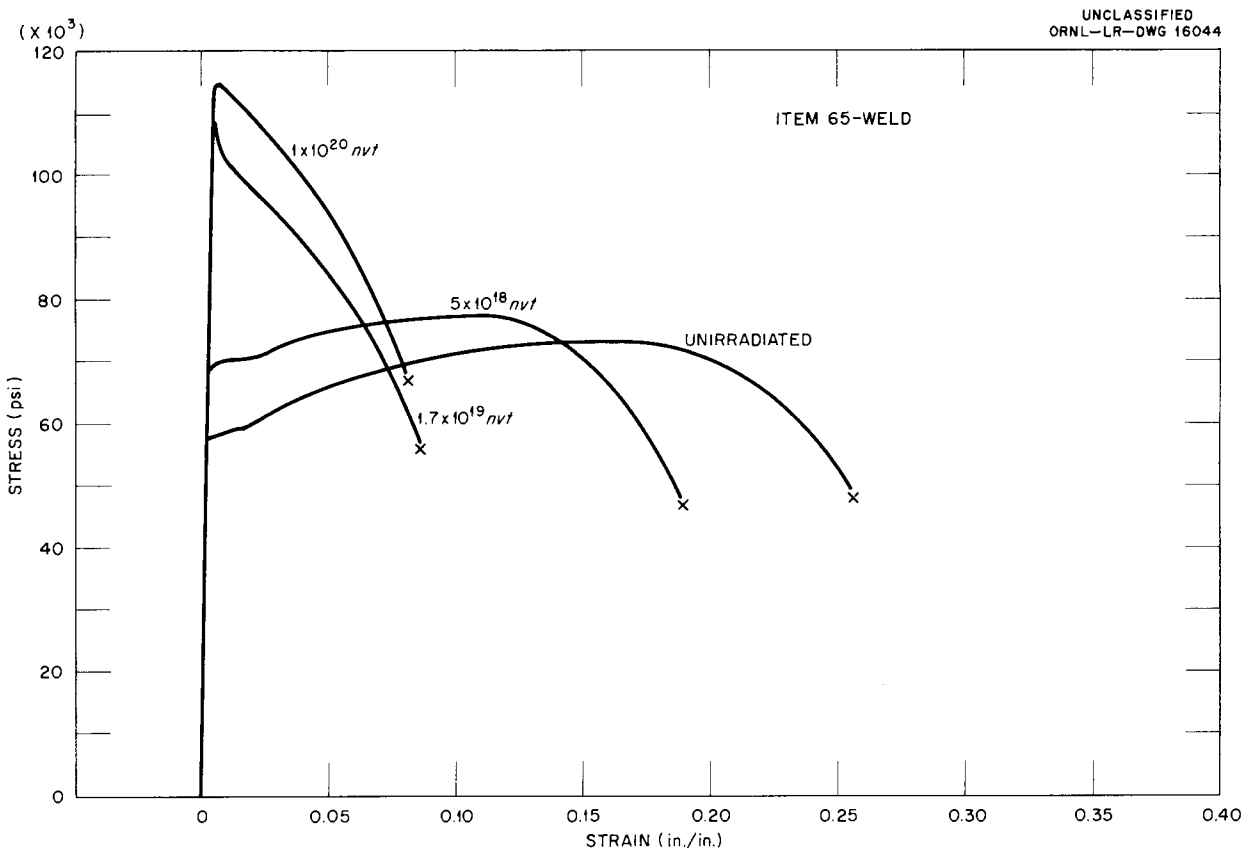

Fig. 12.23. The Effect of Irradiation on Tensile Properties of Weld Metal Deposited from an E7016 Electrode.

Specifically, the GCR-2 back-up program will include the following investigations.

1. Samples of typical weld metals deposited by procedures duplicating the welds that would be used in the pressure vessel will be irradiated, and notch-impact and tensile data will be obtained.
2. Mechanical properties of the irradiated metals will be determined as a function of such variables as: dose rate, effect of stress during irradiation, the effect of irradiation temperature in the range in which the GCR-2 will operate, and orientation of the specimens with respect to the principal weld directions.
3. The effect of mechanical test variables such as strain rate, specimen geometry, and state of stress will be investigated.
4. Wrought metals of the types that have shown the most resistance to deleterious radiation effects will be retested, where necessary, under the temperature and flux conditions expected in the GCR-2.

This program will yield data on the most suitable material presently available and the conditions for fabrication of the GCR-2 pressure vessel. Investigations for more-advanced reactors would require additional studies in order to evaluate more economically desirable, but less familiar, materials of higher strength.

12.7.2 Welding Studies: A considerable amount of data on the welding and weldability of pressure vessel steels are presently available. Satisfactory welding procedures have necessarily been developed for all the materials now used for pressure vessel construction. An experimental program in welding for the GCR-2 as conducted at the Oak Ridge National Laboratory will serve two functions: it will evaluate and, if possible, refine existing welding procedures, and it will supply the carefully controlled specimens required by the radiation-damage and inspection programs.

The studies of welding procedure will help to insure, as actual reactor construction progresses, adherence to the usual high standards of quality required in nuclear equipment. Since the existing welding procedures were, for the most part, developed for non-nuclear service, it would seem to be desirable that active evaluation and improvement of these procedures be undertaken.

The need for carefully structure-controlled weld metal for the radiation-damage program has been discussed above. It is equally necessary that specimens for the inspection work be made under closely monitored conditions. Thus, an integral part of the welding program will be the production of the specimens required for the related efforts.

The welding investigations will include:

1. An evaluation, under Code requirements, of the existing welding procedures for the GCR-2 pressure vessel material.
2. A determination of the limitations, and their possible consequences, of existing procedures.
3. An analysis of suitable modifications designed to overcome the limitations of the existing welding procedures.
4. The production, under specified conditions, of all specimens required in the radiation damage and inspection studies.

In the welding-procedure studies, the data will be evaluated under all the requirements of the ASME Boiler Code, as a minimum test of acceptability. In addition, further tests which appear to be suitable may be applied.

12.7.3 Inspection Methods: Since the pressure vessel welds of the GCR-2 will be made in carbon steel, it is safe to assume that standard techniques of inspection with both radiography and ultrasound can be used. The quality of either inspection method is dependent to some extent upon the configuration of the weld bead. A minimum of push-through and a minimum of cover bead are desirable for both radiographic and ultrasonic inspection. If excessive penetration or excessive cover beads are encountered, ultrasonic inspection is nearly ruled out; these poor welding practices also seriously detract from an acceptable radiographic inspection. It is expected that the plain-carbon steel welds will have reasonably good ultrasonic transmission characteristics. However, should poorly sound-conducting welds be encountered, minor changes in the welding practice may be necessary to produce welds inspectable by ultrasonic methods.

It is recommended that all welds accessible to both radiography and ultrasound be inspected by both means. The use of the two methods is not a repetition, but rather, each approach has its own unique ability to locate a particular type of defect. Joint design and accessibility of the weld may

at times rule out one method or the other; however, the technique that is suitable for the specific problem should then be used for that joint.

Since the ability to employ a given inspection procedure is very dependent upon joint design, a careful study of the design details of the GCR-2 vessel should be made at the earliest opportunity. All joints which will impose inspection difficulties should be sought out. It is possible that some of these joints may be redesigned to permit easy inspection. Those joints which remain non-inspectable by ordinary techniques will supply the incentive for the development of special methods of inspection.

It is felt that the attainment of inspection procedures for the "difficult" joints will comprise the bulk of the experimental work on the inspection program. Some minor amount of effort may be necessary to proof test the routine inspection methods under normal conditions of joint geometry. In addition, where not already available, complete determinations will be made of all of the intrinsic limitations of a given inspection technique.

12.8 Other Reactor Material Components

12.8.1 Shielding Materials: Pyrex glass sheet is considered to be the optimum choice of neutron absorber for the boron curtain, but its suitability for use at the required temperatures must be demonstrated. Prior work has indicated that little damage occurs, except as a result of much larger exposures. However, most previous work has been carried out at lower temperatures and at higher flux levels. Exposure at design temperatures will be likely to cause significant dimensional changes, but may also produce annealing effects.

A number of radiation tests will be performed at the design temperature of 500°F. Damage will be accelerated by flux levels somewhat higher than the reference design. Samples will be exposed to integrated flux levels both equal to and considerably greater than the reference design specifications. Further testing will be performed at temperaturesup to 700°F, since the temperature of parts of the shield may be much higher than the return coolant gas. These tests will be accompanied by bench tests to determine the maximum useful temperature of the pyrex sheet for dimensional stability in the absence of radiation.

Data from these experiments will define the extent of dimensional changes and fragmentation taking place at various flux and temperature levels, and will show the effect of temperature in annealing and restricting the radiation damage.

12.8.2 Control Rod: The basic compatibility of the stainless steel-clad silver control rod is quite well established. At the design temperature of 1100°F there is virtually no solubility of one constituent in the other, and impurities in the gas coolant should have little effect. However, the dimensional and thermal stability of such control rods must be demonstrated.

Silver-base alloy control rods have been under development at other laboratories for some time, but only for use in pressurized water-cooled reactors. The use of pure silver with steel cladding for support has not been attempted, but should prove satisfactory if suitable for control.

Prototype control rods one-half or one-third of final size will be fabricated and tested over many thermal cycles near the design temperature. Rods will be fabricated both with and without an inner cladding of steel, and will be cycled in and out of a furnace held at the maximum reference design temperature, or through cycles much more severe than during the proposed operation.

Data from these experiments should serve to evaluate the chosen type of control rods, and particularly the relative advantages of using an annulus of silver between an inner and outer steel cladding.

12.8.3 Ductwork: In essence, the ductwork for the coolant gas comprises an extension of the pressure vessel. As such, the same requirements for integrity of the pressure vessel must be maintained for the ductwork. There are certain questions associated with the ductwork which should be investigated by a suitable experimental program in order that the reactor construction may proceed with confidence.

The existing welding problems have arisen as a result of necessary reactor design. These problems are associated with the dissimilar-metal joints which must be made in the ductwork system. Such joints will be between the SA-387 (Cr-Mo) steel ducts and the SA-212B pressure vessel, the ducts and the austenitic stainless steel bellows, and the ducts and the Cr-Mo steel heat exchangers.

The most pertinent difficulties attendant to the dissimilar-metal joints discussed above result from the large differences in thermal expansion and conductivity which are significant when thermal cycles are involved. Other investigators[21, 22, 23, 24, 25] have reported a number of transition materials and welding procedures which appear satisfactory. The more recent studies involve the use of nickel-base electrodes such as Inconel BP-65 as transition weld deposits which have coefficients of expansion intermediate between the chromium-molybdenum steels and the austenitic stainless. This technique appears to be more satisfactory than that of using austenitic stainless steel weld deposits.[26, 27]

The experimental studies should include an evaluation of the existing techniques for dissimilar-metal welding in light of the requirements of the GCR-2. Where the limitations of the processes appear to be detrimental, more advanced and reliable methods must be developed. Where the stress pattern of the reactor includes a predictable number of thermal cycles, the stability of the dissimilar-metal joints must be evaluated by a testing program which suitably simulates service conditions.

---

[21] J. T. Tucker, Jr. and F. Eberle, "Development of Ferritic-Austenitic Weld Joint for Steam Plant Application," The Welding Journal, 34, No. 11, 529s (November, 1956).

[22] R. U. Blaser, F. Eberle, and J. T. Tucker, Jr., "Welds Between Dissimilar Alloys in Full-Size Steam Piping," Proc. ASTM, 50, 789 (1950).

[23] H. Weisberg, "Cyclic Heating Test of Main Steam Piping Joints-Between Ferritic and Austenitic Steels--Sewaren Generating Station," Trans. ASME, 71, 643 (1949).

[24] W. C. Stewart and W. G. Schrietz, "Thermal Shock and Other Comparison Tests of Austenitic and Ferritic Steels for Main Steam Piping," Trans. ASME, 72, 1043 (1950).

[25] O. R. Carpenter et al., "Some Considerations in the Joining of Dissimilar Metals for High-Temperature, High-Pressure Service," Proc. ASTM, 50, 809 (1950).

[26] H. Weisberg, loc. cit.

[27] W. C. Stewart and W. G. Schrietz, loc. cit.

Since the ductwork will be operating in two gaseous environments, its behavior in both environments must be studied. The gas inside the ducts will be the hot helium coolant, and the contaminants contained in it may have a deleterious effect on the properties of the material. The outer surfaces of the ductwork will operate in air; thus, the long-time oxidation behavior of the materials must be determined at the temperatures of interest.

An experimental program on the ductwork for the GCR-2 will include the following:

1. Evaluation of existing methods for making dissimilar-metal joints, and a determination of the limitations of these methods.
2. Development of ways to overcome the above limitations if they prove to be harmful.
3. A study of the effects which cyclic thermal stresses have on the life of the joints when superimposed on the residual welding stresses, pressure stresses, and thermal-gradient stresses.
4. A determination of the effects of stress on the behavior of the material in its two gaseous environments.
5. Investigation of the effects of carbon migration from the carbon steel into the austenitic material.

SECTION 13

HAZARDS

13. HAZARDS

CONTENTS

13.1 Introduction.....13.1

13.2 Contamination in the Gas Stream of the GCR-2.....13.3

13.2.1 Neutron Activation of the Helium.....13.9

13.2.2 Activation of the Impurities in the Helium.....13.11

13.2.3 Recoils from Fuel Capsule Wall.....13.12

13.2.4 Corrosion and Erosion.....13.14

13.2.5 Activation of Occluded Gases Emanating from the Graphite.....13.16

13.2.6 Occluded Gas from Metals.....13.17

13.2.7 Residual Gases after Helium Filling.....13.17

13.2.8 Surface Contamination of Fuel Capsule Wall.....13.19

13.2.9 Diffusion through Fuel Capsule Wall.....13.19

13.2.10 Leak through Defect in Fuel Capsule Wall.....13.20

13.3 Release of Fission Gases in the Fuel Capsule.....13.22

13.4 Shutdown Activity and Dose Calculations.....13.28

13.4.1 Activity in Coolant after Shutdown.....13.28

13.4.2 Radiation Level Outside Steam Generator.....13.31

13.4.3 Activity in a Single Fuel Element.....13.39

13.4.4 Shielding Required by Fuel Charging Machine.....13.43

13.4.5 Water Level in Fuel Storage Pond.....13.44

13.5 Removal of Afterheat.....13.45

13.5.1 Shutdown Heat Generation.....13.47

13.5.2 Position of Steam Generators Relative to Reactor.....13.48

13.5.3 Removal of Afterheat by Radiation.....13.48

13.5.4 Removal of Afterheat by Convective Circulation.....13.53

13.5.5 Afterheat Removal with Ruptured Pressure Vessel.....13.59

13.6 Nuclear Excursion.....13.61

13.6.1 Fuel Addition.....13.63

13.6.2 Start-up Accident.....13.63

13.6.3 Continuous Rod Withdrawal at Power.....13.66

13.6.4 Reactivity Addition from Steam Leak..... 13.67
13.6.5 Cold Coolant Accident..... 13.67
13.7 Containment of Radioactivity..... 13.68
13.7.1 Containment Provisions..... 13.69
13.7.2 Rupture of the Pressure Vessel..... 13.69
13.7.3 Discussion of Additional Containment..... 13.72
13.8 Release of Radioactivity..... 13.77
13.8.1 Discharge of Activity up Stack..... 13.77
13.8.2 Emergency Discharge of Activity up Stack (Case 3)..... 13.85
13.8.3 Gas Leakage in the Reactor System..... 13.90
13.8.4 Activity in Building in Event of Pressure Vessel Rupture..... 13.92
13.8.5 Dose From Cold Cloud Following Pressure Vessel Rupture..... 13.94
13.9 Potential Energy of the Graphite..... 13.95
13.9.1 Oxidation of the Graphite..... 13.97
13.9.2 Irradiation Effects on Graphite..... 13.98

13. HAZARDS

13.1 Introduction

The potential hazards associated with the Gas-Cooled Reactor depend upon the containment provided by the system and the probability of incidents which would violate this containment. The GCR-2 is basically safe in that the design of the plant inherently provides: (1) good containment, (2) a stable, temperature-resistant fuel element, (3) a low probability for a nuclear excursion of any kind, and (4) the materials in the system are relatively inert chemically so that there is no strong tendency for them to react with each other or with air.

Containment is afforded both by the fuel capsule wall and the pressurized helium system. Although both of these containers can and will leak to some extent during normal operation, it is shown below that provision has been made for these leaks, and that the rupture of one of the containers without the concurrent rupture of the other will not result in a disaster. Nor is it likely that the failure of one will cause a failure in the other. Thus, it appears that an additional containment vessel is not required.

A type of accident that might prove hazardous is the loss of coolant and/or coolant flow. For this reason, it was considered mandatory that the system be so designed that the afterheat could be removed in spite of a complete electrical power failure. This in turn meant that the heat removal must be accomplished by radiation and thermal convection, assisted by the heat capacity of the graphite. Thermal radiation, together with emission of gamma energy to the graphite, results in the transmission of the bulk of the afterheat to the graphite which, because of its large heat storage capacity, rises only slowly in temperature. Calculations were performed both for the idealized case in which all of the heat is dissipated by radiation with no gas circulation, and for the case in which there is no thermal radiation and the heat from the reactor core is removed by thermal convection in the gas system. The analyses indicate that the loss of coolant or coolant flow does not constitute a serious hazard.

The kinetics of the power plant system, particularly of the reactor, have an important bearing on the hazards problem. As was discussed in Section 7 on Instrumentation and Controls, the reactor is inherently very stable and there exists no means of introducing large-step changes in reactivity. While an abrupt loss of electrical load may occur, this is a common problem in steam power plant practice and is ordinarily handled by using desuperheaters and condensers to absorb the bulk of the load while the initial peak may be taken care of in part by "blowing off" steam. Adequate feed-water storage is provided to take care of such contingencies.

The reactor temperature coefficient is not large and is negative, and normal operation will not require that the reactor be placed on positive periods shorter than approximately 50 min. The various potential nuclear excursions have been examined and on the basis of the present analysis, it appears that all transients may be contained safely by leisurely operator action, automatic protective equipment or both. Analogue simulator studies on these transients have not been made but would not be expected to materially alter the approach outlined here. It appears that there is no serious hazard associated with the control of the reactor.

The radioactive material circulating through the external gas piping system represents an obvious hazard. While there are at least ten potential sources of contamination, only three are significant: (1) activation of the helium, (2) recoils from the fuel capsule wall, and (3) fuel capsule leaks. While the maximum total activity expected in the gas system from each of these sources is 67, 18, and 7 curies, respectively, the activity is diffused over a large volume; moreover, the helium activity is a low-energy beta so that the dose outside the heat exchanger during operation should be less than 3 mr/hr.

The most serious accident that could occur with the reactor is a rupture in the gas system pressure envelope. Perhaps the most likely spot for such a rupture to take place would be at one of the bellows connections designed to accommodate differential thermal expansion in the gas piping. Such a rupture would lead to a crack and a "blowdown". The principal hazard associated with such a rupture would be contamination of the atmosphere downwind of the building by the activity carried in the gas system. However,

the resulting total dose should not exceed 0.1 rem per leaking fuel capsule so that the accident would not become unduly hazardous unless a large number of fuel capsules leak or melt. In view of the improbability of a nuclear excursion and the provisions for the removal of afterheat, it will be shown that there appears to be no mechanism available that will raise the fuel capsule temperature above 2000°F.

The amount of energy that might be released from various components of the system is presented in Table 13.1. Rather large quantities of energy are involved but, as will be shown, because of the large thermal capacity of the system,none of these sources appears capable of causing a serious accident for which additional containment need be provided.

13.2 Contamination in the Gas Stream of the GCR-2

The gas stream of the GCR-2 may become contaminated by any one of the following ten processes:

A. Continuous Sources of Activation Contamination
   - 13.2.1 Helium
   - 13.2.2 Impurities in helium
   - 13.2.3 Recoils from fuel capsule wall
   - 13.2.4 Corrosion and erosion

B. Temporary Sources of Activation Contamination
   - 13.2.5 Occluded gases from graphite
   - 13.2.6 Occluded gases from metal
   - 13.2.7 Residual gases after helium filling

C. Fission Product Contamination
   - 13.2.8 Surface contamination of fuel capsule wall
   - 13.2.9 Diffusion through fuel capsule wall
   - 13.2.10 Leak through defect in fuel capsule wall

Contamination from each of these sources has been examined in terms of the total activity at equilibrium (or the maximum for the case of temporary sources) released to the gas stream under the GCR-2 design operating conditions and the contribution of each is listed in Table 13.2 and presented graphically in Fig. 13.1. A more detailed discussion and analysis is presented under each subheading. Supporting calculations for all but 13.2.4, 13.2.6 and 13.2.7 are also available.[1]

[1] Wm. B. Cottrell and H. N. Culver, Contamination in the Gas Stream of the GCR-2, CF 58-1-119 (January 2, 1958).

TABLE 13.1

VARIOUS ENERGIES IN GCR-2 SYSTEM

	Btu
Fission product heat during first two hours after shutdown	5.8×10^7
Equilibrium irradiation energy in graphite which will be released by a 1000°C anneal	1.8×10^6
Total irradiation energy in graphite after 20 yr exposure*	
Heat released in two hours oxidation of the graphite	$< 2.2 \times 10^4$
Total energy in helium expanded and cooled to atmospheric conditions	8.0×10^6
Internal energy available in helium**	4.86×10^6
Total energy in water and steam expanded and cooled to atmospheric condition	1.1×10^7
Energy available from "flashing" water in steam generators†	7.25×10^5
Thermal energy in graphite above 75°F	5.1×10^8
Thermal energy in steam generator metal above 75°F	1.6×10^8
Thermal energy in pressure vessel metal above 75°F	7.6×10^8

*This energy is of the same order of magnitude as most of the energies listed but there is no apparent mechanism to release it.

**Isentropic expansion to STP (Standard Temperature and Pressure).

†Isentropic expansion to atmospheric pressure of steam evolved (steam assumed to remain as a vapor).

TABLE 13.2. CONTAMINATION IN GCR-2 GAS STREAM

Source of Activity	Nuclear Process	Half Life	Beta Activity[a] Emissions per Disintegration (%)	Beta Activity[a] Energy (Mev)	Gamma Activity Emissions per Disintegration (%)	Gamma Activity Energy (Mev)	Total Curies in System (max)[b] $\alpha = 0$, $\delta = 0$	$\alpha = 0$, $\delta = 0.1$	$\alpha = 0$, $\delta = 0.5$	$\alpha = 1 \times 10^{-5}$, $\delta = <0.5$	Remarks
Helium activation	$He^3(n,p)H^3$	12.26y	100	0.0180			79,500	5730	1212	67.5	Beta active only
Impurities in helium	$H^2(n,\gamma)H^3$	12.26y	100	0.0180			3.12×10^{-5}	2.19×10^{-6}	4.85×10^{-7}	2.66×10^{-8}	Argon and neon cannot be removed by filters: both are beta and gamma emitters; other activities insignificant, assuming filter
	$N^{14}(n,p)C^{14}$	5580y	100	0.1561			5.69	9.4×10^{-4}	1.94×10^{-4}	1.06×10^{-5}	
	$A^{40}(n,\gamma)A^{41}$	1.82h	99.1	1.20	99.1	1.30					
			0.9	2.50			0.119	0.119	0.119	**0.119**	
	$Ne^{22}(n,\gamma)Ne^{23}$	40s	93	4.21	7	3.0					
			7	1.18			0.1397	0.1397	0.1397	**0.1397**	
	$O^{18}(n,\gamma)O^{19}$	29s	70	2.9	70	1.6					
			30	4.5			1.08×10^{-6}	1.08×10^{-6}	1.08×10^{-6}	1.08×10^{-6}	
	$O^{16}(n,p)N^{16}$	7.36s	20	10.3	80	6.7					
			40	4.3							
			40	3.8			3.92×10^{-6}	3.92×10^{-6}	3.92×10^{-6}	3.92×10^{-6}	
Gas evolution from graphite including water vapor desorption	$H^2(n,\gamma)H^3$	12.26y	100	0.0180			1.87×10^{-2}	6.8×10^{-4}	1.45×10^{-4}	7.82×10^{-6}	Includes gases given off at room temperature and up to 1020°C; activity of O^{19} and N^{16} builds up rapidly, then decreases in about one month to less than 0.1 curie, with the bypass streams to filters in operation; C^{14} activity builds up slowly, but also decreases to 0.1 curie in about a month with the filter in operation
	$N^{14}(n,p)C^{14}$	5580y	100	0.1561			45,300	45.5	9.4	0.51	
	$O^{18}(n,\gamma)O^{19}$	29s	70	2.9	70	1.6					
			30	4.5			3.03	3.03	3.03	3.03	
	$O^{16}(n,p)N^{16}$	7.36s	20	10.3	80	6.7					
			40	4.3							
			40	3.8			11.01	11.01	11.01	11.01	
Recoil atoms from type 304 SS fuel capsule wall	$Mn^{55}(n,\gamma)Mn^{56}$	2.58h	60	2.86	100	0.845					During operation Mn^{56}, Ni^{65}, and Cr^{51} are the predominant activities; after shutdown, Fe^{59}, Co^{60}, Co^{58}, and Mn^{54} activities predominate
			25	1.05	30	1.81					
			15	0.75	20	2.13	18.5			18.05	
	$Cr^{50}(n,\gamma)Cr^{51}$	27.8d			9.8	0.32	13.75			1.73	
	$Fe^{58}(n,\gamma)Fe^{59}$	45.1d	54	0.462	57	1.1					
			46	0.271	43	1.29					
			0.3	1.56	2.8	0.191	0.137			1.12×10^{-2}	

TABLE 13.2 (cont'd)

Source of Activity	Nuclear Process	Half Life	Beta Activity[a] Emissions per Disintegration (%)	Beta Activity[a] Energy (Mev)	Gamma Activity Emissions per Disintegration (%)	Gamma Activity Energy (Mev)	Total Curies in System (max)[b] $\alpha = 0$, $\delta = 0$	$\alpha = 0$, $\delta = 0.1$	$\alpha = 0$, $\delta = 0.5$	$\alpha = 1 \times 10^{-5}$, $\delta = <0.5$	Remarks
Recoil atoms from type 304 SS fuel capsule wall	$Co^{59}(n,\gamma)Co^{60}$	5.3y	100	0.309	100	1.33					During operation Mn^{56}, Ni^{65}, and Cr^{51} are the predominant activities; after shutdown, Fe^{59}, Co^{60}, Co^{58}, and Mn^{54} activities predominate
			0.05	1.48	100	1.17	2.52			5.2×10^{-3}	
	$Ni^{64}(n,\gamma)Ni^{65}$	2.56h	57	2.1	29	1.5					
			29	0.60	29	0.37					
			14	1.0	43	1.12	0.69			0.671	
	$Ni^{58}(n,p)Co^{58}$	72d	14	0.475 (β^+)	100	0.805	0.79			4.16×10^{-2}	
	$Fe^{54}(n,p)Mn^{54}$	300d			100	0.835	0.537			7.06×10^{-3}	
Gamma-emitting fission products in the Kr family	Br^{84}	30m			100	1.89					
					80	0.89	1.4×10^{-3}			1.4×10^{-3}	
	Kr^{85m}	4.4h			15	0.31					
					85	0.15	1.7×10^{-2}			1.7×10^{-2}[c]	
	Kr^{87}	78m			<25	2.3					
					<25	1.9	1.9×10^{-1}			1.9×10^{-1}[c]	
	Kr^{88}	2.8h			68	2	5.5×10^{-1}			5.5×10^{-1}[c]	
	Rb^{88}	18m			5	2.8					
					22	1.9	6.0×10^{-2}			6.0×10^{-2}	
	Sr^{91}	9.7h			62	1.4					
					40	1.0	2.3×10^{-3}			2.0×10^{-3}	
	Zr^{95}	65d			99	0.72	6.0×10^{-3}			3.4×10^{-4}	
	Nb^{95}	35d			200	0.75					
					100	0.67	1.3×10^{-1}			1.4×10^{-2}	
	Mo^{99}	67h			17.5	0.78					
					20	0.74	9.0×10^{-2}			6.5×10^{-2}	
							1.0			0.9	
Gamma-emitting fission products in the Xe family	Te^{125m}	58d			200	0.11	4.5×10^{-2}			3.0×10^{-3}	
	Te^{132}	78h			100	0.23	5.5×10^{-1}			3.1×10^{-1}	
	Te^{133m}	63m			100	0.40	8.0×10^{-3}			8.0×10^{-3}	
	I^{131}	8.1d			12	0.7					
					80	0.4	1.3×10^{1}			4.4×10^{0}	

TABLE 13.2 (cont'd)

Source of Activity	Nuclear Process	Half Life	Beta Activity[a] Emissions per Disintegration (%)	Beta Activity[a] Energy (Mev)	Gamma Activity Emissions per Disintegration (%)	Gamma Activity Energy (Mev)	Total Curies in System (max)[b] $\alpha = 0$, $\delta = 0$	$\alpha = 0$, $\delta = 0.1$	$\alpha = 0$, $\delta = 0.5$	$\alpha = 1 \times 10^{-5}$, $\delta = <0.5$	Remarks
Gamma-emitting fission products in the Xe family	I^{132}	2.4h			2.4	2.0					
					9.5	1.4					
					88.0	0.69	2.4×10^{-1}			2.4×10^{-1}	
	I^{133}	21h			1	1.4					
					5	0.85					
					94	0.53	2.8×10^{0}			2.4×10^{-1}	
	I^{135}	6.7h			100	1.8					
					100	1.27	8.0×10^{-2}			7.5×10^{-2}	
	Xe^{131m}	12d			100	0.16	3.3×10^{-1}			3.3×10^{-1}[c]	
	Xe^{133m}	2.3d			100	0.23	3.5×10^{-1}			3.5×10^{-1}[c]	
	Xe^{133}	5.3d			100	0.08	3.5×10^{-1}			3.5×10^{-1}[c]	
	Xe^{135m}	15.6m			100	0.52	1.8×10^{-2}			1.8×10^{-2}[c]	
	Ce^{141}	33d			67	0.15	2.5×10^{-2}			2.3×10^{-3}	
	Ce^{144}	282d			10	0.13					
					10	0.10	2.2×10^{-1}			3.0×10^{-3}	
	Nd^{147}	11.3d			25	0.53					
					25	0.32					
					60	0.09	1.6×10^{-1}			4.1×10^{-2}	
							18.3			6.4	
						Total	19.3			7.3	

[a]The fission product study was performed on the basis of gamma emitters so that any beta associated with the decays listed here would not necessarily be one of the more significant beta decays.

[b]α = fractional bypass to filters,
δ = leak rate (% per day).

[c]It is assumed that the filter will not remove the noble gases.

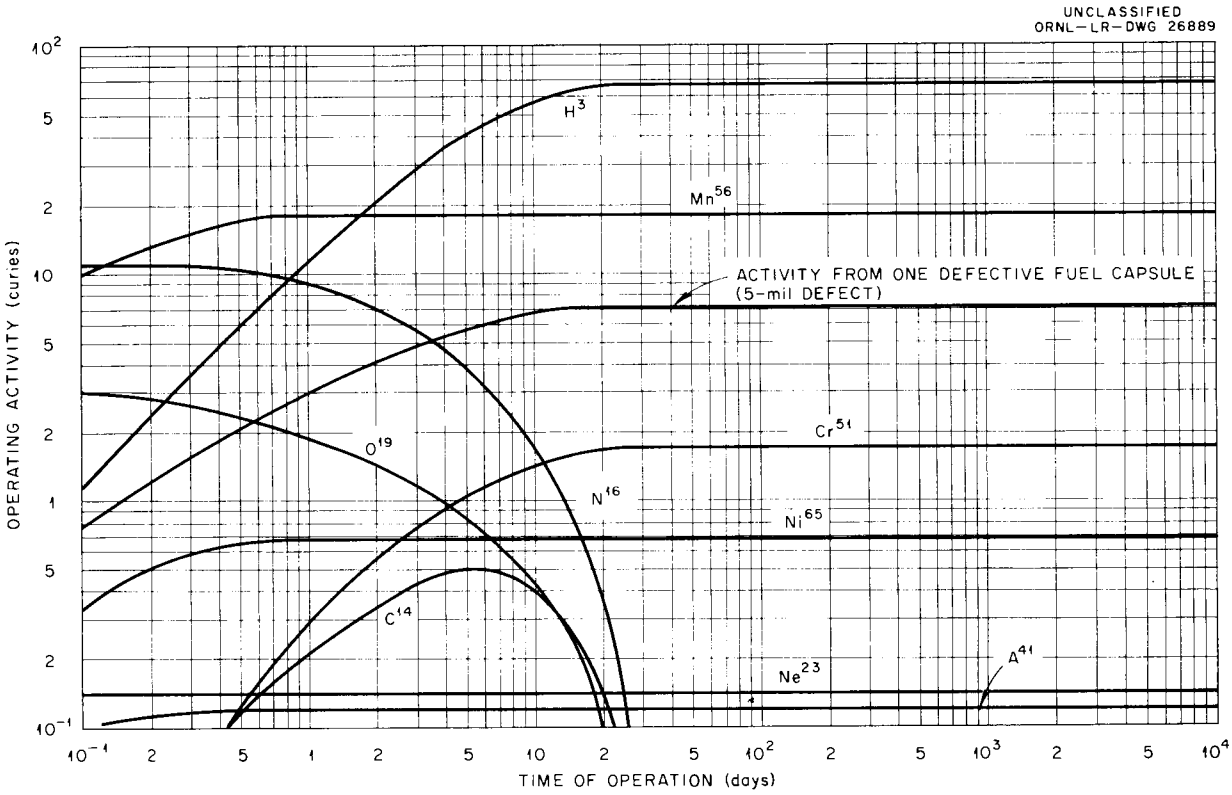

Fig. 13.1. Total Gas Stream Activity During Operation.

By-pass filter systems can be employed advantageously to minimize the gas and system contamination from long-lived activities, including the tritium which is formed by an (n,p) reaction with He^3 as well as activities from recoil diffusion, contamination or defect mechanisms (assuming, of course, that these activities do not plate out immediately on the walls of the containment system).

The differentation of these various sources of contamination into the three groups listed above is significant, not only because the second group is of a temporary nature but also since the sensitivity of the ultimate leak-detection system will be dependent upon the ratio of the various activity levels. The implications of the activity levels described herein, on shielding, fuel element design, leak-detection system, containment, filter system, stack height, etc., will be discussed in other sections of the report.

13.2.1 Neutron Activation of the Helium: The activation of helium is due to an (n,p) reaction with the isotope He^3.

$$ {}_2He^3 + {}_0n^1 \rightarrow {}_1H^3 + {}_1H^1 $$

The build-up of tritium activity will follow the following equation:

$$ A = \frac{\lambda_2}{\lambda_2 + \lambda_3 + \lambda_4} N_1 \phi \sigma \left[1 - e^{-(\lambda_2 + \lambda_3 + \lambda_4)t} \right] $$

where

λ_2 = decay constant for tritium

λ_3 = decay constant to describe the fraction of gas escaping from the system due to leakage

λ_4 = decay constant to describe the fraction of gas being removed from the system by the filters

N_1 = number of atoms of He^3 per cm^3

ϕ = thermal flux, neutrons/$cm^2 \cdot$ sec

σ = thermal cross section for the He^3- np reaction

t = irradiation time in reactor

The equilibrium activity of tritium in the gas can be controlled by the rate of removal of activity from the system either by leakage or by filter mechanism; this may be seen in Fig. 13.2 for leakage rates

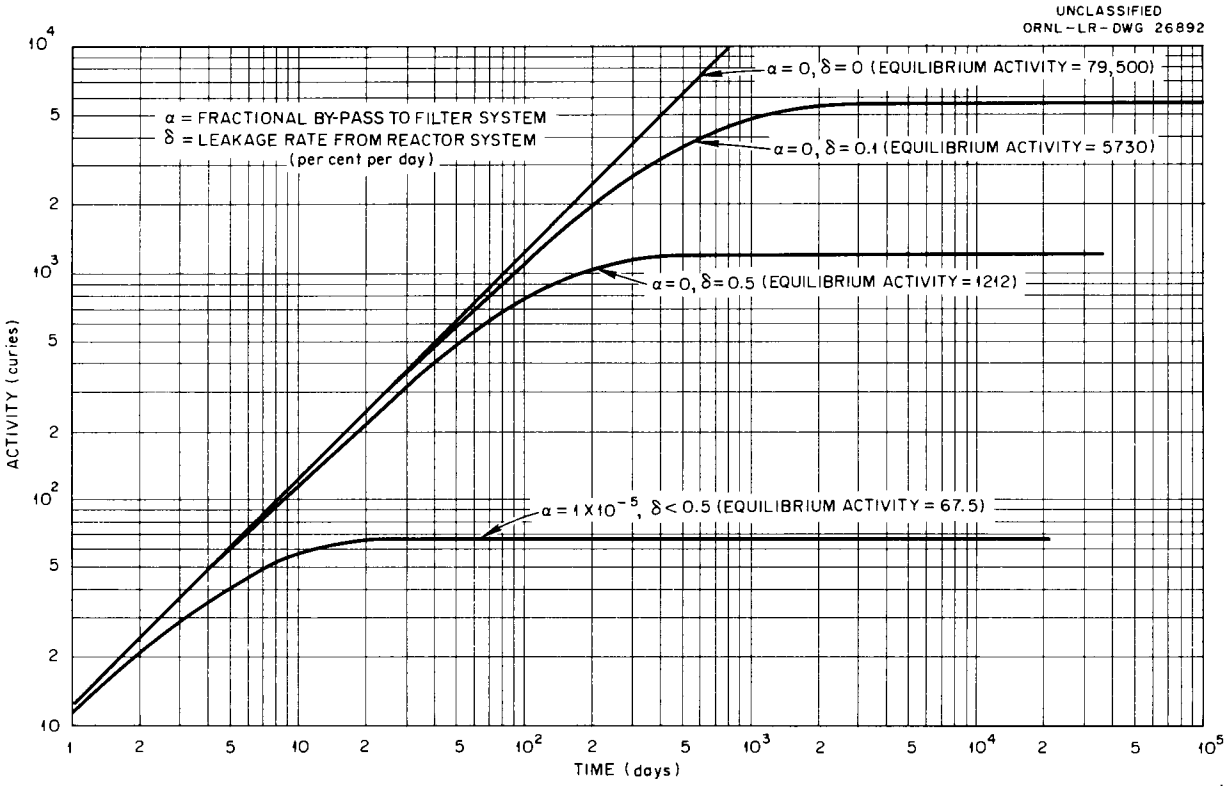

Fig. 13.2. Activity Due to Tritium Build-up.

up to 0.5% per day (with $\lambda_4 = 0$) and for the case where 0.001% of the gas was filtered continuously. Since tritium activity is due to beta disintegration, the activity, if high enough, could be important in contributing to the airborne activity from system leakage. For leakage rates between 0.1% and 0.5% per day and no filter, the activity escaping from the system is approximately constant, indicating that the most hazardous condition would occur if a leak developed after a long period with essentially no leakage from the system. With a by-pass stream through the filter system however, the maximum activity attained in the system is not dependent upon the system leakage rate. For the filtering rate described above, the maximum activity reached in the system is 68 curies. With filters in the system removing tritium, the airborne activity resulting from leakage out of the system will be greatly reduced, and will be directly dependent upon the leakage rate.[2]

13.2.2 Activation of Impurities in the Helium: The activity in the coolant owing to impurities in the helium has been calculated based on the following impurities:

Hydrogen	-	10 ppm
Nitrogen	-	1 ppm
Argon	-	0.2 ppm
Neon	-	10 – 20 ppm
Water Vapor	-	1 ppm
Oxygen	-	None as such, but some as water vapor

The impurities in helium become activated[3] resulting in the build-up of H^3, C^{14}, A^{41}, Ne^{23}, N^{16}, and O^{19} as shown in Table 13.2. The H^3 activity due to the H^2 (n,γ) reactions may be neglected since the activity owing to the (n,p) reaction with He^3 is many orders of magnitude higher. The C^{14} activity, assuming no leakage, is 5.7 curies. This is unimportant since C^{14} has no gamma activity and only a soft beta. The O^{19} activity is negligible (~ 1μc) as is the N^{16} activity. The A^{41} and Ne^{23} have short half-lives and reach an equilibrium activity of less than 0.15 curies. This activity is small compared to the γ activity resulting from recoils in the fuel capsule wall.

---

[2] Wm. B. Cottrell and H. N. Culver, Contamination in the Gas Stream of the GCR-2, Section 1, CF 58-1-119 (January 2, 1958).

[3] Ibid, Section 2.

The equilibrium activity of none of the impurities in helium was high enough to be of concern. Furthermore, the by-pass gas filter system will reduce the concentration of the C^{14} activity in the gas by a factor $\sim 10^6$ so that the resultant activity in the system from impurities will not be significant as compared to other sources of gasborne activity.

13.2.3 Recoils from Fuel Capsule Wall: Nuclear reactions occurring in the type 304 stainless steel fuel capsule wall cause activated atoms to be ejected into the coolant gas stream. The amount of activity caused by recoil atoms is a function of the range of recoil atoms. For thermal neutrons involved in (n,γ) reactions, the range of the recoil atom is estimated to be around 10^{-7} cm. The amount of activity from (n,γ) recoils in the gas will be directly proportional to any error in the calculated ranges. The range of recoil atoms in the fuel capsule wall produced by (n,p) reactions is dependent upon the energy of the fast neutron causing the recoil, and was estimated here by comparison to the Army Package Power Reactor. In any case, the range is so short that atoms escaping from the clad would end up in the gas. The cross section for (n,p) reactions is not too well known for reactions of interest so that experimental results were used.

The following reactions were considered in this study:

$Mn^{55}(n,\gamma)Mn^{56}$	$Fe^{54}(n,\gamma)Fe^{55}$
$Cr^{50}(n,\gamma)Cr^{51}$	$Ni^{58}(n,p)Co^{58}$
$Fe^{58}(n,\gamma)Fe^{59}$	$Fe^{54}(n,p)Mn^{54}$
$Co^{59}(n,\gamma)Co^{60}$	$Fe^{56}(n,p)Mn^{56}$
$Ni^{64}(n,\gamma)Ni^{65}$	

The amount of activity due to the reactions shown above has been investigated[4] based on activation studies performed on the X-10 pile and at the APPR, as well as results from calculated values.

The resulting build-up of activity is shown in Fig. 13.3. This shows the total curies in the system, assuming all recoil atoms remain in the system (no leakage or filtering). The addition of a filter system reduces the activity of the long-lived nuclides and would, therefore, be desirable to reduce the long-term contamination of the system and thus expedite

---

[4] Ibid, Section 3.

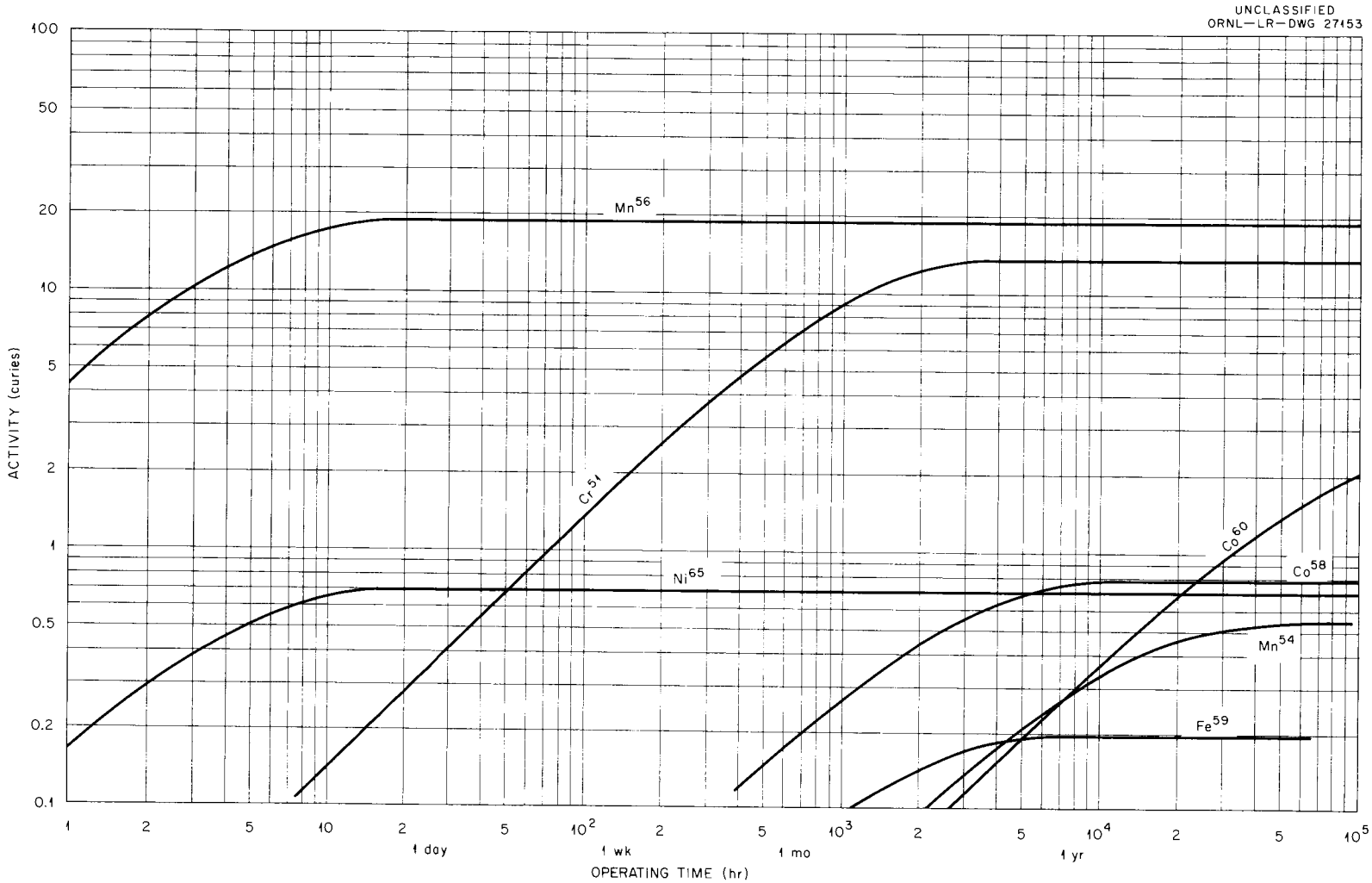

Fig. 13.3. Coolant Activity Due to Recoils from Type 304 Stainless Steel Fuel Capsule Wall.

shutdown maintenance. As one would expect, the Mn^{56} and Ni^{65}, which have short half-lives, are not reduced to any extent by the addition of the filter system. However, this short-lived activity can be outwaited before attempting any maintenance but it still determines the operating dose level of the system. The effect of the filter on the activity in the system is shown in Fig. 13.4.

In view of concern for possible activities with relatively short half-lives, which would probably not have been observed in the experimental references examined, some activation tests were performed on type 304 stainless steel. In these tests counting was begun within one minute after short exposures and no activity comparable to the Mn^{56} activity was observed.

As was previously noted, the activity owing to recoil atoms is directly influenced by the range of the recoil atoms. The first calculations for range were based on the assumption that the recoil atoms would have ranges of the same order as alpha particles of the same energy. Since this assumption was questionable, especially at very low energies, a more exact method for determining the ranges of recoil atoms for small initial velocities was derived based on a method and relationship derived by Bohr.[5] This relationship considers the velocity or energy of the recoil atom, its mass and charge, as well as the mass and charge of the target, and gives ranges which in all cases are about a factor of four less than those first calculated. Since these relationships are at best only approximate, the ranges first calculated were used and considered to be upper limits, although it is believed that the recoil activity should be appreciably smaller.

13.2.4 Corrosion and Erosion: The extent of corrosion and erosion of the stainless steel fuel capsules in the GCR-2 is not known. Studies of the activity in a reactor coolant indicate that the longer the half-life the greater the fraction of any particular isotope in the coolant from corrosion as opposed to recoil processes. Furthermore, in a water system

---

[5]Niels Bohr, The Penetration of Atomic Particles Through Matter (Hafner Publishing House, 1948).

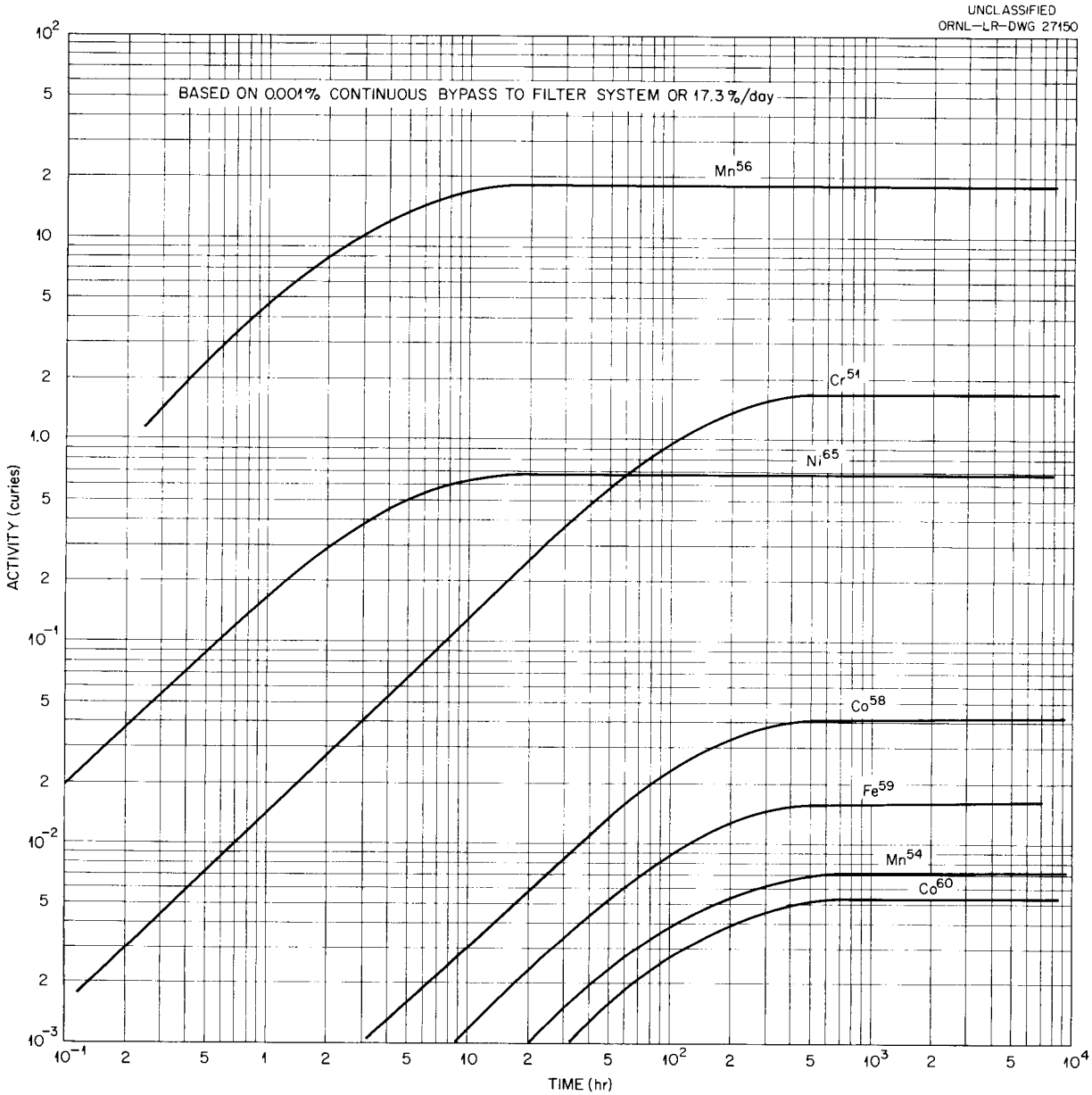

Fig. 13.4. Coolant Activity Due to Recoils from Type 304 Stainless Steel Fuel Capsule Wall Using a By-Pass Filter System.

the activity of any isotope due to corrosion is always more predominant than the activity of that isotope due to recoil. On the other hand, in a gas system the corrosion is believed to be sufficiently low that only for very long-lived isotopes is it possible for the corrosion activity to become predominant.[6] However, until and unless experimental data to the contrary are obtained, it will be assumed that these corrosion and erosion processes in the GCR-2 are less significant than recoil processes in contaminating the main fluid stream. In any case, activities involved would be the same as those discussed in the recoil case, although their relative magnitudes may be affected.

13.2.5 Activation of Occluded Gases Emanating from the Graphite: The occluded gases emanating from the graphite will become activated and thus contribute to the contamination of the gas stream. The gases[7] desorbed in significant quantities include N_2, O_2, CO_2, CO, and H_2 as well as appreciable quantities of water.[8] These sources may combine to release the equivalent of $\sim 4.5 \times 10^6$ liters of O_2 and $\sim 2 \times 10^5$ liters of N_2 to the gas stream. Associated with these elements, the significant activities are C^{14}, O^{19}, and N^{16}.

The above data on the amount of gases released are only a first approximation, since little is known about the effects of manufacturing processes on the absolute or even the relative amount of these contaminants. Furthermore, since there was little information on the rate at which these contaminants

---

[6] H. N. Culver, Cooling Water and Demineralizer Activities in NMSR, ORNL CF-58-4-81 (April 29, 1958).

[7] C. A. Odening and J. C. Bowman, Recent Developments in Gas Pruification of Graphite, National Carbon Research Laboratories, Tech. Memo., TM-274 (August 12, 1957).

[8] R. V. Moore, "The Design and Construction of the Plant," J. British Nuclear Energy Conf., 2, No. 2, 64 (April, 1957).

would be evolved, it was assumed that they would be released instantaneously at a time when the reactor was at full power. The calculated activities,[9] therefore, represent a maximum although the time to this maximum and the duration of the activity surge are not necessarily significant. Furthermore, it would be expected that start-up procedures, particularly system evacuation prior to He filling, isothermal operation at 450°F and a slow heat-up, plus the effect of the system filter would substantially reduce the maximum levels indicated.

The radioactive nuclides formed from the impurities introduced into the gas stream are H^3, C^{14}, O^{19}, and N^{16}. The H^3 activity due to the (n,γ) reaction with H^2 is much less than the activity from the (n,p) reaction with He^3 and may therefore be neglected. The C^{14} activity is shown in Fig. 13.5 for leakage rates from zero to 0.5% per day. Since this activity involves beta emission (and not gamma emission) it is relatively unimportant, compared to the recoil activity. However, the activity due to $O^{18}(n,\gamma)O^{19}$ from both gas evolution and water vapor desorption and that from $O^{16}(n,p)N^{16}$ attain maximum values of 3.03 and 11.0 curies, respectively. Both of these activities have short half-lives so that the maximum activity is reached in a very short time. Furthermore, neither system leakage, nor the by-pass filter will affect these maximum levels, although both affect the rate at which these activities disappear. On the other hand, the C^{14} has a long half-life, which causes it to build up slowly to the maximum level, and this maximum is dependent upon system leakage and by-pass filter rates. The build-up and decrease of the level of each of these activities is shown in Fig. 13.1 for the design condition.

13.2.6 Occluded Gas from Metals: The activation of the occluded gases in the metal has not been evaluated. However, these gases are the same as those absorbed in graphite and, although the relative amounts of the gases in the metal and graphite may differ, the amount contained in the metal is expected to be orders of magnitude less.

13.2.7 Residual Gases after Helium Filling: The proposed start-up technique includes evacuation of the gas system before helium filling.

---

[9] Wm. B. Cottrell and H. N. Culver, Contamination in the Gas Stream of the GCR-2, Section 4, CF 58-1-119 (January 2, 1958).

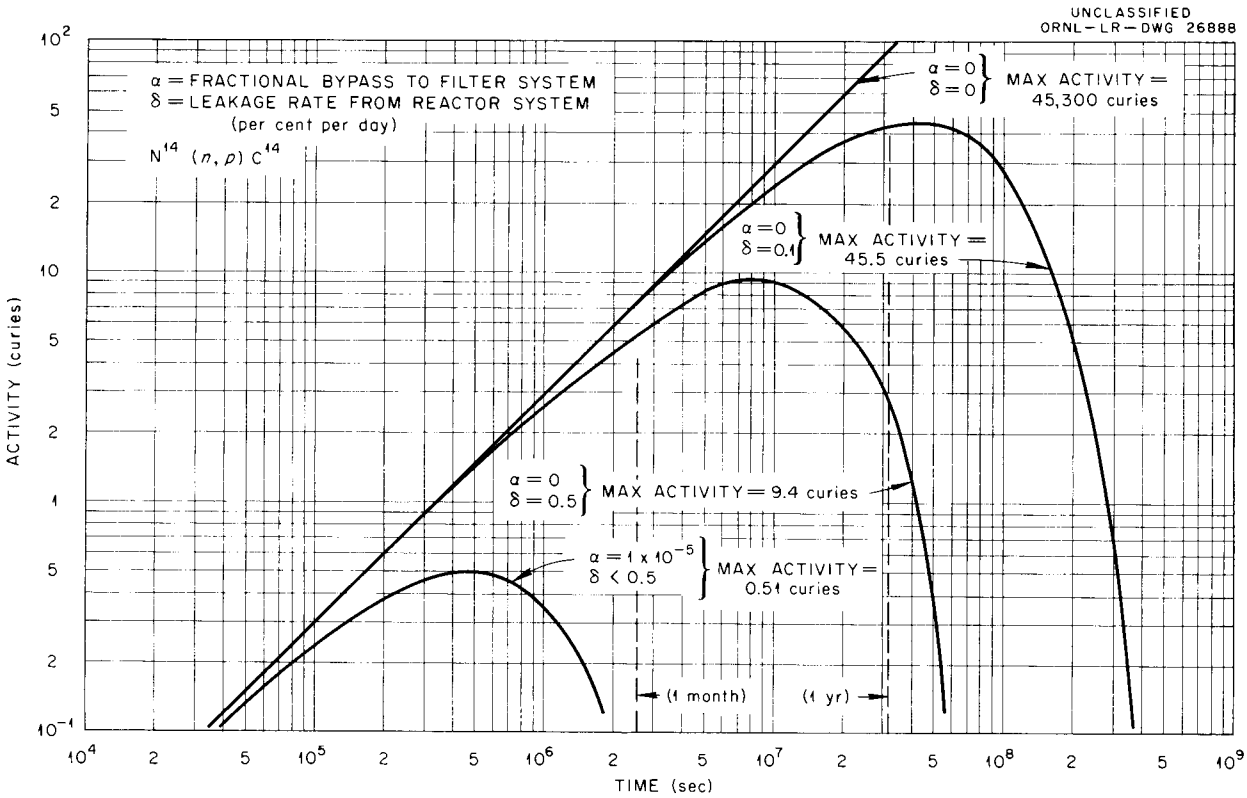

Fig. 13.5. C^{14} Activity Due to Gas Evolution From Graphite.

This process will also be effective in desorbing a portion of the gases in the graphite as well as metal. Thus, after evacuation, the make-up of the residual gas in the system will be governed by the desorption of the graphite. Since the activation of these gases was considered above, no separate calculation was made.

13.2.8 Surface Contamination of Fuel Capsule Wall: No information was available on the surface contamination of UO_2 fuel capsules of the type proposed for use in the GCR-2. If the surface contamination were to be 10^{-9} g/cm^2, or 1/3 the maximum specified for rolled Materials Testing Reactor type fuel elements, then on the 4.1×10^7 cm^2 of fuel element surface in the GCR-2, this would cause 1.65×10^{10} fissions/sec (i.e., ~ 0.5 w of power would be produced by the surface contamination on the capsule).

The effect of this surface contamination on the sensitivity of the defective fuel capsule leak detector was discussed in detail in Section 7 on Instrumentation and Controls.[10] It was shown that the ratio of concentrations in the gas capsule from surface contaminations and from the leak is

$$\frac{N_{surface}}{N_{leak}} = \frac{2.5 \times 10^{-9}}{\nu}$$

where ν is the escape coefficient (probability of escape, see 13.2.10) for a particular isotope. Thus, for those isotopes with an escape coefficient of 2.5×10^{-9} (see 13.2.10) the number of atoms in the helium due to surface contamination is the same as that from the leak. In any case, it would appear that the surface contamination of the UO_2-stainless steel fuel capsules should be substantially less than that for the rolled metal plates described above, and, furthermore, contamination on the stainless steel capsules could be reduced by an acid rinse.

13.2.9 Diffusion through Fuel Capsule Wall: In lieu of experimental data on diffusion coefficients for fission products in stainless steel, a conservative quasi-theoretical method of estimating the diffusion coefficient

---

[10] Ibid, Section 5.

as developed by M. R. Gustavson, was employed.[11] This method gave a value for the diffusion coefficient at 1300°F of 3×10^{-13} cm^2/sec. If this coefficient is used for the fission product gasses,[12] it gives a total gas contamination equivalent to a leak from one fuel capsule. However, this diffusion coefficient applies only to the metallic fission products. The use of this approach to other fission products is questionable, particularly with regard to Xe and Kr, which it is believed do not diffuse through the metal at all. Preliminary results of tests[13] on the diffusion of fission products through the fuel capsule wall in the temperature range of interest indicate that no significant amount of diffusion occurs. While these tests are not yet quantitative, they do support the conclusion that at the temperatures in question diffusion should not be of concern.

13.2.10 Leak through Defect in Fuel Capsule Wall: Aside from the initial surge of activity that might result from activity accumulated up to the time of the onset of the leak, there would subsequently be a continuous leakage of activity to the gas stream. Escape rate coefficients (defined as the fraction of the total amount of an isotope in the fuel escaping per second) have been measured for a number of isotopes for a predetermined defect.[14,15] The existing data have then been interpolated to permit an evaluation of the total activity in the gas stream from all isotopes. The resulting values of escape rate coefficients are listed in Table 13.3. The various escape rates have a number of possible errors associated with them including:

1. Measurement of a value for ν (escape rate coefficient for a particular isotope).

---

[11] M. R. Gustavson, Diffusion of Fission Products through Cladding, AGN Note No. 306, (October 14, 1957).

[12] Cottrell and Culver, op. cit., Section 6.

[13] L. P. Crocker and C. E. Creek, Fission Product Diffusion through Clad Cermet Fuel Elements, CF 57-12-69 (December 16, 1957).

[14] B. Lustman, Release of Fission Gases from UO_2, WAPD 173, Westinghouse Electric Corp., Bettis Plant, Pittsburgh, Pennsylvania, Contract AT 11-1-Gen-14 (March, 1957).

[15] J. D. Eichenberg et al., Effects of Irradiation on Bulk UO_2, WAPD 183, Westinghouse Atomic Power Division (October, 1957).

TABLE 13.3

ESCAPE RATE COEFFICIENTS USED TO DETERMINE THE GAMMA ACTIVITY IN THE GAS STREAM FROM A FUEL CAPSULE LEAK

Element	$\nu(sec^{-1})$	Remarks*
Te	3×10^{-9}	Average single isotope
I	4×10^{-8}	Average of two isotopes
Xe	7×10^{-8}	Average of three isotopes
Cs	1×10^{-7}	Average of four isotopes
Ba	6×10^{-10}	Average of two isotopes
La	1×10^{-11}	Similar to Ce
Ce	1×10^{-11}	Average of single isotope
Pr	1×10^{-11}	Similar to Ce
Nd	4×10^{-10}	Similar to Mo
Se	3×10^{-9}	Similar to Te
Br	6×10^{-9}	Average of two isotopes
Kr	1×10^{-7}	Average of single isotopes
Rb	1×10^{-7}	Similar to Cs
Sr	7×10^{-10}	Average of five isotopes
Y	2×10^{-12}	Average single isotope
Zr	1×10^{-11}	Average single isotope
Nb	4×10^{-10}	Similar to Mo
Mo	4×10^{-10}	Average of single isotope

* There are from 1 to 4 valid measurements per isotope.

2. Use of this value of ν for all isotopes of this element. (Although there may be some reason to think ν is dependent upon λ [decay constant], the limited data available do not support this.) Furthermore, some isotopes, such as Rb^{88}, would be expected to be dependent upon immediate precursors rather than direct escape.
3. Where no data are available on a particular isotope, an escape rate coefficient has been assumed to be either that of its predecessor or that of the element whose chemical and physical properties are most similar for which escape rates have been measured, whichever was the greater.
4. The experimental escape rates were based upon a pressurized water system rather than a 300 psi helium system. The latter should be lower because solution in water would not take place.
5. A 5-mil capsule wall defect was assumed.
6. The 5-mil defect was assumed to result in leak rates in the 40-in. GCR-2 fuel elements which were comparable to those in the 10-in. Pressurized Water Reactor fuel elements.

The escape rate coefficients shown in Table 13.3 have been used to calculate[16] the gamma activity in the gas stream as a function of time as shown in Fig. 13.6. It may be seen that the equilibrium activity owing to the above assumed fission product release is of about the same order as that existing in the gas stream owing to the recoil activity.

Since the majority of the activity attributed to the Xe family comes from I (Xe is the second most prolific activity in this family), the use of a filter would be effective in lowering the equilibrium concentration (by a factor of ~ 3). The filter would not significantly affect the total activity originating in the Kr family since Kr itself is the most prominent member of this group.

13.3 Release of Fission Gases in the Fuel Capsule

The fission gases released from the UO_2 slugs will cause the gas pressure within the fuel capsule to increase. This phenomenon is important in the

[16] Cottrell and Culver, op. cit., Section 7.

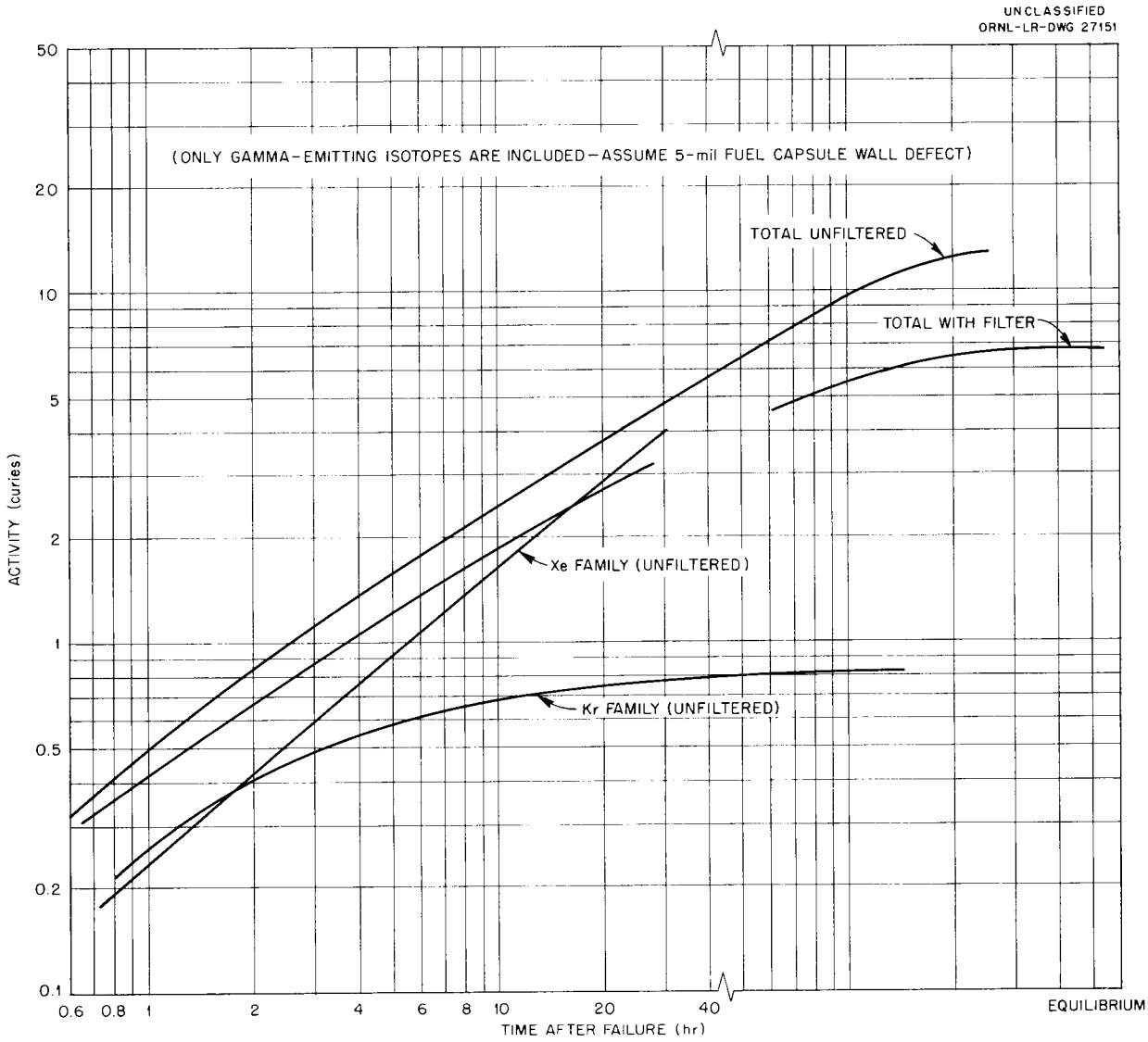

Fig. 13.6. Fission Product Activity in System as Function of Time after Fuel Capsule Defect.

design of the capsule both for normal operating conditions and for the shut-down situation in which the helium system is reduced to atmospheric pressure.

The quantity of fission gas (Xe and Kr) existing as a function of operating time is listed in Table 13.4 and shown in Fig. 13.7. This information was obtained by dividing the isotopes of each element into two groups: (1) Those which are stable or have half-lives greater than 10 yr and (2) those which have shorter half-lives (and would, therefore, reach an equilibrium concentration). The contribution of the second group is significant only at operating times of 100 hr or less as the accumulation of the stable isotopes predominates at longer times. The data shown in Fig. 13.7 must be adjusted for a particular operating temperature and UO_2 density in order to evaluate the quantity diffusing from the oxide matrix into the gas space within the fuel capsule.

By extrapolating the data in WAPD-173, a relationship between the fraction of gas escaping as a function of the center temperature of the UO_2 slug for the various UO_2 densities of interest can be obtained as shown in Fig. 13.8. As may be seen in Fig. 13.8, the gas release from an oxide having a density of 93% of the theoretical value is 1.5 times that from an oxide having a density of 95%, and the release is reduced by another factor of five if the density is increased from 95% to 97%.

The pressure build-up in the capsule can be determined from the calculated amount of gas release and the known void volume within the capsule. Since the amount of gas release is dependent upon the oxide temperature which in turn is dependent upon the gas temperature rise, an iterative calculation is required. Calculations of the pressure build-up within the GCR-2 fuel elements are presented in Section 3. It has been shown that the maximum pressure will always be less than 300 psia. As the helium design pressure is 300 psia, the pressure differential during operation will always be inward, but when the helium system is reduced to atmospheric pressure there will exist a positive pressure within the fuel element even after it has cooled off. This pressure will not subject the fuel capsule to excessive stresses although it will lead to immediate ejection of the contained gases in the event that a defect develops in the capsule.

TABLE 13.4. FISSION GAS RELEASE AS A FUNCTION OF OPERATING TIME

Principal Isotope	Number of Atoms per Fission, γ	λ (sec^{-1})	$\left(\frac{\gamma f}{\lambda}\right)^{*}_{equil}$	Number of Atoms Released — Operating Time (hr) 100	1,000	10,000	100,000
Xe-131	3×10^{-2}	Stable		2.4×10^{23}	2.4×10^{24}	2.4×10^{25}	2.4×10^{26}
Xe-132	4.5×10^{-2}	Stable		3.6×10^{23}	3.6×10^{24}	3.6×10^{25}	3.6×10^{26}
Xe-133	6.6×10^{-2}	1.5×10^{-6}	9.7×10^{23}				
Xe-134	7.8×10^{-2}	Stable		6.2×10^{23}	6.2×10^{24}	6.2×10^{25}	6.2×10^{26}
Xe-135^{m}	1.7×10^{-2}	7.4×10^{-4}	5.0×10^{20}				
Xe-135	6.6×10^{-2}	2.1×10^{-5}	6.9×10^{22}				
Xe-136	6.4×10^{-2}	Stable		5.1×10^{23}	5.1×10^{24}	5.1×10^{25}	5.1×10^{26}
Total			1×10^{24}	1.7×10^{24}	1.7×10^{25}	1.7×10^{26}	1.7×10^{27}
Total stable and radioactive				2.7×10^{24}	1.8×10^{25}	1.7×10^{26}	1.7×10^{27}
$\div 6.02 \times 10^{23}$ to get moles				4.5	30	280	2800
$\div$ 56,000 to get moles per capsule				8.0×10^{-5}	5.4×10^{-4}	5×10^{-3}	5×10^{-2}
Kr-83	4.7×10^{-3}	Stable		3.7×10^{22}	3.7×10^{23}	3.7×10^{24}	3.7×10^{25}
Kr-84	8.7×10^{-3}	Stable		6.9×10^{22}	6.9×10^{23}	6.9×10^{24}	6.9×10^{25}
Kr-85^{m}	8.5×10^{-3}	4.4×10^{-5}					
Kr-85	3.8×10^{-3}	Stable**		3.0×10^{22}	3.0×10^{23}	3.0×10^{24}	3.0×10^{25}
Kr-86	1.7×10^{-2}	Stable		1.3×10^{23}	1.3×10^{24}	1.3×10^{25}	1.3×10^{26}
Kr-87	2.7×10^{-2}	1.5×10^{-4}	4.0×10^{21}				
Kr-88	3.8×10^{-2}	7.0×10^{-5}	1.2×10^{22}				
Total			2.0×10^{22}	2.7×10^{23}	2.7×10^{24}	2.7×10^{25}	2.7×10^{26}
Total stable and radioactive				2.9×10^{23}	2.7×10^{24}	2.7×10^{25}	2.7×10^{26}
$\div 6.02 \times 10^{23}$ to get moles				0.48	4.5	45	450
$\div$ 56,000 to get moles per capsule				8.6×10^{-6}	8×10^{-5}	8×10^{-4}	8×10^{-3}

*Where f is the total number of fissions per sec and λ is the decay constant.

**Half life 10.6 years, essentially stable for present purpose.

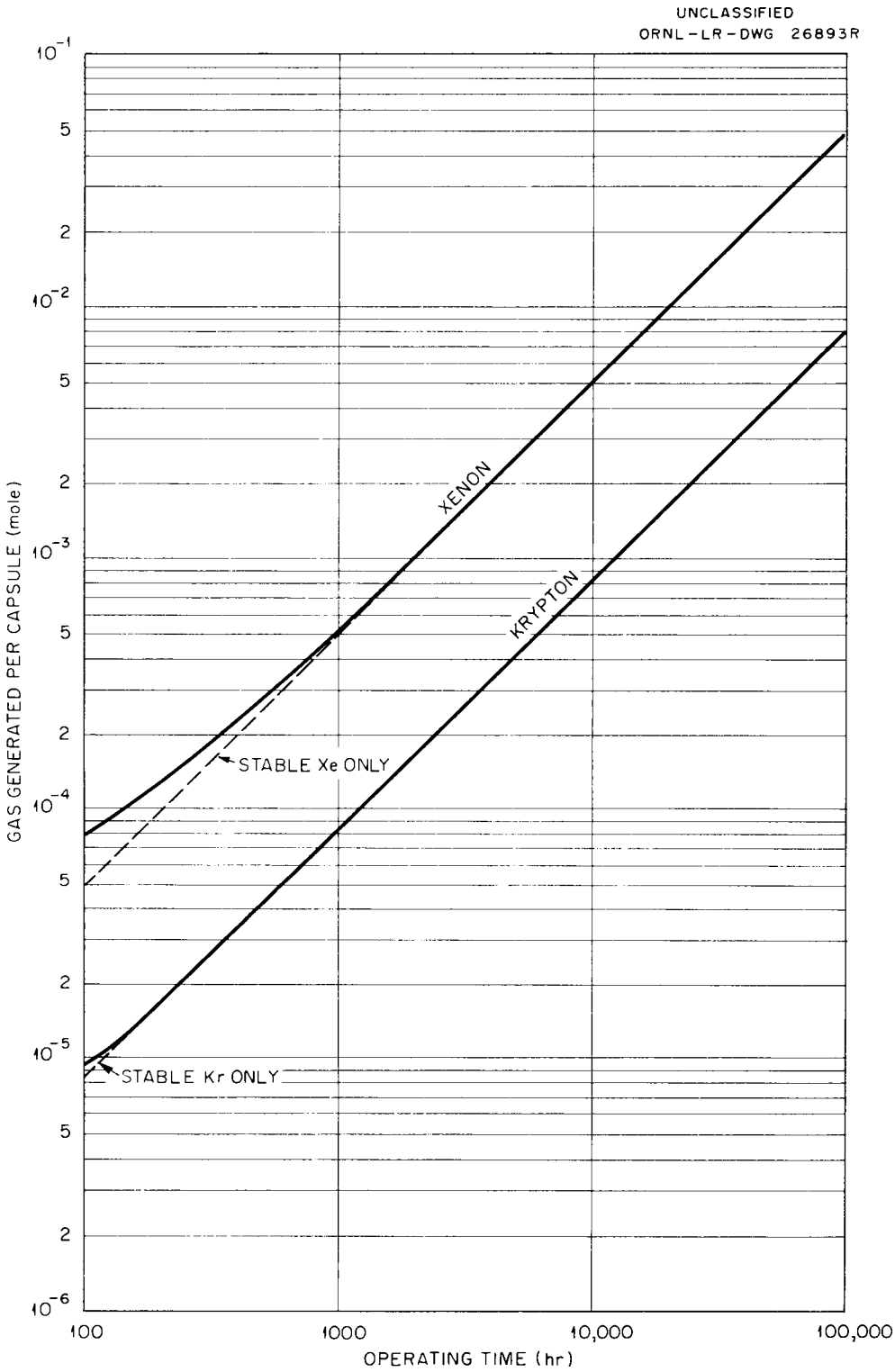

Fig. 13.7. Gas Generated Per Capsule as Function of Operating Time at 700 Mw (56,000 Capsules).

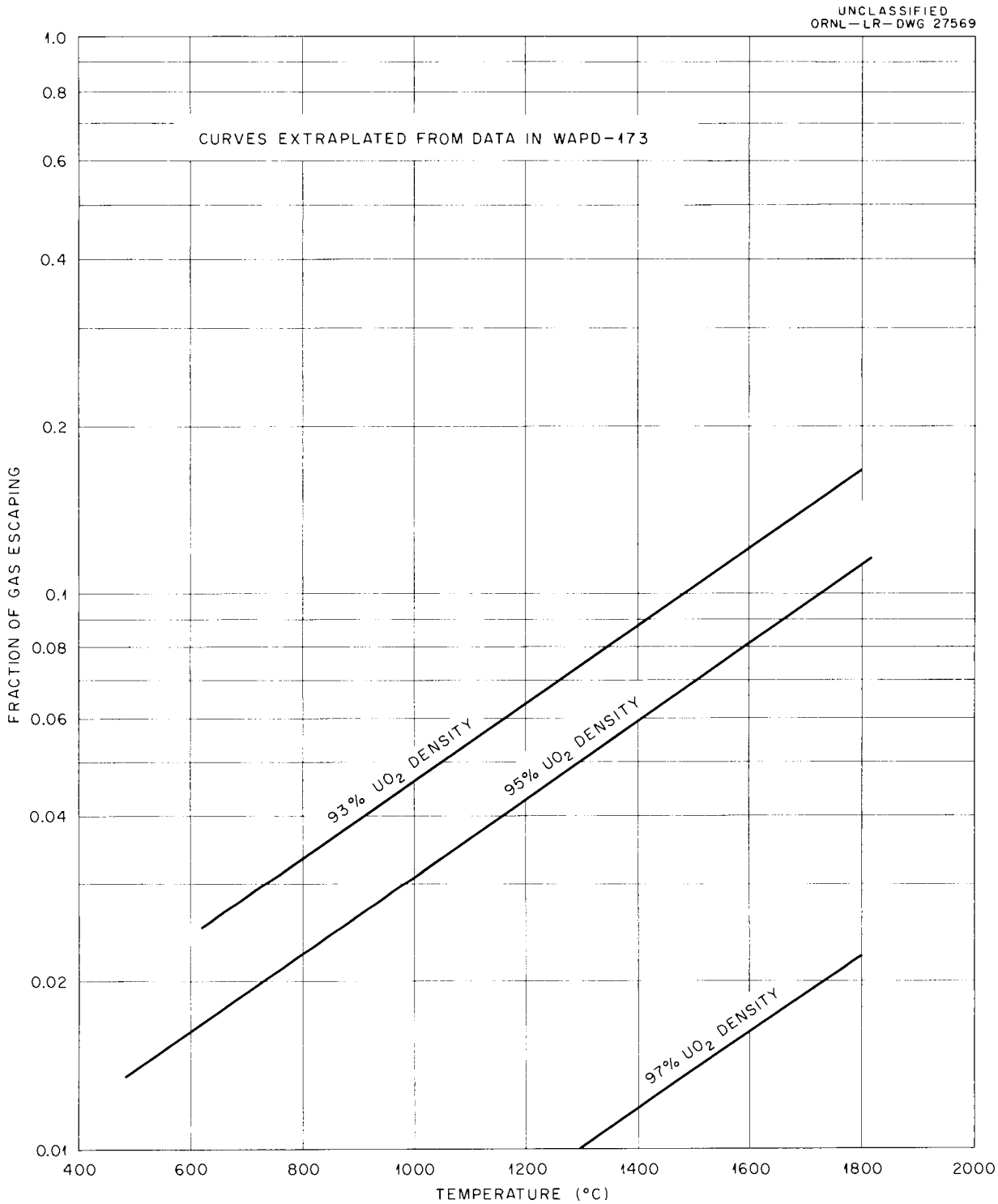

Fig. 13.8. Fraction of Kr Escaping vs Center Temperature.

13.4 Shutdown Activity and Dose Calculations

13.4.1 Activity in Coolant after Shutdown: The activity in the GCR-2 coolant after shutdown will be greatly influenced by the following factors:

1. The time of operation previous to shutdown.
2. The power level at which reactor has been operating previous to shutdown.
3. The leakage rate from the reactor, or the frequency of pressure relief in the reactor.
4. The effectiveness of the by-pass purification system in removing activity from the gas.
5. The number of fuel capsules leaking, the time the fuel-leaking capsule has been in reactor (i.e., the effective nvt to which the capsule has been exposed) and the time since the defect developed.
6. The effectiveness of the surfaces of the gas system in removing activity from the gas.

The activity in the GCR-2 will consist of the activity in the gas stream and the activity which has collected on the surfaces of the reactor (i.e., heat exchangers, fuel elements, moderator, ducts, etc.).

The equilibrium activity and the activity for various times after shutdown for the fission products leaking from one fuel capsule are tabulated in Tables 13.5 and 13.6. These values assume no decrease in activity owing to a purification system. Since the plant has a gas-purification system, it can be expected to reduce the activity in the gas stream by a factor of $\frac{\lambda}{\lambda + \frac{\alpha}{T}}$ where λ is the usual decay constant for a particular nuclide, and α is the fraction of the total flow being bypassed to the purification system and T is the circuit time in seconds ($\frac{\alpha}{T} = 2 \times 10^{-6}$ sec). It is readily seen that the real benefit of the purification system is for nuclides with long half-lives (i.e., H^3, Sr^{90}, etc.).

The data in Tables 13.5 and 13.6 are only approximate for the following reasons:

1. The contribution of daughters was not considered.
2. Some of the data represent crude estimates based on measured escape rate coefficients.

TABLE 13.5. AFTER-SHUTDOWN ACTIVITY LEVEL FROM XENON CHAINS FROM ONE LEAKING FUEL CAPSULE (WITHOUT FILTER)*

Isotope	λN_{ex}**	$\lambda N_{ex} e^{-\lambda t}$ (disintegrations/sec)				
		Time After Shutdown (sec)				
		10^5	10^6	10^7	5×10^7	10^8
Te^{125m}	9×10^{13}	9×10^{13}	7.8×10^{13}	2.3×10^{13}	9×10^{10}	
Te^{129m}	2.63×10^{15}					
Te^{131m}	4.2×10^{13}	7.1×10^{9}				
Te^{131}	3.9×10^{12}					
Te^{132}	1.1×10^{15}	1.1×10^{15}	9.1×10^{13}			
Te^{133m}	1.6×10^{13}					
Te^{133}	6.3×10^{11}					
I^{131}	2.6×10^{16}	2.6×10^{16}	9.6×10^{15}			
I^{132}	4.8×10^{14}	1.6×10^{11}				
I^{133}	5.6×10^{15}	2.2×10^{15}	5.0×10^{11}			
I^{135}	1.6×10^{14}	8.8×10^{12}				
I^{136}	3.2×10^{12}					
Xe^{131m}	6.6×10^{14}	6.6×10^{14}	3.4×10^{14}	8.3×10^{11}		
Xe^{133m}	7.0×10^{14}	4.9×10^{14}	2.1×10^{13}			
Xe^{133}	7.0×10^{14}	6.0×10^{14}	1.5×10^{14}			
Xe^{135m}	3.6×10^{13}					
Cs^{136}	2.2×10^{11}	2.2×10^{11}	1.2×10^{11}	6.0×10^{8}		
Cs^{138}	3.6×10^{11}					
Ba^{137m}	1.9×10^{11}					
Ba^{139}	5.6×10^{12}					
Ba^{140}	1.3×10^{15}					
La^{140}	2.7×10^{12}	1.7×10^{12}	2.2×10^{10}			
La^{141}	1.9×10^{11}	1.1×10^{9}				
Ce^{141}	5.0×10^{13}	5.0×10^{13}	4.0×10^{13}	4.6×10^{12}		
Ce^{143}	2.2×10^{12}	1.2×10^{12}	6.6×10^{9}			
Ce^{144}	4.3×10^{14}	4.3×10^{14}	4.3×10^{14}	3.3×10^{14}	1.1×10^{14}	2.58×10^{13}
Ce^{146}	8.5×10^{9}					
Pr^{146}	1.5×10^{10}					
Nd^{147}	3.1×10^{14}	3.1×10^{14}	1.5×10^{14}	2.6×10^{11}		
Nd^{151}	4.8×10^{9}					
Total	3.63×10^{16}	31.9×10^{15}	10.9×10^{15}	35.3×10^{13}	1.1×10^{14}	2.58×10^{13}

*Wm. B. Cottrell and H. N. Culver, Contamination in the Gas Stream of the GCR-2, CF 58-1-119 (January 2, 1958).

**Ibid. Data in this column taken from Table 5. The symbol N_{ex} denotes the total number of atoms of isotope which have escaped from leaking fuel capsule.

TABLE 13.6. AFTER-SHUTDOWN ACTIVITY LEVEL FROM KRYPTON CHAINS FROM ONE LEAKING FUEL CAPSULE (WITHOUT FILTER)*

Isotope	λN_{ex}**	$\lambda N_{ex} e^{-\lambda t}$ (disintegrations/sec) Time After Shutdown (sec)		
		10^5	10^6	10^7
Se^{83}	2.7×10^{11}			
Br^{84}	2.8×10^{12}			
Br^{87}	2.6×10^{11}			
Kr^{85m}	4.1×10^{13}	5.1×10^{11}		
Kr^{87}	3.8×10^{14}			
Kr^{88}	1.1×10^{15}	1×10^{13}		
Rb^{88}	1.2×10^{14}			
Sr^{91}	4.5×10^{12}	6.1×10^{11}		
Y^{91m}	4.6×10^{9}			
Y^{93}	1.5×10^{10}	2.3×10^{9}	3.3×10^{9}	
Zr^{94}	2.1×10^{8}			
Zr^{95}	1.2×10^{13}	1.2×10^{13}	1.1×10^{13}	3.6×10^{12}
Nb^{95m}	2.8×10^{11}	2.3×10^{11}	3.4×10^{10}	
Nb^{95}	2.5×10^{14}	2.5×10^{14}	2.0×10^{14}	2.5×10^{13}
Nb^{97m}	4.8×10^{9}			
Nb^{97}	3.5×10^{11}			
Mo^{99}	1.8×10^{13}	1.4×10^{13}	1×10^{11}	
Total	1.93×10^{15}	12.9×10^{14}	2.1×10^{14}	2.9×10^{13}
Total from Table 13.5		31.9×10^{15}	10.9×10^{15}	35.3×10^{13}
Total		34.8×10^{15}	11.1×10^{15}	38.2×10^{13}
$\div (5.6 \times 10^4 \times 3.7 \times 10^{10})$ (curies in system per rod defect)		16.7	5.4	0.18

*Wm. B. Cottrell and H. N. Culver, Contamination in the Gas Stream of the GCR-2, CF 58-1-119 (January 2, 1958).

**Ibid. Data in this column taken from Table 4. The symbol N_{ex} denotes the total number of atoms of isotope which have escaped from leaking fuel capsule.

3. Even if the daughter calculations were included (as they can be) this list would not show any gamma-emitting daughters that might come from a beta-emitting parent (beta-emitting parents were not included in this list).
4. Gaseous fission products could be purged out of the system before servicing.

Table 13.7 shows the activities from recoil atoms for various times after shutdown assuming an effective purification system. The total system activity due to recoil atoms, fission product atoms from one leaking fuel element, impurities in the helium, and helium activation are shown in Fig. 13.9 for various times after shutdown. This curve has been drawn from the data of Tables 13.5, 13.6, and 13.7, modified where necessary for a by-pass filter rate of 2.10^{-6} per sec.

13.4.2 Radiation Level Outside Steam Generator: Using the activities calculated in 13.4.1, the radiation level immediately outside a steam generator may be calculated as a function of time after shutdown. However, it is difficult to predict what fraction of this activity will remain in the gas stream and what fraction will collect on the metal or graphite surfaces exposed to the gas. Although virtually all of the activity will be in the form of atomic size particles in the solid phase, it is not conservative to assign the amount of activity in a heat exchanger in proportion to the heat exchanger gas volume as compared to the total system gas volume. It might be noted that the equilibrium activity for a particular nuclide has been determined previously based on a filtration removal rate of $\frac{\alpha}{T} = 2 \times 10^{-6}$ per sec (see 13.4.1). This assumed that the activities in question were uniformly concentrated in the gas stream. If the nuclides were being removed by another process at a rate higher than 2×10^{-6} per sec, and if this process involved the collection of nuclides on surfaces in the system, the equilibrium activity in the gas stream would be substantially reduced. Although this would be beneficial as far as airborne activity from escaping gases is concerned, it would at the same time increase the equilibrium activity in the system (i.e., the surfaces would be collecting the activity instead of the filter system). It is, therefore,

TABLE 13.7. ACTIVITIES IN GAS STREAM AFTER SHUTDOWN (WITH FILTER)

Source	Half Life	Decay Const. λ (sec^{-1})	Activity in Gas* (curies)										
			Time After Shutdown (sec)										
			0**	1	10	10^2	10^3	10^4	10^5	10^6	10^7	10^8	10^9
H^3	12.26y	1.79×10^{-9}	67.5	67.5	67.5	67.5	67.5	67.5	67.5	67.5	66.3	56.4	7.83
A^{41}	1.82h	1.06×10^{-4}	0.119	0.119	0.119	0.117	0.107	0.041					
Ne^{23}	40s	1.74×10^{-2}	0.14	0.138	0.118	0.025							
Mn^{56}	2.58h	7.45×10^{-5}	18.05	18.05	18.05	17.92	16.75	8.57	0.01				
Cr^{51}	27.8d	2.88×10^{-7}	1.73	1.73	1.73	1.73	1.73	1.73	1.68	1.28	0.097		
Ni^{65}	2.56h	7.52×10^{-5}	0.671	0.671	0.671	0.666	0.622	0.316	0.0004				
Fe^{59}	45.1d	1.775×10^{-7}	1.12×10^{-2}	1.12×10^{-2}	1.12×10^{-2}	1.12×10^{-2}	1.12×10^{-2}	1.12×10^{-2}	1.1×10^{-2}	9.39×10^{-3}	1.9×10^{-3}		
Co^{60}	5.3y	4.14×10^{-9}	5.2×10^{-3}	5.2×10^{-3}	5.2×10^{-3}	5.2×10^{-3}	5.2×10^{-3}	5.2×10^{-3}	5.2×10^{-3}	5.18×10^{-3}	4.99×10^{-3}	3.43×10^{-3}	8.32×10^{-5}
Co^{58}	72d	1.115×10^{-7}	4.16×10^{-2}	4.16×10^{-2}	4.16×10^{-2}	4.16×10^{-2}	4.16×10^{-2}	4.16×10^{-2}	4.08×10^{-2}	3.72×10^{-2}	1.36×10^{-2}		
Mn^{54}	300d	2.68×10^{-8}	7.06×10^{-3}	7.06×10^{-3}	7.06×10^{-3}	7.06×10^{-3}	7.06×10^{-3}	7.06×10^{-3}	7.04×10^{-3}	6.87×10^{-3}	5.40×10^{-3}	4.8×10^{-4}	

*Initial activities tabulated are with the purification system in operation, and it was assumed that the purification system became inoperative at shutdown. To obtain activity at time t with no benefit from the purification system, multiply the tabulated values by $(\lambda + 2 \times 10^{-6})/\lambda$.

**From Table 13.2.

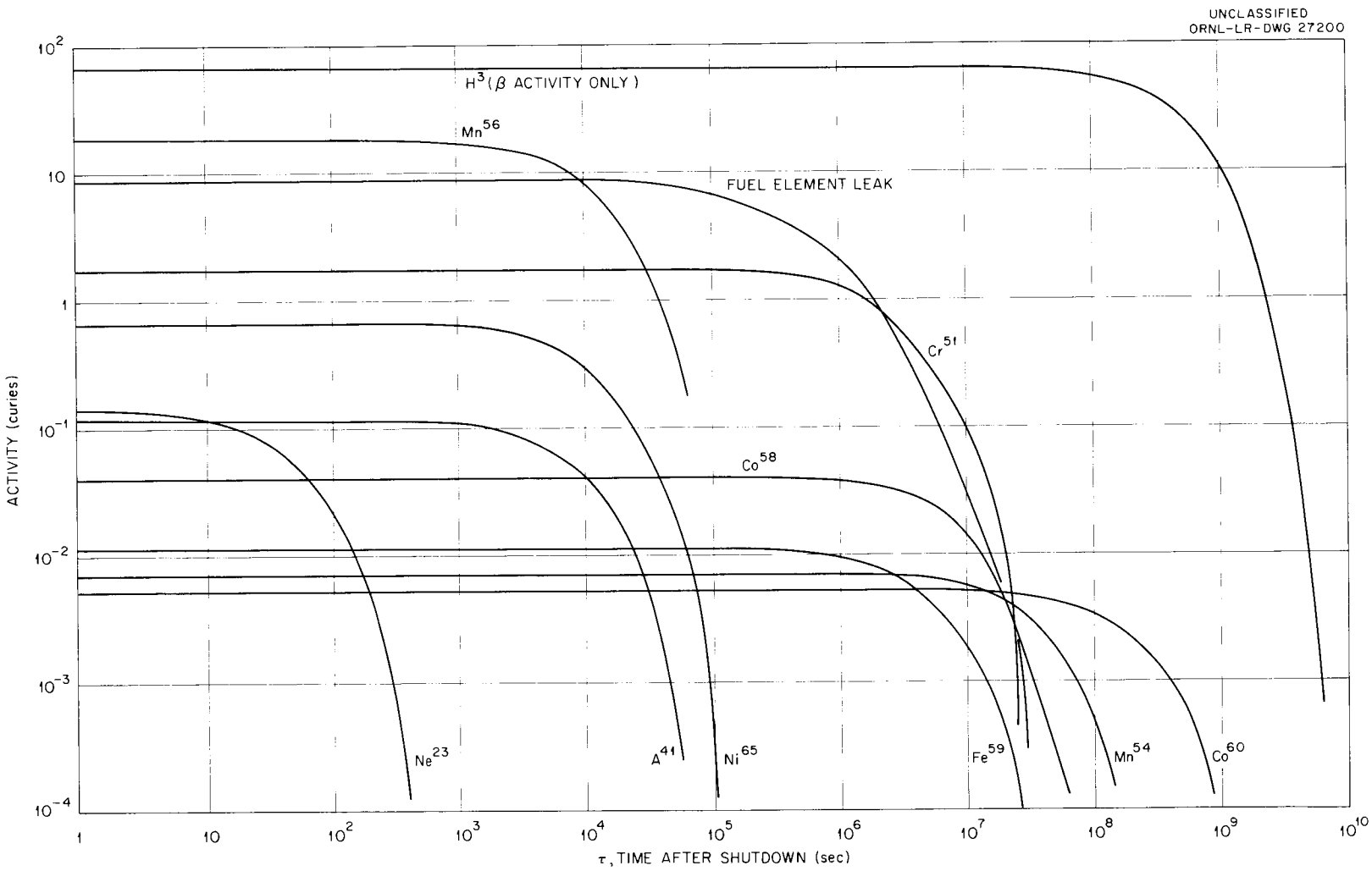

Fig. 13.9. After Shutdown Activities in Gas System.

important to know where the nuclides will collect in the system, as well as what fraction will be removed by each process. In the absence of any experimental data, the activity assigned to each heat exchanger was 25% of the total system activity with no filter in the system. This further implies that the fission products and recoil atoms will collect on the heat exchanger tubes and shell in preference to the moderator, fuel elements, or pipes.

In order to determine the dose at a heat exchanger, the important gamma-emitters in Tables 13.5 through 13.7 were tabulated in Tables 13.8 and 13.9 for a system with and without a filter, respectively. As a convenience in calculating the dose outside the steam generator, the data in Tables 13.8 and 13.9 may be grouped by combining activities of like energy to obtain Tables 13.10 and 13.11 for the system with and without the filters, respectively. Assuming the filter system is ineffective in removing activity from the system, the activities as tabulated in Table 13.11 will be important in the total system for various times after shutdown.

The dose at a heat exchanger was also calculated on the assumption that each heat exchanger would have 25% of the activities shown in Table 13.11, and that the activity would be uniformly distributed in the heat exchanger.

The geometry of a heat exchanger is as shown in Fig. 13.10.

The dose at the surface of the steam generator is calculated assuming the activity to be a homogeneous volume source, externally shielded by the shell of the steam generator and with internal self-shielding calculated by homogenizing all the metal (i.e., tubes, etc.) within the shell. Thus, the average metal densities ρ in the economizer, boiler and superheater sections of the steam generator are respectively:

$$\rho\ (\text{economizer}) = \frac{\text{weight of economizer tubes, etc.}}{\text{volume of economizer section}} = \frac{5.25 \times 10^7 \text{g}}{7.1 \times 10^7 \text{m}^3} = 0.74\ \text{g/cm}^3$$

$$\rho\ (\text{boiler}) = \frac{\text{weight of boiler tubes, etc.}}{\text{volume of boiler section}} = \frac{6.40 \times 10^7 \text{g}}{1.065 \times 10^8} = 0.60\ \text{g/cm}^3$$

$$\rho\ (\text{superheater}) = \frac{\text{weight of superheater tubes, etc.}}{\text{volume of superheater section}} = \frac{6.76 \times 10^7}{1.38 \times 10^8} = 0.49\ \text{g/cm}^3$$

TABLE 13.8. PREDOMINANT GAMMA ACTIVITIES AFTER SHUTDOWN (WITH FILTER IN SYSTEM)

Nuclide	Gamma Energy (Mev)	Gamma Activity (photons/sec)				
		Time After Shutdown (sec)				
		0	10^5	10^6	10^7	10^8
		Photons from Recoils				
Mn^{56}	0.845	6.68×10^{11}	3.87×10^8			
	1.81	2×10^{11}	1.16×10^8			
	2.13	1.33×10^{11}	7.7×10^7			
Cr^{51}	0.32	6.25×10^9	6.07×10^9	4.69×10^9	3.5×10^8	
Ni^{65}	1.12	1.07×10^{10}	5.88×10^6			
	1.5	7.24×10^9	3.98×10^6			
	0.37	7.24×10^9	3.98×10^6			
Co^{58}	0.805	1.55×10^9	1.53×10^9	1.39×10^9	5.08×10^8	
Mn^{54}	0.835	2.62×10^8	2.61×10^8	2.55×10^8	2.0×10^8	1.78×10^7
Fe^{59}	1.1	3.34×10^8	3.28×10^8	2.80×10^8	5.68×10^7	
	1.29	2.52×10^8	2.48×10^8	2.11×10^8	4.28×10^7	
Co^{60}	1.33	1.92×10^8	1.92×10^8	1.91×10^8	1.84×10^8	1.27×10^8
	1.17	1.92×10^8	1.92×10^8	1.91×10^8	1.84×10^8	1.27×10^8
		Photons from Fission Products (one capsule leaking)				
Br^{87}	5.4(56%)	2.60×10^6				
	3.0(14%)	6.50×10^5				
Kr^{87}	2.3(25%)	1.72×10^9				
	1.89(25%)	1.72×10^9				
Kr^{88}	2.40(35%)	6.86×10^9				
	2.19(15%)	3.53×10^9				
	1.85(15%)	2.94×10^9				
	1.55(14%)	2.74×10^9				
	1.20(4%)	7.84×10^9				
	0.85(23%)					
I^{135}	1.8(50%)	1.34×10^9	7.38×10^7			
	1.27(50%)	1.34×10^9	7.38×10^7			
Cs^{136}	0.9(100%)	0.34×10^5	8.47×10^5	5.02×10^5		
Ba^{140}, La^{140}	3.0(1%)	5.80×10^7	5.45×10^7	3.09×10^7	1.16×10^5	
	2.5(5.4%)	3.13×10^8	2.94×10^8	1.67×10^8	6.2×10^5	
	1.6(94%)	5.45×10^9	5.12×10^9	2.91×10^9	1.09×10^7	

TABLE 13.9. PREDOMINANT GAMMA ACTIVITIES AFTER SHUTDOWN (WITH NO FILTER IN SYSTEM)

Nuclide	Gamma Energy (Mev)	Gamma Activity (photons/sec)				
		Time After Shutdown (sec)				
		0	10^5	10^6	10^7	10^8
		Photons from Recoil Atoms				
Mn^{56}	0.845	6.85×10^{11}	3.97×10^8			
	1.81	2.05×10^{11}	1.19×10^8			
	2.13	1.36×10^{11}	7.89×10^7			
Cr^{51}	1.32	4.98×10^{10}	4.84×10^{10}	3.74×10^{10}	2.85×10^9	
Ni^{65}	1.12	1.10×10^{10}	6.05×10^6			
	1.5	7.46×10^9	4.10×10^6			
	0.37	7.46×10^9	4.10×10^6			
Co^{58}	0.805	2.94×10^{10}	2.91×10^{10}	2.64×10^{10}	9.65×10^9	
Mn^{54}	0.835	1.99×10^{10}	1.96×10^{10}	1.94×10^{10}	1.52×10^{10}	1.35×10^9
Fe^{59}	1.1	4.09×10^9	4.01×10^9	3.42×10^9	6.95×10^8	
	1.29	3.08×10^9	3.03×10^9	2.58×10^9	5.24×10^8	
Co^{60}	1.33	9.30×10^{10}	9.30×10^{10}	9.26×10^{10}	8.92×10^{10}	6.15×10^{10}
	1.17	9.30×10^{10}	9.30×10^{10}	9.26×10^{10}	8.92×10^{10}	6.25×10^{10}
		Photons from Fission Products per Capsule Leaking				
Br^{87}	5.4	2.60×10^6				
	3.0	6.50×10^5				
Kr^{87}	2.3	1.72×10^9				
	1.89	1.72×10^9				
Kr^{88}	2.40	6.86×10^9				
	2.19	3.53×10^9				
	1.85	2.94×10^9				
	1.55	2.74×10^9				
	1.20	7.84×10^9				
I^{135}	1.8	1.43×10^9	7.89×10^7			
	1.27	1.43×10^9	7.89×10^7			
Ba^{140}, La^{140}	3.0	2.43×10^8	2.28×10^8	1.29×10^8	4.86×10^5	
	2.5	1.31×10^9	1.23×10^9	7.00×10^8	2.62×10^6	
	1.6	2.28×10^{10}	2.15×10^{10}	1.22×10^{10}	4.57×10^7	

TABLE 13.10. PREDOMINANT GAMMA-ACTIVITY ENERGY GROUPS AFTER SHUTDOWN (WITH FILTER)

Gamma Energy (Mev)	Gamma Activity (photons/sec)				
	Time After Shutdown (sec)				
	0	10^5	10^6	10^7	10^8
5.4	2.6×10^6				
3.0	5.9×10^7	5.5×10^7	3.1×10^7	1.16×10^5	
2.5	8.9×10^9	3.5×10^8	1.7×10^8	6.3×10^5	
2.0	3.5×10^{11}				
1.8		5.3×10^9			
1.6			3×10^9	1×10^7	
1.3				3×10^8	2.5×10^8

TABLE 13.11. PREDOMINANT GAMMA-ACTIVITY ENERGY GROUPS AFTER SHUTDOWN (WITHOUT FILTER)

Gamma Energy (Mev)	Gamma Activity (photons/sec)				
	Time After Shutdown (sec)				
	0	10^5	10^6	10^7	10^8
5.4	2.6×10^6				
3.0	2.43×10^8	2.3×10^8	1.3×10^8	4.9×10^5	
2.5	1×10^{10}	1.2×10^9	7×10^8	2.6×10^6	
2.25	1.4×10^{11}				
2.0	3×10^{11}				
1.6		2.2×10^{10}	1.3×10^{10}	4.6×10^7	
1.3		2.3×10^{11}	2.2×10^{11}	1.8×10^{11}	1.2×10^{11}

UNCLASSIFIED
ORNL-LR-DWG 27188

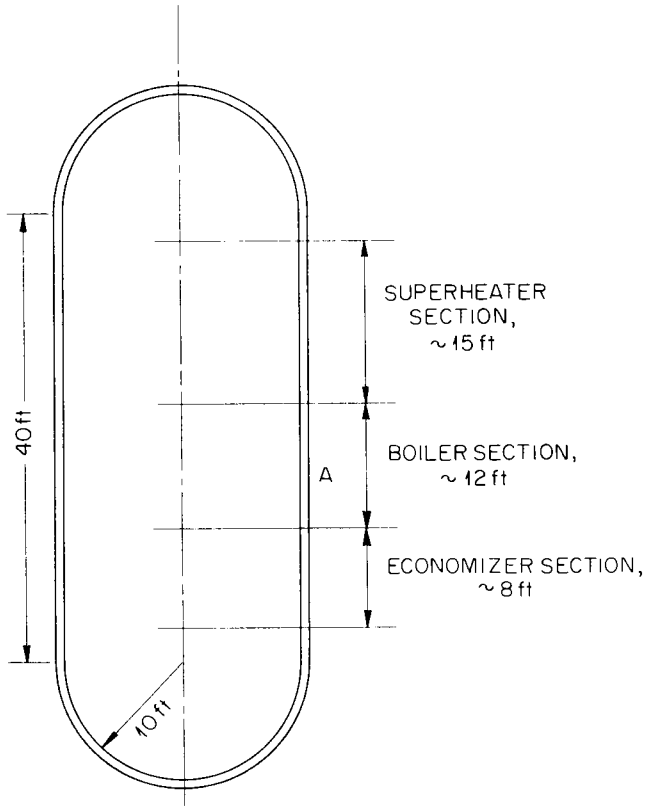

TOTAL VOLUME INSIDE SHELL =

$$\frac{\pi D^2 L}{4} + \frac{4}{3}\pi\frac{D^3}{8} = 1.67 \times 10^4 \text{ ft}^3 = 4.75 \times 10^8 \text{ cm}^3$$

LENGTH OF SUPERHEATER TUBES = 26,880 ft

LENGTH OF BOILER TUBES = 28,283 ft

LENGTH OF ECONOMIZER TUBES = 23,222

VOLUME OF SUPERHEATURE TUBES =

$20(26{,}880) = 537{,}600 \text{ in.}^3 = 8.81 \times 10^6 \text{ cm}^3$

WEIGHT = 6.76×10^7 g

VOLUME OF BOILER TUBES =

$18(28{,}283) = 509{,}090 \text{ in.}^3 = 8.34 \times 10^6 \text{ cm}^3$

WEIGHT = 6.40×10^7 g

VOLUME OF ECONOMIZER TUBES =

$18(23{,}222) = 417{,}996 \text{ in.}^3 = 6.85 \times 10^6 \text{ cm}^3$

WEIGHT = 5.25×10^7 g

$$V_e = \frac{\pi D^2 L}{4} = \frac{\pi (20)^2}{4} 8 = 2510 \text{ ft}^3 = 7.1 \times 10^7 \text{ cm}^3$$

$V_B = 1.065 \times 10^8 \text{ cm}^3$

$V_S = 1.38 \times 10^8 \text{ cm}^3$

Fig. 13.10. Schematic Drawing of Steam Generator.

If all the metal (i.e., tubes, supports, spacers, etc.) inside the steam generator were uniformly distributed, the average density (i.e., including the large plenum regions at the top and bottom) would be ~ 0.4 g/cm^3. However, these plenum regions also lack the surface area for the activity to plate out upon so that the dose calculations were based upon a self-shielding derived from the average metal density in the tube sections of the steam generator for which a conservative value of 0.55 g/cm^3 was used.

Since the source is considered to be a uniform volume cylindrical source containing 25% of the unfiltered activity, the volumes source strength, p, (in photons/cm^3·sec) is:

$$p = \frac{0.25\ P(E)}{3.57 \times 10^8 cm^3}$$

where

P(E) = photons/sec of energy E (taken from Table 13.11)

The calculation is outlined and the terms defined in Fig. 13.11. In these calculations

R_o (radius of cylinder) = 3.05×10^2 cm

a = t (thickness of shell) = 7.62 cm

The results shown in Fig. 13.12 and Table 13.12 indicate that the maximum dose at a steam generator is only 2.57 mr/hr, and this occurs during operation. This dose depends upon the assumptions previously noted, and represents the maximum dose with one fuel capsule leaking. From the data of Table 13.9, it may also be seen that the dose at a heat exchanger will not increase greatly during operation unless more than 10 fuel capsules are leaking simultaneously. This is because the Mn^{56} activity predominates during operation. After shutdown, the dose decreases rapidly since Mn^{56} has a short half-life. After 10^5 sec, the main source of activity is from Co^{60} and Ba^{140}-La^{140}. Since the Co^{60} has the longest half-life, it predominates at long times and, therefore, decreases the importance of the activity from fuel capsule leaks.

13.4.3 Activity in a Single Fuel Element: The gross activity from fission products at time τ is given by,[17]

$$A \approx 1.4\ P\ [(\tau - T_o)^{-0.2} - \tau^{-0.2}]\ \text{curies}$$

[17] Samuel Glasstone, "Nuclear Reactions and Radiations," Principles of Nuclear Reactor Engineering, (New York: Van Nostrand, 1955) p. 120.

UNCLASSIFIED
ORNL-LR-DWG 27187

$$\phi = \frac{Bp R_0^2}{2(a+z)} F(\theta, b_2)$$

WHERE

B = BUILDUP FACTOR

p = SOURCE STRENGTH (photons/cm^3·sec)

R_0 = RADIUS OF SOURCE VOLUME (cm)

Z = EFFECTIVE SELF-ATTENUATION DISTANCE (cm)

a = DISTANCE FROM POINT WHERE DOSE IS BEING DETERMINED TO VOLUME SOURCE (cm)

F = EXPONENTIAL FUNCTION

μ_s = MACROSCOPIC CROSS SECTION OF SOURCE MATERIAL (cm^{-1})

μ = MACROSCOPIC CROSS SECTION OF SHIELD MATERIAL (cm^{-1})

t = THICKNESS OF SHIELD (cm)

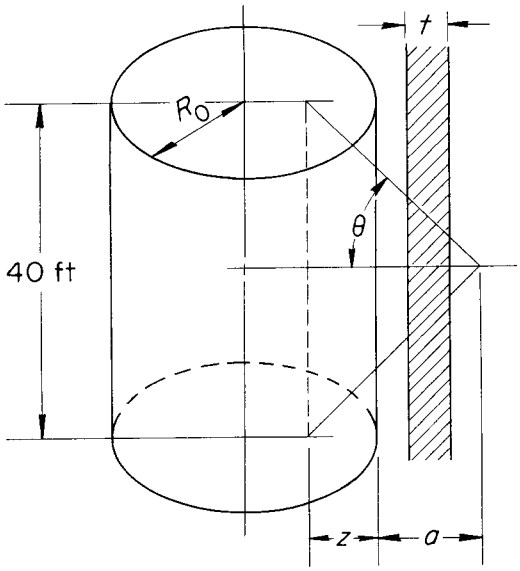

$b_2 = b_1 + \mu_s z$,
$b_1 = \mu t$,
$b_2 = \mu_s z + \mu t$

REF., REACTOR SHIELDING DESIGN MANUAL, TID 7004

Fig. 13.11. Shielding Configuration – Cylindrical Source.

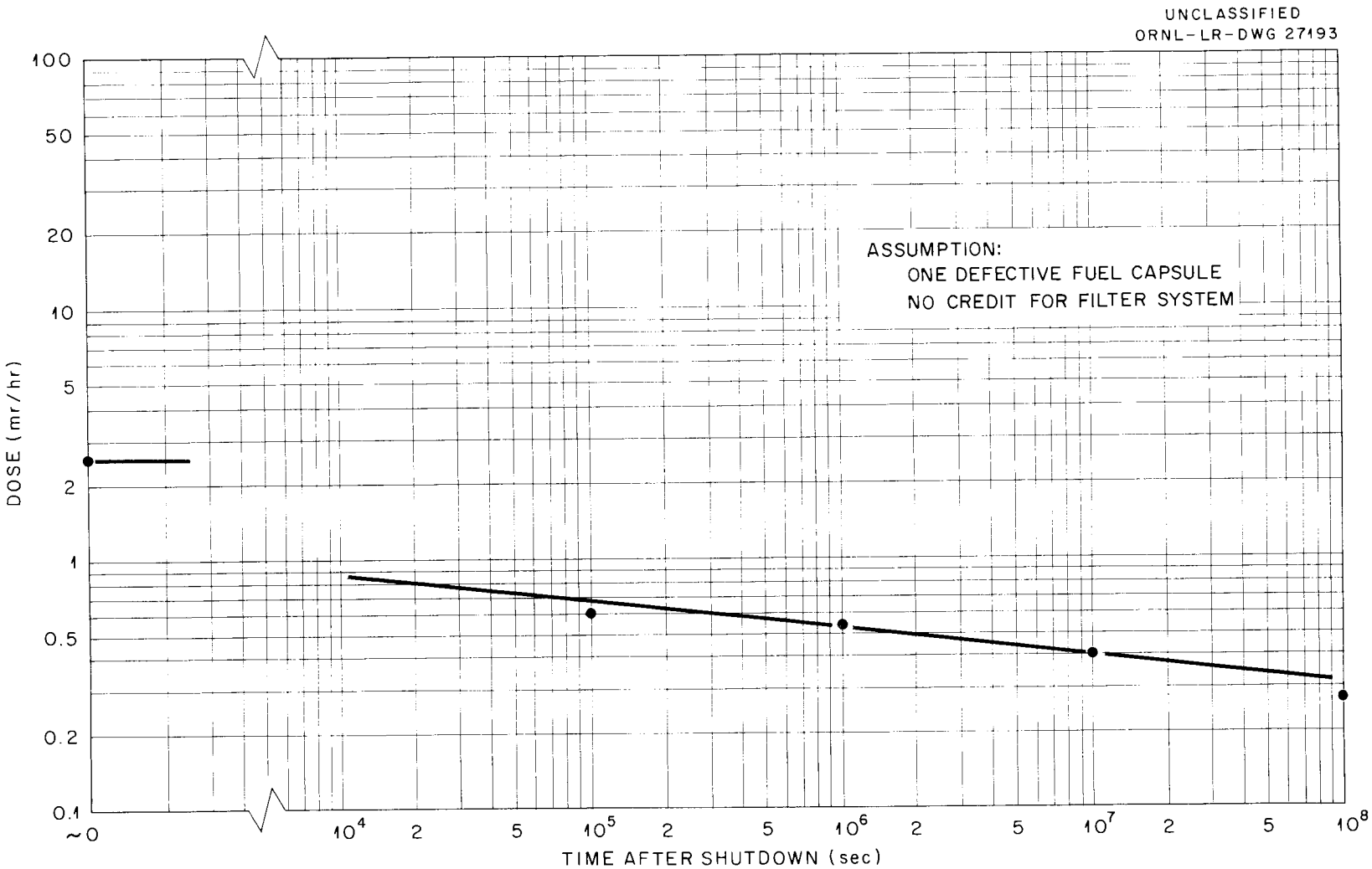

Fig. 13.12. Dose at Steam Generator Surface after Shutdown.

TABLE 13.12. CALCULATION OF DOSE AT A STEAM GENERATOR SURFACE AFTER SHUTDOWN

Gamma Energy (Mev)	p	μ_s	μt	z	$\mu_s z$	b_2	θ	$F(\theta,b_2)$	B	ϕ	Dose (mr/hr)
					At Time = Zero						
5.4	1.82×10^{-3}	0.0181	1.81	162	2.94	4.75	74.4	4.5×10^{-3}	3.30	7.4×10^{-3}	~0
3.0	1.7×10^{-1}	0.021	2.10	150	3.15	5.25	75.5	2.6×10^{-3}	4.5	5.67×10^{-1}	~0
2.5	7.0	0.023	2.30	143	3.28	5.58	76.1	1.85×10^{-3}	5.20	20.8	0.078
2.25	9.8×10^{1}	0.0237	2.37	142	3.37	5.74	76.2	1.5×10^{-3}	5.60	256	0.896
2.0	2.1×10^{2}	0.0247	2.47	139	3.44	5.91	76.4	1.25×10^{-3}	6.0	499	1.6
										Total	2.57
					At Time = 10^5 sec						
3.0	1.61×10^{-1}	0.021	2.10	150	3.15	5.25	75.5	2.6×10^{-3}	4.5	5.37×10^{-1}	~0
2.5	8.4×10^{-1}	0.023	2.30	143	3.28	5.58	76.1	1.85×10^{-3}	5.20	2.5	~0
1.6	1.64×10^{1}	0.0276	2.76	132	3.63	6.39	77.1	7.7×10^{-4}	7.40	33	0.092
1.3	1.61×10^{2}	0.0309	3.09	125	3.85	6.94	77.7	4.3×10^{-4}	8.80	214	0.514
										Total	0.606
					At Time = 10^6 sec						
3.0	9.1×10^{-2}									3.04×10^{-1}	
2.5	4.9×10^{-1}									1.46	
1.6	9.1									18.3	
1.3	1.54×10^{2}									205	
										Total	0.54
					At Time = 10^7 sec						
3.0	3.43×10^{-4}									1.45×10^{-3}	
2.5	1.82×10^{-3}									5.4×10^{-3}	
1.6	3.22×10^{-2}									6.49×10^{-2}	
1.3	1.26×10^{2}									167.5	
										Total	0.402
					At Time = 10^8 sec						
1.3	8.4×10^{1}									111.5	0.268

Symbols:

p = volume source strength, photons/cm^3·sec

μ_s = macroscopic cross section of source material, cm^{-1}

μ = macroscopic cross section of shield material, cm^{-1}

t = shield thickness, cm

z = effective self-attenuation distance, cm

$b_2 = \mu_s z + \mu t$

θ = an angle defined by a, z, and the height of the source such that $\theta = \tan^{-1}[(b/2) \div (z + a)]$

$$F = \int_0^{\theta} e^{-b_2} \sec\theta \, d\theta$$

B = build-up factor

$$\phi = \frac{BpR_0^2}{2(a + z)} F(\theta,b_2) \text{ , photons/cm}^2\text{·sec}$$

where

P = power in watts

T_o = operating time, days

τ = time after start-up days

Since there are about 10,000 fuel elements and the reactor power is 700 Mw, the power per element is 7×10^4 w. Assuming that the reactor has operated (at power) for ~ 10 yr, $\tau^{-0.2} = 0.194$, and

$$A = P\,(1.4)\,[t^{-0.2} - \tau^{-0.2}] = 7 \times 10^4\,(1.4)(t^{-0.2} - 0.194)$$

where t is the time after shutdown in days. One minute after shutdown, $A = 4 \times 10^5$ curies of fission products per fuel element (per bundle of 7 capsules).

13.4.4 Shielding Required by Fuel Charging Machine: Shielding will be required for the fuel elements during the process of removal from the reactor and after they are removed and stored in a cooling pond. The predominant activity was found to be that of La^{140}, since this isotope has both a high yield and a high gamma energy.

The number of La^{140} atoms per capsule after an infinite operating time is a function of the fissioning rate and the yield. Since each fuel capsule produces ~ 10^4 w, the number of fission per second (per capsule) is 13.2×10^{14} which is identical to $\Sigma_f \Phi$.

Thus,

$$N_o^{235} = \frac{\Sigma_f \Phi}{\sigma_f \Phi} = \frac{3.2 \times 10^{14}}{(580 \times 10^{-24})(3 \times 10^{13})} = 2 \times 10^{22}$$

For the case $\Phi = 3 \times 10^{13}$ neut/cm^2/sec, this yields[18]

$$N_s^{140}/N_o^{235} = 2.3 \times 10^{-4}$$

---

[18] J. O. Blomeke and Mary F. Todd, Uranium-235 Fission Product Production, ORNL-2127, Pt. 1, p. 64 (August 19, 1957).

Therefore, $N(La^{140}) = (2.3 \times 10^{-4})(2 \times 10^{22}) = 4.6 \times 10^{18}$ atoms.

The shutdown activity of $La^{140} \cong N_s \lambda_L e^{-\lambda_B t}$ where λ_B is the decay constant for Ba^{140} and λ_L is the decay constant for La^{140}. At t = 0

$$A = \frac{(4.6 \times 10^{18})(6.27 \times 10^{-7})}{3.7 \times 10^{10}} = 80 \text{ curies}$$
$$= 3 \times 10^{12} \text{ dps}$$

La^{140} has the following gamma transitions of importance (> 1 Mev).

Per Cent	Energy	Photons/sec
1	3.0	3.1×10^{10}
5.4	2.5	1.68×10^{11}
94	1.596	2.92×10^{12}

The dose external to a lead shield of 8- and 10-in. thickness was computed for the case of a lead shield of 36-in. ID containing eighteen fuel elements of seven capsules each. The calculations indicated that a 10-in.-thick annular shield would result in a dose of 12 mr/hr and that a 8-in. shield would give 20 mr/hr. Thus, the design of the fuel unloading machine must provide for ~ 8 in. of lead. Were the unloading machine to be designed for only six hot elements at one time rather than the eighteen assumed here, some slight reduction in the required lead-shield thickness could be realized.

13.4.5 Water Level in Fuel Storage Pond: The cooling pond will have to be of sufficient size in order to contain all of the fuel elements in the event that the reactor has to be completely unloaded, and of sufficient depth so that the water above the fuel elements will reduce the dose to tolerable levels. As in the previous calculation, the thickness of the

required shield is determined by the La^{140} activity. Since there are 9600 fuel elements in the reactor, each containing seven capsules, the La^{140} activity of one element is 2.1×10^{13} dps (disintegrations per sec) at shutdown. Since the half-live of the Ba^{10}-La^{14} pair is long, the calculations are made on the basis of this shutdown activity.

Total activity in pond = $(9{,}600)(2.1)10^{13} = 2 \times 10^{17}$ dps.

Assume cooling pool is 100 ft by 25 ft. If the elements are 40-in. high, the volume the fuel occupies is $(100)(25)(\frac{40}{12}) = 8.33 \times 10^3$ ft^3 $= 2.36 \times 10^8$ cm^3.

Assuming a homogeneous source, the source strength will be,

$$S = \frac{2 \times 10^{17}}{2.36 \times 10^8} = 8.5 \times 10^8 \text{ dis/cm}^3\cdot\text{sec.}$$

$p = (8.5 \times 10^8)(10^{-2}) = 8.5 \times 10^6$ photons/cm^3·sec of Mev γ's

$p = (8.5 \times 10^8)(5.4 \times 10^{-2}) = 4.6 \times 10^7$ photons/cm^3·sec of 2.5 Mev γ's

$p = (8.5 \times 10^8)(0.94) = 8 \times 10^8$ photons/cm^3·sec of 1.6 Mev γ's.

The dose at the surface of the water was then calculated as a thick-slab volume heat source by homogenizing the water and fuel in the bottom of the pond (to allow for the self shielding) and determining the required water thickness above the fuel to reduce the dose to tolerable levels. These calculations indicated that the dose at the surface of the water will be 17 mr/hr if there is 104 in. of water above the top of the fuel elements. Since the fuel elements are 40-in. long, a storage pond should have a depth of at least 12 ft of water.

13.5 Removal of Afterheat

Adequate provision has to be made for the removal of fission product decay energy to prevent excessive temperatures in the fuel capsules following any emergency shutdown. A significant feature of the GCR-2 fuel capsule is that both the UO_2 and the stainless steel wall are capable of withstanding a temperature of as much as 2000°F for brief periods, although the peak fuel capsule-wall temperature even in the event of the abrupt loss of all four helium blowers would be less than 1400°F. There

are several processes of heat removal including radiation, convection, and conduction which will be effective in removing the decay energy from the fuel capsules. Heat is transferred by these processes either to the graphite or the gas, or both. Inasmuch as the radiation mechanism is independent of helium system pressure, whereas convection is not, the heat losses through these two principal processes have been examined separately.

Since the graphite represents a large heat sink, radiation of heat to the graphite is alone sufficient to limit the maximum fuel capsule-wall temperature during the initial transient after an abrupt shutdown to less than 1400°F. Thermal convection of the helium will further restrict the maximum temperature excursion caused by afterheat following an emergency. Preliminary calculations presumed that the UO_2 would be in contact with the capsule wall. Although this would almost certainly be true, further calculations have shown that, were this not the case, and even if the pressure vessel were to be ruptured, the resulting temperature excursion to which the hottest fuel capsules would be subject would not cause the capsule wall to melt.

In the calculations which follow, it is assumed that the fuel temperature coefficient drives the reactor subcritical at the start of the excursion. The details of the resultant transient are difficult to analyze rigorously; however, the assumption is certainly reasonable since if there is no temperature rise, there is no excursion; whereas, if there is a rise, the reactor must become subcritical. The situation is further complicated, as in the case when there is a loss of coolant flow, by the blower coast-down. This behavior causes the reactor to operate at decreasing power levels before becoming subcritical, instead of experiencing a step change from 700 Mw(T) to subcritical as assumed above.

Analogue simulator studies may be performed on the various shutdown transients of interest. However, the calculations which have been made demonstrate that even if the gas system is assumed to be evacuated (no forced or convective-gas flow) the after heat may be radiated to the graphite. After several hours, it is desirable to presume some convective heat removal from the reactor in order to limit the maximum average graphite

temperature. It should be noted that this single case covers but does not distinguish between loss of coolant or loss of coolant flow by any of several mechanisms. The resulting transient is quite nominal. Furthermore, the presence of convection will further reduce the excursion from that described by radiation alone, although the excursion, if it were hypothesized that convection were the only heat-removal process, would be much more severe. However, such an excursion is impossible to attain: radiation will be the principal mechanism which limits the initial excursion with convection limiting the average temperature rise of the heat sink (i.e., graphite).

The reactor gas system has been designed to permit the required convective circulation. The amount of circulation is sensitive to the relative heights of the reactor and steam generator, as well as to the piping and any restrictions (i.e., valves). It should be noted that when a blower is off, the normal position of the valve is closed. Appropriate interlocks will be provided to keep the valve open, or to open all gas valves, should a power failure occur for all four blowers.

The removal of afterheat is contingent also upon the capacity of the heat sink. So long as the hot well and boiler feed pumps are operating this is no problem. In the event of station power failure, however, special pumps operated by the emergency power system will pump water from the cold well reservoir to the steam generators, where the decay heat produces steam which is dumped at low pressure.

13.5.1 Shutdown Heat Generation: The afterheat as a function of time after shutdown is given for an infinite operating time by the following expression:[19]

$$P(t) = P_o \, 5.7 \times 10^{-2} \, t^{-0.2} \qquad (13.1)$$

where $P(t)$ is the afterheat at time t in watts, P_o is the operating power level in watts, and t is the time after shutdown in seconds. This expression includes both beta and gamma energies, and its use in the following calculations for the heat to be removed from the fuel is conservative since most of the gamma photons will be absorbed in the

[19] Glasstone, op. cit., p. 119.

graphite rather than in the fuel. Both the above expression and its integral are shown in Fig. 13.13 as a function of time after shutdown, normalized to an operating power of one watt.

In addition to afterheat, there will be a finite source of heat arising from the power produced by the delayed neutrons as they decay after the reactor is subcritical. However, if it is assumed that the reactivity is reduced at a rate of 0.1% Δk/sec, this power production rate is only 10% of that of the afterheat at one second and decreases rapidly so that at 20 sec it is only 1% of the afterheat generation rate. Actually, the fuel temperature coefficient will bring the reactor subcritical at a much faster rate than the rods so that the contribution of this heat source has been neglected in the following studies.

13.5.2 Position of Steam Generators Relative to Reactor: In case of a blower failure, it is desirable to remove the afterheat following shutdown by means of natural convection. This can be affected by installing the steam generator so that its centerline is above the centerline of the reactor core.

Figure 13.14 shows the necessary difference in elevation of the centerlines of the steam generator and the reactor to insure sufficient natural convection to remove 2.3×10^7 Btu/hr afterheat with a reactor outlet temperature of 950°F and an inlet temperature of 450°F. The difference in elevation for other heating rates may be obtained from Fig. 13.14 by means of the following relationship:

$$\left(\frac{\Delta h_1}{\Delta h_2}\right)^{1/2} = \frac{Q_1}{Q_2}$$

As it was desired to have convective circulation remove the afterheat for the generation rate after not longer than 1.5×10^3 sec, a difference in elevation between the centerlines of the reactor and steam generator of 16 ft was chosen. This should be regarded as a minimum difference in elevation and further increase would improve the convection heat removal.

13.5.3 Removal of Afterheat by Radiation: The transfer of heat from the fuel capsules to the graphite is virtually independent of the helium system pressure; thus, the temperatures attained by the fuel

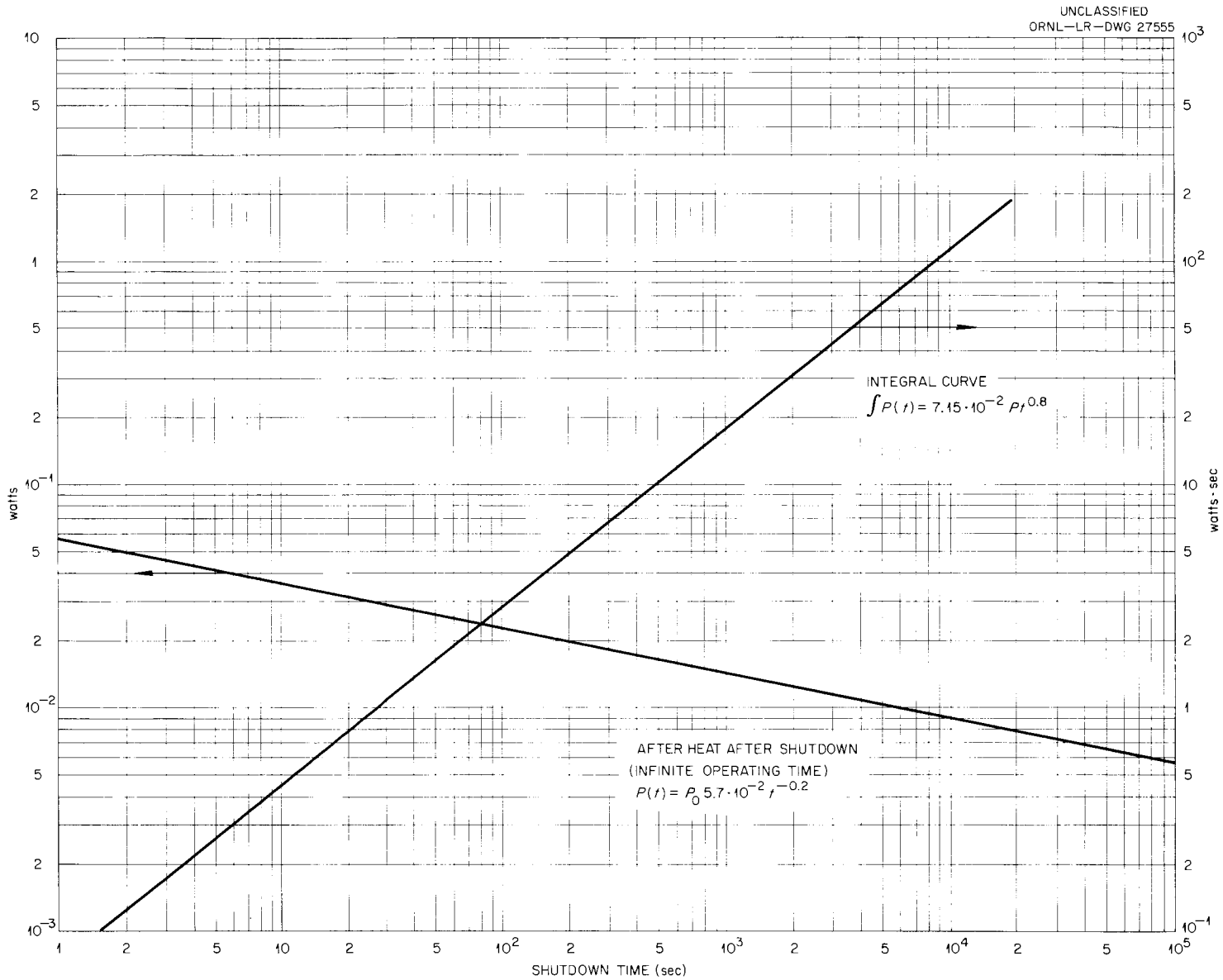

Fig. 13.13. Afterheat as a Function of Time after Shutdown.

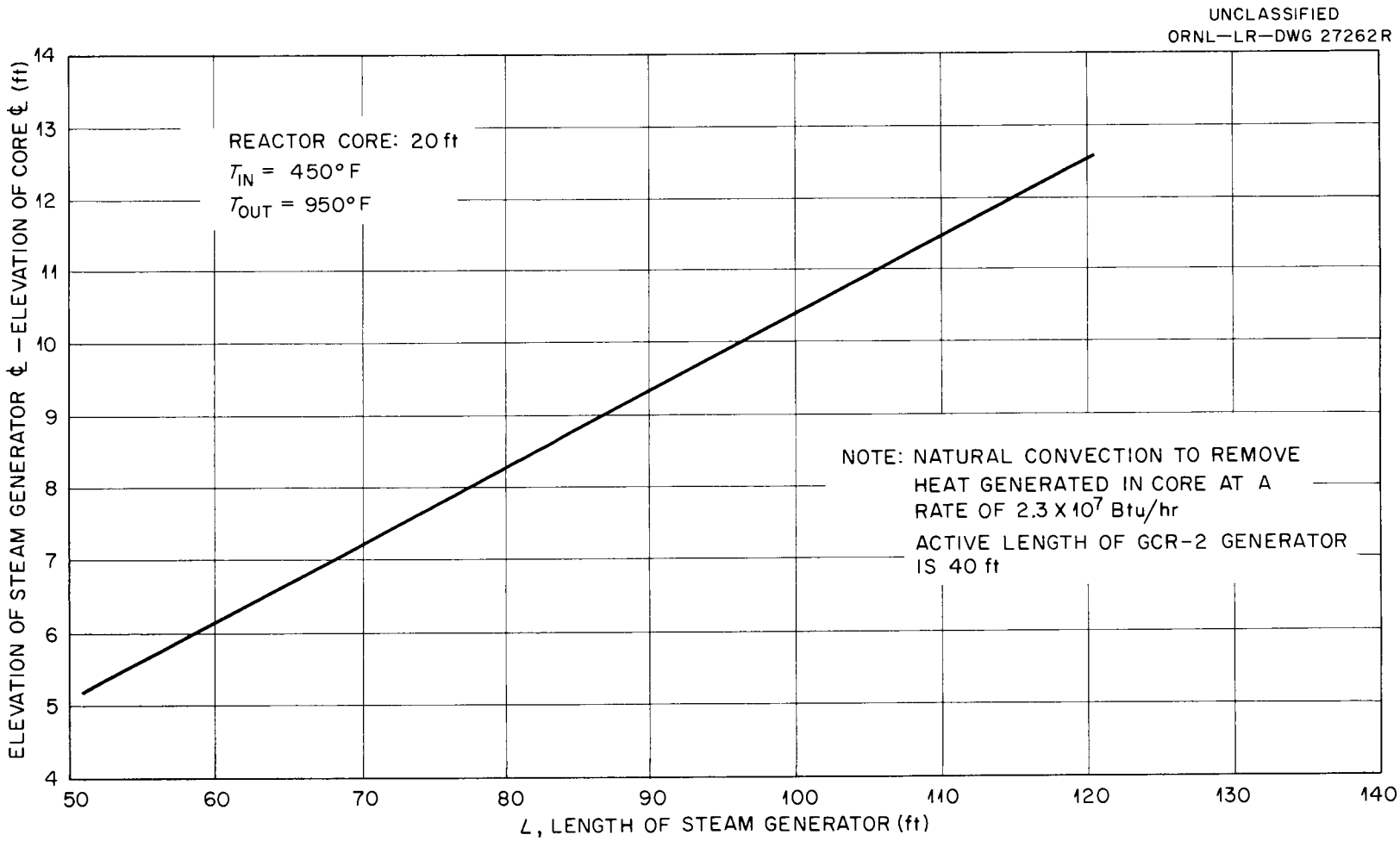

Fig. 13.14. Elevation of Steam Generator Relative to Reactor Core.

capsules when losing heat by radiation only may be regarded as an upper limit. In this situation it was assumed that:

1. No gas flow (it is immaterial to this calculation whether because of a station power failure, simultaneous blower failures, simultaneous valve failure, or complete loss of all coolant).
2. The reactor was shut down. Since the rods cannot be dropped in, it is assumed that the fuel temperature coefficient will hold the reactor subcritical until the rods take over.
3. The fuel capsule wall is collapsed on the UO_2.
4. The residual heat in the UO_2 is removed by the gas which estimates indicate will circulate for approximately 2 min at diminishing flow as the blowers coast to a stop.

On this basis, a calculation has been made of the temperature of the fuel and graphite after shutdown with no convective heat losses for the hottest fuel capsule. The afterheat raised the fuel capsule temperature to 1355°F at which value the heat radiated by the fuel to the graphite is equal to the afterheat generation rate. The local graphite temperature will rise as it absorbs this radiant energy; however, in time this energy will be conducted away to colder portions of the graphite and cause a more or less uniform rise in the bulk temperature.

Figure 13.15 shows the fuel capsule surface temperature and the graphite surface temperatures at two points in the reactor as a function of time after shutdown. The two points chosen were: (1) the point of maximum fuel capsule surface temperature in the center channel at steady-state operating conditions, and (2) the center of the reactor, which is the point of maximum heat flux.

The geometrical view factor (to account for line-of-sight blockage of graphite surface by adjacent capsules) was determined graphically and was found to be 0.521 for the outer six capsules and about 0.115 for the central capsule. To insure a conservative result, it was assumed that the heat generated in the central capsule was radiated to the outer capsules. The heat generated in the outer capsules plus that absorbed from the central capsule is then radiated to the graphite.

The fission product decay energy converted to heat in the fuel was taken as 6/7 of the total while 1/7 was considered to be transmitted to

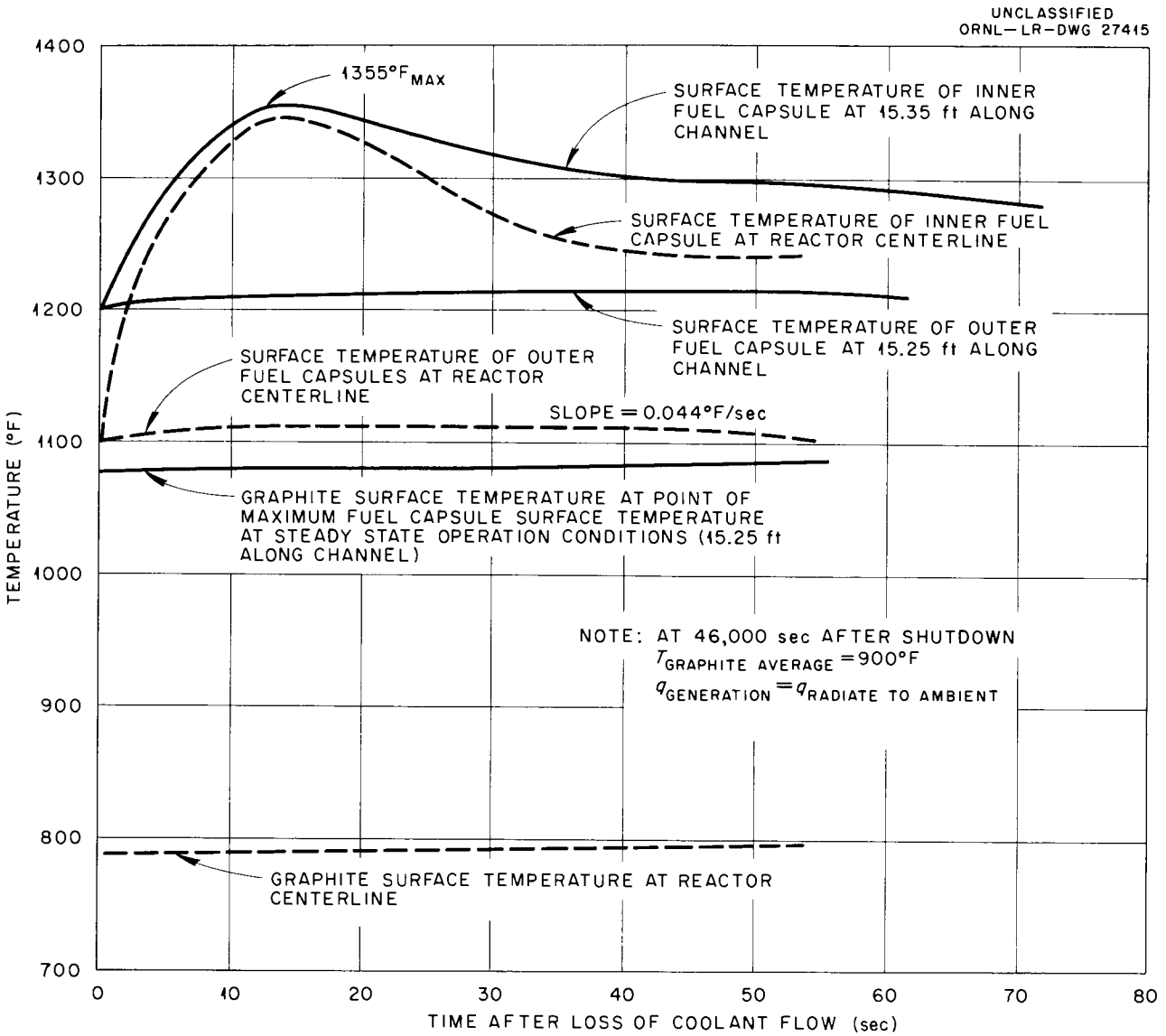

Fig. 13.15. Fuel and Graphite Surface Temperatures Assuming Afterheat Dissipated by Radiation.

the graphite by gamma radiation. The difference between the heat transferred to the graphite and the heat generated in the fuel capsule will cause the fuel capsule temperatures to rise. In turn, these higher temperatures will allow more heat to be radiated to the graphite. A maximum temperature will be reached in 13 sec, at which time the heat-radiation rate will be equal to the heat-generation rate. After this time, the capsule temperatures will decrease as a consequence of the decreasing heat-generation rate.

The maximum fuel capsule surface temperature in the hottest zone, which is about 15.25 ft from the channel inlet, was found to be about 1355°F. The peak fuel capsule temperature at the center of the reactor was 1345°F.

It can be seen in Fig. 13.15 that the graphite temperatures changed very little in the short time required for the fuel capsule to reach the peak. If no other mechanism of heat removal existed, the graphite temperature will continue to rise and with it the temperature of the capsule. Since the pressure vessel is surrounded by 4 in. of insulation, no significant quantity of heat will be radiated by the pressure vessel, although the mass of metal in the pressure vessel will lower the rate of graphite temperature rise. At the end of 2000 sec if all the afterheat is assumed to have been absorbed by the graphite, the graphite temperature will have risen approximately 50°F. Even if the pressurized helium were displaced by atmospheric air, convection circulation of the air will be adequate to remove the afterheat at the rate it is being generated at this time. Thus, even in the event of a large-scale pressure vessel rupture (see further discussion below), the mean temperature rise of the graphite will be not more than 50°F. Furthermore, should the excursion be initiated by the closure of the gas valves, there will be adequate time (> 30 min) to manually open the valves.

13.5.4 Removal of Afterheat by Convection Circulation: The temperature excursion to which the fuel capsule would be subjected if thermal radiation were the only mechanism of heat dissipation, was shown in 13.5.3 to be tolerable. In addition, appreciable quantities of heat are also removed

by convective circulation. As previously noted, this mechanism is dependent upon the system pressure and gas composition. The temperature transients to which the fuel capsules and the gas would be subjected in the event of the loss of all four helium blowers are of interest for a number of situations including the following:

1. Convective circulation of 300 psia helium.
2. Convective circulation of gas with a large leak causing the gas system to lose pressure rapidly.

Inasmuch as the temperature transients in the first situation will be much less severe than the second, the latter has been examined in detail with no credit taken for the thermal-radiation heat losses. In the subsequent calculations the following relationships are used:

a. Heat generation rate [Cf. Eq. (13.1)]

$$q(\theta) = q_o \left(5.7 \times 10^{-2}\ t^{-0.2}\right) \tag{13.2}$$

where $q(\theta)$ is the heat-generation rate (watts) at time θ, q_o is the initial heat-generation rate, and θ is the time after shutdown in seconds.

b. Pressure leak in the system

$$\frac{p(\theta)}{p_i} = e - c_d \left[\frac{A}{Q}\right] \sqrt{2g_c RT\left(\frac{k}{k-1}\right)(p_{r,cr})^{2/k} - (p_{r,cr})^{\frac{k+1}{k}}} \tag{13.3}$$

This equation was derived from the equation for gas flow:[20]

$$\frac{W}{a} = c_d \sqrt{\frac{2g_c k}{k-1}\ \frac{p_o}{v_o}\ \left(\frac{p}{p_o}\right)^{2/k} - \left(\frac{p}{p_o}\right)^{\frac{k+1}{k}}} \tag{13.4}$$

where,

$p(\theta)$ = system pressure at time (θ), lb/ft^2

p_i = initial system pressure, lb/ft^2

c_d = discharge coefficient

A = area of opening, ft^2

Q = volume of system, ft^3

g_c = 32.2 = conversion constant, $ft/sec^2 \left(\frac{lb\ mass}{lb\ force}\right)$

k = c_p/c_v = specific heat ratio = 1.66 for helium

---

[20] O. A. Mooney, Mechanical Engineering Thermodynamics, (New York: Prentice Hall, Inc., 1953).

ν_o = specific volume in system; ft^3/lb

p_o = pressure in system, lb/ft^2

p = pressure at nozzle throat, lb/ft^2

$p_{r,cr}$ = critical pressure ratio; $\left(\frac{p}{p_o}\right)_{cr}$ = 0.4875 for helium

Note: Equation (13.2) holds until the pressure in the system reaches approximately 30 psia,then the pressure will decrease more slowly.

c. Pressure differential due to buoyancy[21]

$$= \Delta P_b = \frac{\beta_o \rho_o \; g \; Z(t - t_o)}{g_c} = \frac{\beta_o \rho_o \; g \; Z(\bar{q}_{He})}{g_c \; c_p \; \bar{w}} \qquad (13.5)$$

where,

ΔP_b = pressure differential due to buoyancy, lb/ft^2

β_o = coefficient of thermal expansion, $\frac{1}{^oR}$

ρ_o = cold leg (helium inlet) density, lb/ft^3

g = acceleration due to gravity, ft/sec^2

g_c = 32.2, conversion constant, $ft/sec^2 \left(\frac{\text{lb mass}}{\text{lb force}}\right)$

Z = difference in elevation of centerlines of steam generator and reactor - ft

t = coolant outlet temperature, °F

t_o = coolant inlet temperature, °F

$\bar{q}_{He}$ = average heat transferred to coolant, Btu/hr

c_p = specific heat of coolant, Btu/lb °F

$\bar{w}$ = average flow rate of coolant, lb/hr

d. System flow resistances

$$\Delta P_R = W_T^2 \left[k_1 \left(\frac{T_H}{T_{H_i}}\right) + k_2 \left(\frac{T_c}{T_{c_i}}\right) + k_3 \left(\frac{T_{m_c}}{T_{m_i}}\right) + k_4 \left(\frac{T_{m_c}}{T_{m_i}}\right) \right] \frac{p_i}{p\theta} \qquad (13.6)$$

[21] C. F. Bonilla, Nuclear Engineering, (New York: McGraw-Hill, 1957).

where,

ΔP_R = pressure drop, lb/ft^2

W_T = total flow rate, lb/hr

T_H = coolant outlet temperature, °R

T_{H_i} = initial steady-state coolant outlet temperature, °R

T_c = coolant inlet temperature, °R

T_{c_i} = initial steady-state coolant inlet temperature, °R

T_{m_c} = mean coolant temperature in core and steam generator, °R

T_{m_i} = initial steady-state coolant mean temperature, °R

p_i = initial steady-state system pressure, psia

$p\theta$ = system pressure at time θ, psia

k_1 = resistance coefficient of flow path from core to heat exchanger (hot), $hr^2/ft^2 \cdot lb$

k_2 = cold-leg resistance coefficient, $hr^2/ft^2 \cdot lb$

k_3 = core resistance coefficient, $hr^2/ft^2 \cdot lb$

k_4 = the heat exchanger resistance coefficient, $hr^2/ft^2 \cdot lb$

k_1, k_2, k_3, k_4 were obtained as shown in Section 6.

e. Coolant outlet temperature (symbols as above)

$$t = \frac{q}{w_{cp}} + t_o$$

f. The fuel capsule surface temperature was found in a manner similar to that explained in Section 3, once the flow rates and coolant inlet and outlet temperatures were found.

It was assumed that the following events occurred simultaneously:

1. All four blowers stopped, either because of a station electrical power failure or simultaneous blower failures.
2. A rupture equivalent to a one-square-inch area hole existed in the pressure system.

3. The reactor was shut down. Again it was assumed that the temperature coefficient will be effective in bringing the reactor subcritical.
4. The fuel capsule wall is collapsed on the UO_2.
5. The residual heat in the UO_2 as well as the initial afterheat for two seconds after shutdown would be removed by the gas stream which continues to circulate by the inertia of the blowers; (a reasonable approximation since the blowers will not come to rest for about 2 min after the power is interrupted.
6. All afterheat generated more than 2 sec after shutdown is then removed by natural convection assuming the steam generator to be an infinite sink.
7. The initial conditions assumed were as follows: time - 2 sec after shutdown; reactor inlet temperature - 450°F; the reactor outlet temperature is assumed to be that as required to force the convective circulation to remove heat at the rate it is being generated; helium initial pressure - 300 psia; difference in elevation of reactor and steam generator horizontal centerlines - 16 ft.

Figure 13.16 shows the effects of the assumed incident on reactor gas pressure, maximum fuel capsule surface temperature and maximum coolant outlet temperature as a function of time after shutdown.

Inasmuch as the temperatures were assumed to be those required to make the convective heat removal and afterheat generation rates equal, no credit was taken for the quantity of heat which will be absorbed by the fuel capsules. Thus, while convection alone would result in undesirably high-fuel capsule-wall temperature, the actual capsule-wall temperature will be limited by radiative process to significantly lower temperatures as discussed in the preceding paragraph and indicated by the dotted line in Fig. 13.16.

With no allowance for radiation, the temperatures would reach a peak within a few seconds after shutdown, the coolant outlet and maximum fuel capsule surface temperature would decrease for the first several minutes after shutdown, while the afterheat generation rate dropped and the system

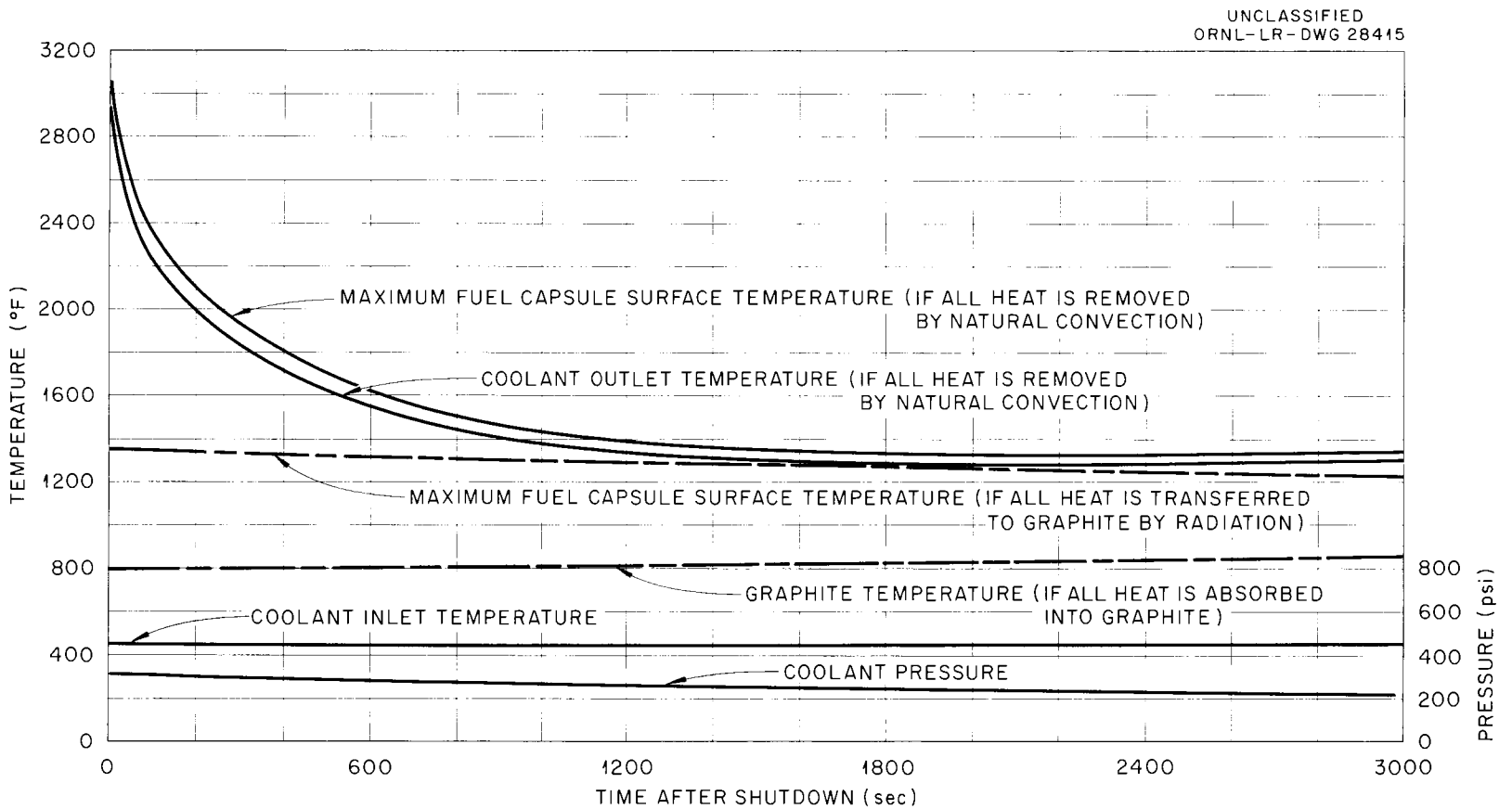

Fig. 13.16. Fuel and Helium Temperature Assuming Afterheat Removed by Thermal Convection Circulation of the Gas with a Pressure Vessel Leak.

is still highly pressurized. At about 500 sec after shutdown, the heat removal capacity will have decreased with the decreasing pressure, and the temperatures will begin to level off. As the system pressure continues to decrease, the heat removal by thermal convection of the helium will decrease, and the temperature rise of the gas through the reactor will begin to increase. A maximum temperature will occur when the system reaches atmospheric pressure at about 5 hr after shutdown. The plant operator has one variable under control in that he can manipulate the steam system to reduce the helium inlet temperature, which would increase the heat removal capacity of the gas because of the increased inlet density. Thus, the outlet temperature decreases more than the inlet temperature. The heat removal requirement at about 1000 sec after shutdown is less than 0.005 times its normal operating value. The amount of steam generated could easily be dumped into the condenser. Thus, the afterheat curve levels off and the system pressure continues to decrease, at times beyond that shown in Fig. 13.16, the helium outlet temperature will rise. This effect can be partly counteracted by further decreasing the helium inlet temperature to a minimum practical value of around 200°F. However, by the time this rise occurs the heat generation rate is but a small fraction of its initial value and the heat that cannot be dissipated by convection at the reduced pressures will be transferred to the graphite by radiation at temperatures considerably below the peaks indicated in the preceding paragraph.

It should be noted that, in the case described in Fig. 13.16, the helium system was assumed to decrease to atmospheric pressure over a period of several hours. Faster leakage rates would decrease the thermal convection heat removal,and, for the extreme case, temperatures would approach those given earlier for thermal radiation only. With no leakage the temperature would continue to decrease with time.

13.5.5 Afterheat Removal with Ruptured Pressure Vessel: A burst-type rupture of the pressure vessel will cause the helium system to approach atmospheric pressure within a fraction of a second. In this event, convective circulation of the gas will remove smaller quantities of heat; moreover, the circulation of the gas as the blowers coast to a stop will

be insufficient to remove the residual heat in the fuel, with the result that higher fuel capsule-wall temperatures will occur.

However, assuming that the capsule wall remains in contact with the oxide after the shutdown, the maximum temperature reached by the capsule wall would be that calculated above for thermal radiation alone, plus the difference in the mean temperatures of the oxide and the wall. Since the mean oxide temperature is approximately 300°F above the surface temperature, the initial fuel capsule-wall temperature at shutdown would then be approximately 1500°F.

Should the oxide not remain in contact with the wall when the pressure vessel failed (as might be the case because of the internal fuel capsule pressure), the initial wall temperature would be substantially less than the 1500°F attained above. In either event the subsequent temperature excursion of the capsule wall caused by afterheat would be similar to that described in 13.5.3, but the temperature excursion would be < 300°F higher when allowance is made for increased radiation at the higher temperature.

Although the above cases cover the various situations which are believed to be possible, it is of interest to observe the temperature excursion for the most extreme situation conceivable, i.e., that in which a gap exists between the capsule wall and the UO_2 during operation, so that the temperature of the UO_2 outer surface initially might be 2200°F rather than 1200°F. In this case, it was assumed that there existed a radial gap of 0.005 in. and the gases in the capsule consist of 70% xenon, and 30% helium, since this combination will have a much lower thermal conductivity than pure helium. It was further assumed that the top of the reactor pressure vessel would blow off and a power failure would occur at the same time.

The mechanism of heat transfer is conduction and radiation from the oxide to the stainless steel capsule, and radiation and convection from the capsule surface to the graphite and the gas, respectively. The coolant initially would be helium until the natural thermal convection would replace it with air in about one second. The central capsule radiates heat partly to the outer six capsules and partly to the graphite, while the

outer capsules radiate directly to the graphite. Convective cooling is the same for both.

If the top of the reactor were to blow off, the system would reach atmospheric pressure in about 0.3 sec (helium would flow from the heat exchanger pressure vessels to the reactor during this period).

Figure 13.17 shows the results of this analysis and even for this improbable situation the melting temperature of the capsule wall is not attained. The maximum outer capsule-wall temperature 1987°F is reached in 12 sec. At this time, the maximum central capsule-wall temperature is 2240°F. The temperature of the outside surface of the oxide in the outer six capsules illustrates the fact that the heat removal rate from the oxide to the capsule for the initial temperature conditions is much greater than the afterheat generation, causing an immediate reduction in its temperature.

13.6 Nuclear Excursion

Nuclear excursions are a potential hazard with any nuclear reactor although the consequences vary over a wide range from one reactor to another depending upon the amount of excess reactivity available, the neutron lifetime, the nuclear controls, the temperature coefficient, as well as the heat capacity of the system and the coupling of the reactor to the load. Analytical studies of all these relationships have not been undertaken, but it is immediately evident that the GCR-2 appears to be quite favorable on all of the above counts. Neither the reactor control system nor the various nuclear excursions can be specified in detail until analogue simulator studies of the reactor and control system have been completed. Furthermore, at that time rod drive speed, set points, interlocks permissives, and control rate will be established so as to realize a conveniently operable, yet safe, system. In lieu of such information a number of pertinent situations have been examined, based on extrapolation from previous simulator studies or simple relationships; these include potential nuclear excursions following fuel additions, start-up rod withdrawal, rod withdrawal at power, steam leak and the introduction of cold helium into the core.

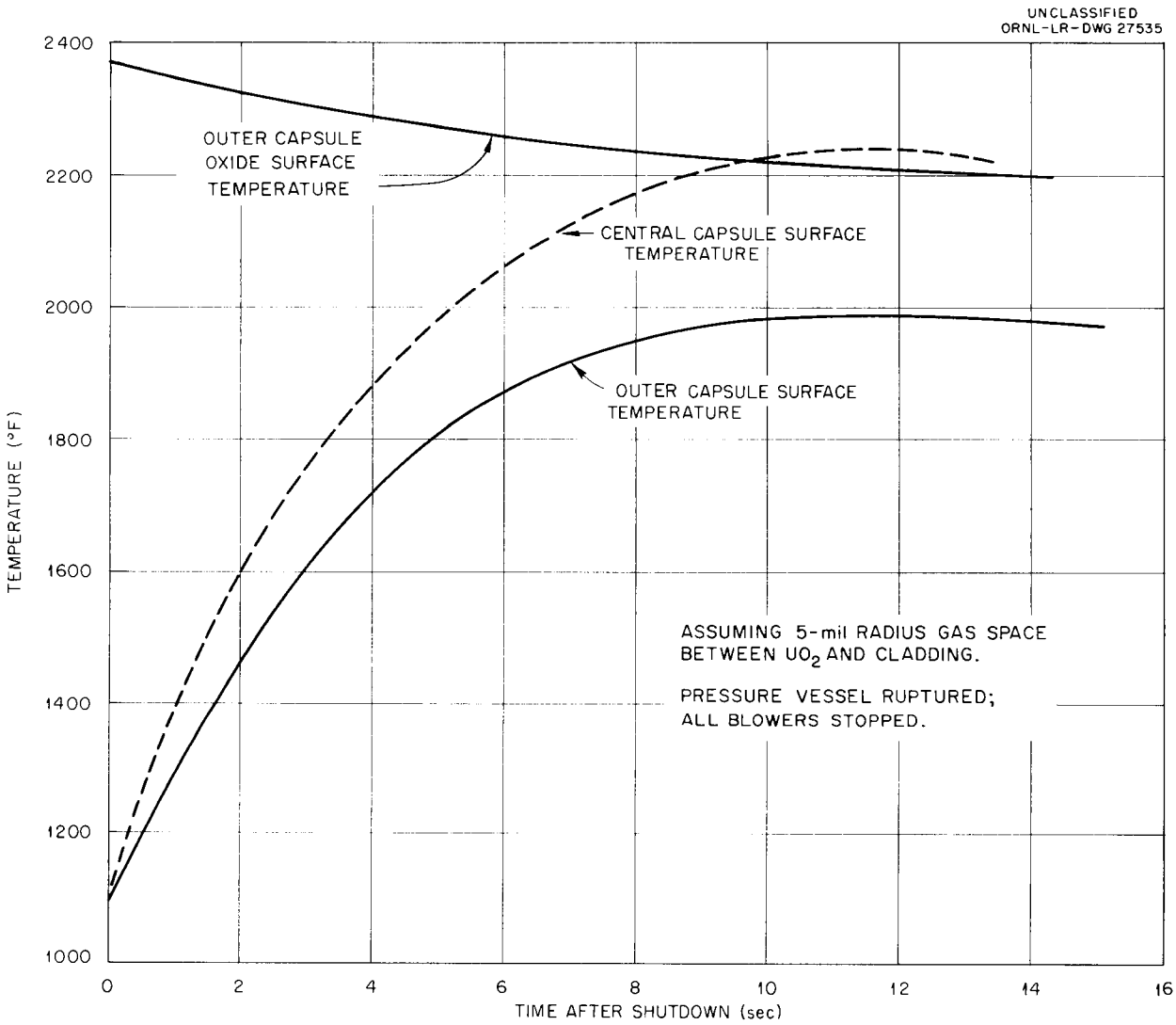

Fig. 13.17. Capsule-Wall Temperature After Shutdown for Worst Conceivable Accident.

Each of these situations is discussed in the light of the philosophy described in Section 7 of the report, namely to provide the "conventional" shutdown protection at low power and a minimum of automatic action at high power, relying in the latter regime on the inherent nature of the reactor supplemented by annunciators to direct the operators attention to any incipient fault. While this philosophy has advantages in any power reactor, it is most suited to the large graphite power reactors in which the heat capacity of the system is so large that the system time constants are long.

13.6.1 Fuel Addition: In any reactor system the possibility exists of adding more reactivity in the fuel than can be compensated for by the negative reactivity in the control rods. While it is not practical to instrument against such an eventuality, administrative control of the loading operation and the critical experiment can preclude any such accident.

In the GCR-2 the control rods have > 5% excess reactivity in the cold, clean reactor. Furthermore, there are about 10,000 fuel elements (each a cluster of seven fuel capsules) so that a $k \cong 1$ the average reactivity in each fuel element is 0.01%. Thus, during the critical loading, the reactor is first charged with the maximum amount of fuel for which it can be proven that the reactor cannot become critical. The rods are then withdrawn and a count taken. If the rods are then inserted, up to 500 fuel elements may be added without danger of taking the reactor critical.

In actual practice the reactor will be loaded outward from the center and the amount of fuel which can be added safely each time will be determined on the basis of the counting rate for the previous loading, the uncertainty in the control rod worth, and fuel element worth. As the reactor approaches criticality the reactivity of fuel elements added at each step will be < 1/10 the negative reactivity available in the rods.

13.6.2 Start-Up Accident: The temperature and power excursions which will result as a consequence of the continuous withdrawal of all the control rods at their maximum rate starting from source power is designated the "start-up accident". As noted in Section 7, Instrumentation and Controls, the rods may be withdrawn at a rate of 0.01% per sec. Since the reactor is initially at < 0.95 multiplication, the continuous withdrawal

of all rods will require over eight minutes to bring the reactor critical. It is felt that this time is about as short as can be allowed if the potential excursions using this withdrawal rate are not to be hazardous.

It is readily apparent that nuclear excursions may be reduced in magnitude if the rate of reactivity addition is reduced, and in the extreme, if the rate is zero there is no hazard since the reactor will not go critical. However, it is believed that prolonged start-up time can be in itself a hazard. If the start-up proceeds too slowly, there will be no perceptable effect on the control instrumentation and this may lead to a loss in the operator's attention.

During all start-ups, the reactor will be protected by automatic annunciation and controls. These protective devices will first annunciate, then stop rod withdrawal, then insert rods at slow speed and finally insert the rods at fast speed if the preceding action was unable to contain the excursion. The excursion may be indicated by any one of the power, period or temperature instrumentation. The set points for each of these automatic actions will be spaced to allow the system to respond to the new condition before imposing another control action. At no time during this regime can the reactor become prompt critical so the insertion of the rods will immediately stop any excursion. Thus, there are a multiplicity of circuits, any one of which would prevent the "start-up accident".

It is of interest, however, to consider the progress of the excursion if none of the automatic protective devices were functioning. The rods are assumed to be continuously withdrawn from source power, 7 w, and the withdrawal is allowed to continue regardless of period, power and temperature instrumentation. At the same time, it must be appreciated that with the number of independent signals provided, any one of which would cause the reactor to shut down, that subsequent withdrawal of the rods is a virtual impossibility. Analogue studies[22] of such transients in a system in which the initial multiplication was 0.9, the neutron lifetime 10^{-4} sec and the rod withdrawal rate 10^{-4} δk/sec, gave the results tabulated in Table 13.13.

---

[22] E. G. Good, Subpower Range Start-Up Transients, WAPD-TM-1 (March, 1956).

TABLE 13.13

START-UP ACCIDENT WITH $\ell = 10^{-4}$ sec; $\delta k/\delta t = 10^{-4}$ sec^{-1}

$\log_{10} n/n_o$	period, sec	δk,%
2	17.0	0.12
4	3.0	0.41
6	1.43	0.52
8	1.0	0.56
10	0.68	0.60
12	0.50	0.64

where n_o is the initial, or source, power level.

The effect of the temperature coefficient is not included in this excursion although it would begin to be felt after about six decades of power increase (i.e., ~ 1% of design). Up to this time the above excursion would be similar to that in the GCR-2 except that the GCR-2 excursion would be somewhat less severe as its neutron lifetime is 1.6×10^{-4} sec and the reactor would become critical sooner because of its higher initial reactivity. Thus, although it would take over 8 min to become critical, the GCR-2 power could increase from 10^{-4}% to 1% in 40 sec (i.e., from $\log_{10} n/n_o = 2$ to 6 from Table 13.13. Even at this time were the operator to insert the rods, the "excursion" would be abruptly terminated with no deleterious effects. It is also pertinent to a consideration of this excursion that even were the reactor power to increase through twelve decades the reactor would not be prompt critical so that insertion of the rods even at that time would bring the excursion to an end.

Were the excursion to be allowed to continue above 1% of design power, again assuming the failure of all protective control instrumentation and no action taken on the part of any of the operators in the control room, the excursion would eventually be slowed down by the fuel temperature coefficient which in the GCR-2 is 3×10^{-5} $\delta k/°F$. Although analogue simulator studies of this particular excursion have not been undertaken as yet, the extrapolation of existing data[23] indicates that the negative temperature coefficient of the fuel will limit the initial power excursion to ~ 300% of design at which time the maximum average fuel temperature would be ~ 2500°F and that of the capsule wall

[23] PWR Hazard Summary Report, WAPD-SC-541, Section 5 (September, 1957).

appreciably less. If still no action is taken, the temperature will subsequently increase at a rate of ~ 4°F/sec and fuel capsule melting will eventually occur.

13.6.3 Continuous Rod Withdrawal at Power: Any time that the reactor is operating at an appreciable fraction of its design power and the control rods are withdrawn, the reactor temperature will increase although the power will remain essentially unchanged. This behavior is characteristic of a power reactor with a negative temperature coefficient. The automatic nuclear excursion protection which was necessary during start-up is a potential source of inadvertent shutdown during power operation which, in addition to the power outages involved, will reduce the fuel element life by unnecessary temperature cycling; therefore, this protection will be inoperative when the reactor is at power. At any time, excessive temperatures will be annunciated and the operator will be expected to act accordingly.

If, however, the four control rods on the temperature servo were to be continuously withdrawn because of equipment malfunction, the reactor temperature would increase at a rate of ~ 12°F per min. If the operator ignored the temperature annunciation from the reactor helium or the steam generator, the rods would withdraw to their upper limit. Since the rods would be operating near their midpoint, the maximum temperature increase would be less than 200°F over a 15-min interval. Additional reactivity could not be automatically inserted into the reactor even if the malfunctioning servo continued to demand it unless the operator made it available by repositioning the control rods.

It is of interest to consider the resulting excursion if, regardless of temperature, the operator were to continuously withdraw all reactor control rods at their maximum rate. The temperature would increase at the rate of 4°F/sec and would continue until fuel melting occurred. It should be noted that in this instance the operator would have had to physically hold a spring-loaded switch in the withdrawn position as the equipment in this circuit is "fail safe". It is felt that this accident would require deliberate sabotage on the part of an operator and that sabotage of this nature could not be prevented by an automatic shutdown

from a temperature signal. Some consideration was given to the use of a mechanical interlock on the rod withdrawal knob which would require resetting after ~ 30 sec of continuous group rod withdrawal, but it did not appear to be warranted.

13.6.4 Reactivity Addition from Steam Leak: A leak in the steam generator could admit steam to the helium system and, in the case of the GCR-2 reactor, would result in an increase in reactivity. However, the increase in reactivity, if the helium were completely saturated with steam, would be only 0.1% k. According to Glasstone,[24] this would correspond to a stable period of ~ 60 sec. If introduced as a step change and no corrective action occurred, a temperature rise of 33°F would occur. Actually some finite time would be required for the steam concentration in the helium to build up, which if not greater than 0.01% k/sec will be matched by the insertion of the rods. It is calculated that the complete rupture of all tubes in one steam generator will not be able to attain this rate. The presence of water in the helium will have been detected by at least one, if not all, of the moisture detectors on each helium loop as well as in the case of the rupture of a large number of tubes, having been observed as an increase in helium system pressure or a decrease in steam pressure. Any of these developments require that the reactor be shut down; although if the leak were small enough, it might be possible to shut down only the leaking steam generator loop.

13.6.5 Cold Coolant Accident: With the reactor critical, the sudden introduction of cold helium into the reactor will cause an increase in reactivity because of the effect of the negative-temperature coefficient. This might conceivably occur in the GCR-2 when the fourth steam generator is placed into operation following a period of operation with only three generators in service. In actual practice the helium in the fourth generator will first be heated up by recirculating the helium in that loop and when the proper (450°F) temperature is attained, the main gas valve will be manually opened gradually to the same position as the valves in the other loops, at which time the control of the valve position will be transferred to automatic temperature servo. For additional information

[24] Samuel Glasstone, "Reactor Theory: Disturbance of the Steady State," Principles of Nuclear Reactor Engineering, (New York: Van Nostrand, 1955) p. 238.

of this operation, see Section 8. If, however, the valve is opened at its maximum rate (3 min) before the helium temperature has been brought up to the reactor inlet condition,the cold coolant situation will exist.

For this analysis it is assumed that the steam generator to be placed in service has cooled to 100°F; the actual temperature will probably be somewhat higher as there is no valve in the hot gas line coupling the reactor and steam generator, so that the resulting two directional convective circulation in that duct would be significant. The 100°F gas in returning to the reactor will first mix with the return helium from the other steam generators as all four loops discharge helium spirally about the periphery of the pressure shell, in order that the gas be well mixed before entering the core). The core inlet gas temperature is reduced 87.5°F, from 450 to 362.5°F. Since the fuel temperature coefficient is 3×10^{-5} δk/°F, the cold helium will be equivalent to 2.63×10^{-3} δk if no credit is taken for the heat capacity of the system. The reactivity will have been inserted at the rate of 8.6×10^{-4} δk/min because of the three-minute valve opening time. This reactivity rate is about twice that available in the four rods on servo so that after three minutes when the valve is fully opened the maximum power excursion will be 137% of design power and > 25 sec period. The excess power will go into heating up the cold loop as well as slightly overheating other parts of the system.

While the consequences of such an excursion are not serious, they may be readily and conveniently avoided by interlocking the valve drive motor so that it cannot be opened until the helium temperature in that loop is within ±20°F of that in the reactor inlet.

13.7 Containment of Radioactivity

The design of the gas-cooled reactor system provides two containment barriers between the fuel and the surrounding area: the first of these is the fuel capsule itself, and the second is the pressurized helium system. Both are discussed in Section 3. In view of the inherent safety afforded by these two containers, the improbability of accidents which would violate them, as well as the fact that a failure of one will not cause a failure of the other, it is not believed necessary to add an additional

envelope to provide over-all containment of the entire system, as has become the practice with power reactors in this country. In view of the interest in an over-all containment vessel, the sequence of events following a postulated rupture of the reactor pressure vessel is discussed, and the resultant dose to the surroundings as a function of the number of leaking fuel capsules in given in 13.8 of this report. While the consequence of such a rupture might prove to be disastrous to the occupants of the building (as is ordinarily the case when the container for any type of reactor is assumed to rupture), the maximum dose to the surrounding area will be less than 25 rem even if 250 fuel capsules are assumed to be leaking (as in the defect case described in 13.2.10), but not melted.

13.7.1 Containment Provisions: As noted in 13.7, the fuel element capsule wall and the pressurized helium system provide the two major containment barriers in the gas-cooled reactor. Although both of these are assumed to have some nominal leakage, the design of the system has provided for safe handling of these leaks so that short of a gross rupture of the pressurized helium system they do not constitute a hazard.

The physical properties of the UO_2-stainless steel fuel element are such that for short periods, it can tolerate temperatures in excess of 1000°F above the normal operating values. (See Section 3) Even more important, this fuel element assembly is not subject to a progressive failure induced by oxidation even if a defect were to develop and if by some means an oxidizing atmosphere were to exist in the system.

The pressurized helium system has been designed for service at 300 psi at system temperature with a factor-of-safety of four. The reactor pressure vessel is spherical (to attain the most favorable structural configuration), and the necessary penetrations of the vessel are conservatively designed and provided with ample room for growth and distortion.

13.7.2 Rupture of the Pressure Vessel: While it is exceedingly unlikely that an abrupt and large-scale rupture or burst of the main pressure vessel would occur in the gas-cooled reactor, it is of interest to examine the consequences of such a rupture. Failure experience with pressure vessels made of a ductile material indicates that in most cases

a crack opens up but a large fragment is not blown out. However, it seems worthwhile to consider this as the worst imaginable case, however remote its likelihood.

If the reactor pressure vessel were to burst, the helium would first expand into the clearance space between the outer perimeter of the spherical pressure vessel and the inside surface of the concrete shielding. The volume available in this region is approximately equal to the total volume of the gas system including the steam generators and piping. (One reason for this is that a substantial proportion of the volume of the reactor and heat exchanger pressure vessels is occupied by graphite, heat exchanger tubes, etc.) The gas escaping from the vessel into the shield would undergo a throttling process so that its temperature would be the same as the average temperature had been in the reactor system, but the pressure level would be reduced to approximately one-half. The shield should be so designed that it will contain adequate steel reinforcing in the form of hoops so that the vertical cylindrical walls of the shield will not rupture, but instead the flat shield cover at the top will blow off. As soon as this cover starts to lift, helium will begin to escape through the annulus between the cover and the cylindrical portion of the concrete. The helium inside of the shield will expand isentropically with the energy going into the kinetic energy of the escaping helium stream. Helium will flow out through the annular opening at sonic velocity.

Table 13.14 presents a quantitative estimate of the sequence of events following this worst possible rupture of the pressure vessel as a function of the time in seconds from the instant of rupture. Values are tabulated for the pressure and temperature of the helium inside the shield, and the weight of helium escaping during each increment of time. The acceleration, velocity and the distance traveled by the top of the shield in a vertical direction are also given. The values at the end of a time interval were used as the conditions prevailing at the beginning of the next time increment.

While these calculations are very rough, they indicate that the bulk of the pressure energy in the helium will be dissipated in eddies in the helium leaving the gap between the cylindrical portion of the shield and the shield cap. Some of the pressure energy will go into accelerating the shield cap

TABLE 13.14. CALCULATION OF KINETICS OF PRESSURE SHELL RUPTURE

Time	Δt	Pressure Inside Shield, p_1	Helium Temperature Inside Shield, T_1	Weight of Helium Inside Shield, W_s	Weight of Helium Leaving Shield During Δt, W_A	Acceleration of Shield	Velocity of Shield Top at End of Increment	Average Velocity of Shield Top During Increment	Distance Lifted During the Increment	Total Distance Lifted	Average Distance Lifted During Increment	Volume Inside Shield	Helium Temperature Inside Heat Exchanger	Helium Pressure Inside Heat Exchanger	Weight of Helium in Heat Exchanger	Weight of Helium Leaving Heat Exchanger
(sec)	(sec)	(psia)	(°R)	(lbs)	(lbs)	(ft/sec^2)	(ft/sec)	(ft/sec)	(ft)	(ft)	(ft)	(ft^3)	(°R)	(psia)	(lb)	(lb)
0	0	93	1200	3540	0	0	0	0	0	0	0	139,240	1200	315	6180	0
0.05	0.05	93	1200	3540	270	141	7.05	3.525	0.176	0.176	0.088	139,488	905	154	4020	2160
0.10	0.05	143	1200	5430	880	252	19.65	13.35	0.6675	0.8435	0.5097	140,680				
			Since the pressure inside the shield ≈ pressure inside the heat exchanger, consider the system as acting together													
0.10	0.05	143	1200	9450	880	252	19.65	13.35	0.6675	0.8435	0.5097	202,680				
0.15	0.05	122	1120	8570	1770	183	28.8	24.22	1.211	2.0545	1.449	205,330				
0.20	0.05	81	952	6800	2310	114	34.5	31.65	1.5830	3.6375	2.846	209,280				
0.25	0.05	39.4	913	4490	1760	22	35.6	35.0	1.75	5.3875	4.512	213,940				
0.3	0.05	16.7	650	2730		−29.8	34.5	35.05	1.75	7.1375	6.262					
1.3	1.0	15	640			−32.2	2.3	18.4	18.4	25.5375						
1.35	0.05					−32.2	0.7	1.5	0.075	25.6125						
1.37	0.02					−32.2	0.05	0.375	0.0075	25.62						

vertically, so that the cap will rise about 25 ft from its initial position and then will fall back. Some pertinent system data are given below:

Initial Conditions

Part of System	Gas Volume (ft^3)	Weight of Helium (lb)
Pressure Vessel	41,240	3540
Steam Generator Loops (4)	72,000	6180
Total System	113,240	9720
Inside Shield	88,000	No Helium present

At time zero, it was assumed that all of the gas in the pressure vessel expands into the area inside the shield. The volume inside the shield (including the volume inside the pressure vessel) is about 139,240 ft^3. The amount of air between the shield and the pressure vessel is not large and its effects on the physical properties of the gas inside the shield were neglected because the over-all effects on the results would be small.

13.7.3 Discussion of Additional Containment: The two containment barriers, i.e., the fuel capsule and the pressurized helium system, are not completely independent (i.e., events which perturb one may also perturb the other) but the failure of one will not cause a failure of the other. It is most significant in this connection to note that the degree of containment provided by the fuel capsule and the helium system is adequate for any disaster which does not both, (1) rupture the helium pressure vessel, and (2) melt a significant fraction of the fuel elements.

Accidents which melt fuel capsules, but which do not rupture the helium pressure system, would raise the activity in the system to uncomfortable levels (whether or not the third container was provided), but would not release excessive amounts of activity outside the system. On the other hand, the rupture of the pressure system would have comparable effects on the building occupants (whether or not a third container was provided), and would result in a maximum exposure downwind of the building of $\sim$ 0.1 rem, if the rupture were to occur at the same time that there was a leaking fuel capsule in the system. This latter exposure could be avoided by the use of a third container, but unless the activity in the system were increased significantly, as by the concurrent melting of a number of

fuel capsules, it would be entirely unnecessary.

The events which seem to be most likely to cause melting of fuel capsule (i.e., nuclear excursions and/or afterheat), have been considered and in all cases have been found to be incapable of producing the required temperatures, principally because of the large heat sink provided by the graphite to which the fuel capsules radiate heat as their temperature increases. As this radiation process serves to limit the temperature of the fuel element, attention is therefore directed to mechanisms by which the graphite temperature may be significantly increased. Two possible mechanisms have been considered, oxidation and stored-energy release, but neither of these appear to be remotely capable of producing the required temperatures; however, it should be noted that there are many uncertainties regarding the intricacies of these processes.

Mechanical damage to a large number of fuel capsules as a consequence of the pressure vessel rupture would of course increase the resulting dose. This possibility is minimized by the design and support of the fuel elements.

While a postulated failure was described in 13.7.2 it should be noted that the pressure vessel is designed with a large safety factor as assurance against just such an incident. Further, if a pressure vessel leak were to occur it would probably take the form of a split rather than the brittle burst assumed, and the resulting loss of pressure would occur at a much slower rate.

Although it is not believed to be necessary for additional containment to be provided, the high velocity of the helium that might be ejected from the shield (initially ~ 4500 ft/sec) raises concern over the possibility that projectiles might penetrate the container. Since 4500 ft/sec is of the order of the muzzle velocity for antitank guns, if an outer containment vessel is deemed necessary, it would appear that a heavy annular belt of armour also should be placed around gaps through which projectiles might be ejected. Even more important, the shield and its various components should be designed so that a piston-cylinder or projectile-gun barrel type of acceleration would not occur. For example, a shield plug in a fuel loading well at the top of the reactor could form such a projectile in the event of a flange failure at the top of the well. Where (as in this

instance) such conditions are hard to avoid, heavy armour plate should be mounted over the reactor to protect an outer containment vessel if one were to be used.

The fluid volume after expansion at constant enthalpy to atmospheric pressure is of the order of 2,000,000 ft^3 for the helium and 200,000 ft^3 for the steam. The volume of a 200-ft-dia sphere would be of the order of 4,000,000 ft^3. Thus, it would appear that the pressure within such a sphere would be increased to approximately an absolute pressure of about 25 psia in the event of the simultaneous ruptures of both the helium and steam systems. This would require a pressure vessel wall thickness of approximately 1-1/4 in. at the top with somewhat thicker walls at the sides and bottom to accommodate the stresses associated with the weight of the vessel walls. As a matter of interest, a layout was prepared to show one way in which the equipment might be arranged within a over-all containment vessel. This layout is shown in Fig. 13.18 and should be considered as very preliminary because the containment vessel would introduce many problems in construction which could not be investigated in the time available.

The containment vessel would also present many problems in the routine operation and maintenance of the plant as it would be necessary to pass through a lock in the vessel wall to reach any of the heat exchanger, blower or reactor equipment.

The addition of a secondary containment vessel to the GCR-2 would impose some additional costs including:

The Containment Vessel
Additional Gas Piping
Additional Steam Piping
Additional Instrument Runs
Supplemental Foundations
Additional Crane Service
Additional Operating Areas

A cost tabulation is given in Table 13.15. Additional overhead and construction fund costs have been included because the containment vessel will add at least six months to the construction period.

A 50% contingency has been added because time was available for only a cursory examination of the problems. Others for which cost allowances were not included in the base estimate are:

UNCLASSIFIED
ORNL-LR-DWG 27427

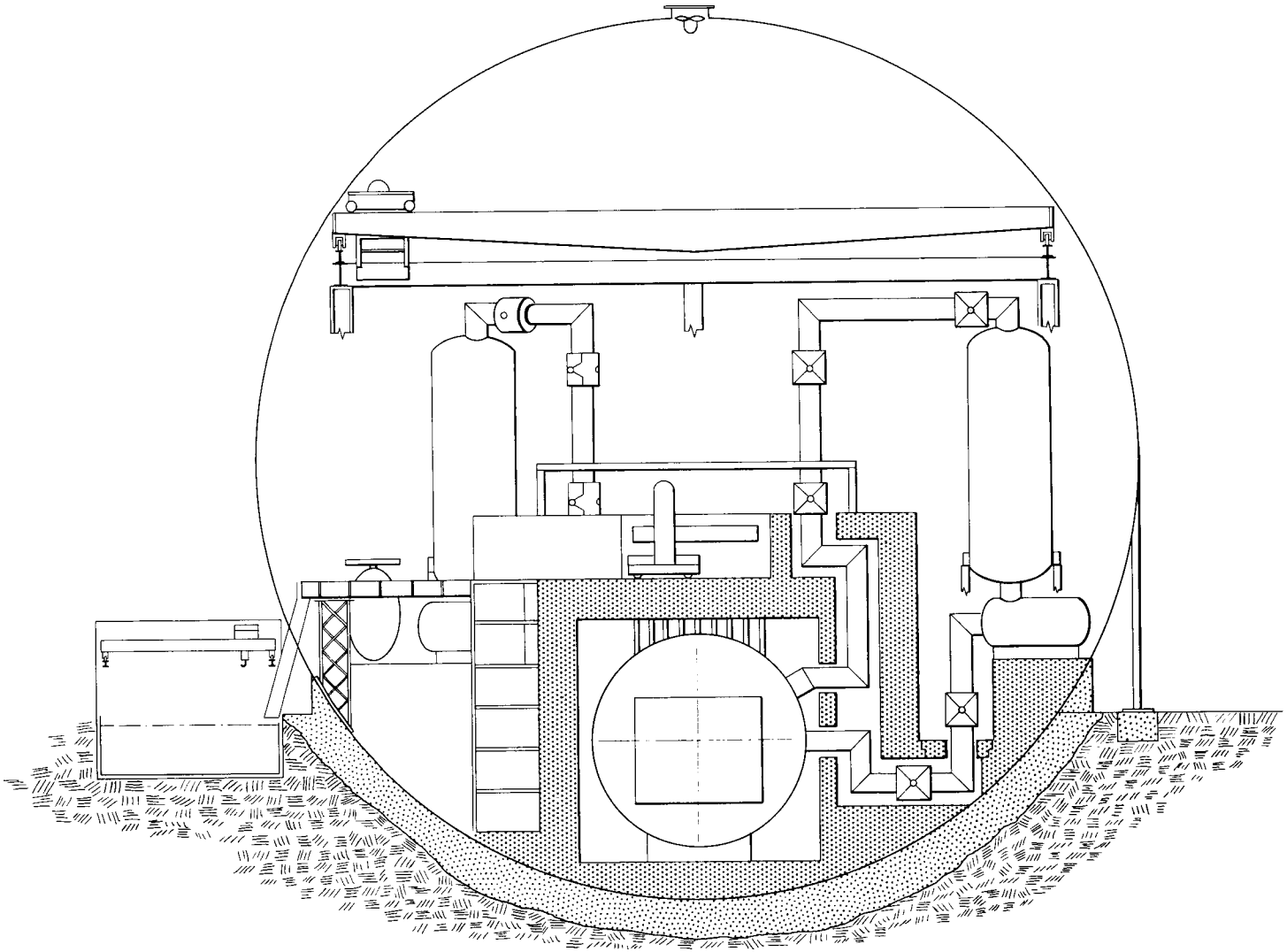

Fig. 13.18. Preliminary Layout for Gas-Cooled Reactor Enclosed by Containment Vessel.

TABLE 13.15

TABULATION OF COST ADJUSTMENTS FOR THE GCR-2 SYSTEM ENCLOSED WITHIN A CONTAINMENT VESSEL

Additional Costs

1.	Containment vessel, 210 ft dia, 3600 t at $ 0.45/lb	$ 3,250,000
2.	Armor plate to protect vessel from missiles	750,000
3.	Piping and supports (169 ft of 6 ft dia hot pipe) (96 ft of 6 ft dia cold pipe)	1,250,000
4.	Bridge crane (100 t - 210 ft span) (two 50 t, one 20 t trolleys)	200,000
5.	Structural steel (50 t at $ 1000/t	50,000
6.	Instrumentation	250,000
7.	Additional building space outside vessel for hot and cold change houses, hot and cold service areas, battery room, air compressor and dryers. 5000 sq ft at $ 20/sq ft.	100,000
8.	Shield cooling Space cooler 600,000 Btu/hr	50,000
9.	Air decontamination equipment	50,000
10.	Extension of construction period $80,000,000 x 6% Int. x 6 mo.	2,400,000
11.	Overhead for 6 mo. extended construction period	1,000,000
12.	Steam system addition	500,000
	Subtotal Additional Costs	$ 9,850,000

Reduced Costs

1.	Eliminate reactor building exterior walls and roof	$ 100,000
2.	Eliminate floor space for equipment moved outside vessel. (See 6 under Additional Costs)	50,000
3.	Eliminate reactor building superstructure and 20 t crane	75,000
4.	Eliminate fuel tunnel	50,000
5.	Eliminate weatherproofing of piping and heat exchangers	50,000
	Subtotal Reduced Costs	$ 325,000
	Total Added Costs	$ 9,525,000
	Total with 50% Contingency	$14,000,000

1. Complications of partial-erection operations inside the containment vessel.
2. Construction interference problems caused by erecting the top of containment vessel after the reactor equipment is installed.
3. Escalation Costs.

With the contingency, the over-all estimate for this plant addition is $14,000,000 which amounts to 1.15 mills/kwh, and added to the over-all power costs in Table 11.11 would give a total escalated power cost of 12.27 mills/kwh.

13.8 Release of Radioactivity

13.8.1 Discharge of Activity up Stack: Radioactivity in the gas stream may be released from the system under three conditions: the first two representing normal operating conditions, and the third condition representing an emergency condition. The stack height was calculated so that the resulting ground concentrations from the two "normal" cases would be less than the maximum permissible values for continuous exposure while that from the emergency case would not exceed 2.5 rem to the bone. After preliminary calculations, the number of leaking fuel capsules which could be tolerated was determined for each condition and a stack height of 150 ft elevation was chosen as adequate. The assumptions for the three conditions are listed below.

For all cases:

a. Radioactivity in the gas stream has reached an equilibrium condition resulting from one leaking fuel capsule, recoil activity from the stainless steel capsule wall, and helium activation.
b. By-pass filters in the main loops have been effective in reducing long-lived activities.
c. Activity is a function of the number of fuel capsules that are releasing fission products.

Case 1 - System Leakage

a. The only activity leaking from the system is in gaseous form (i.e., only tritium and the fission product gases are assumed to escape).

b. Leakage of helium shall not exceed 1%/day, shall be continuous, and shall be swept up the stack by the shield cooling air flow.

Case 2 - Venting

a. System pressure is relieved up the stack at the rate of 1 psi/hr.

b. Escaping activity may be due to either gases or solid atoms circulating in the gas.

c. In the following calculations, credit is taken for the fraction of time the activity is released.

Case 3 - Emergency Pressure Relief

a. The entire gas system is depressurized up the stack in a short period of time and will be considered as an instantaneous release for this case.

A. <u>Normal Discharge of Activity up the Stack</u>.

System volume $V_1 = 1.76 \times 10^9$ cm^3 at 300 psig and 750°F

System volume V_2 at atmospheric pressure and 0°F

$$V_2 = \left(\frac{T_2}{T_1}\right)\left(\frac{p_1}{p_2}\right)V_1$$

$$= \left(\frac{460}{1210}\right)\left(\frac{315}{15}\right)1.76 \times 10^9 = 1.41 \times 10^{10} \text{ cm}^3 \text{ at STP}$$

Case 1

Leakage rate - 1%/day

$$\text{Vol released} = \frac{(1.41 \times 10^{10})(0.01)}{(3.6 \times 10^3)(24)} = 1.63 \times 10^3 \text{ cm}^3/\text{sec at STP}$$

Case 2

Pressure release of 1 psi/hr

$$\text{Vol released} = \frac{1.41 \times 10^{10} \text{ cm}^3}{(300)(3.6)10^3} = 1.31 \times 10^4 \text{ cm}^3/\text{sec}$$

The curies released from the system per second at the stack is equal to:

$$Q_z = \frac{fA_z F}{V_s} \text{ curies/sec}$$

where f is the fraction of isotope passing stack filter, A_z is the equilibrium activity in system (curies), F is the rate of gas release (cm^3/sec), and V_s is the volume of gas in system, (cm^3). From a continuous point source,[25]

$$X_{max} = \frac{2Q'}{\pi e \bar{u} h^2}$$

where X_{max} is the maximum ground concentration for continuous exposure, (in μc/cm^3), Q' is the source strength (curies/sec), $\bar{u}$ is the mean wind speed (meters/sec), and h is the height of source (meters).

Since the allowable concentration of the different isotopes varies, it is necessary, in order to place all the isotopes of interest on the same basis (in this instance all isotopes are compared with Sr^{90}), to take

$$Q_z^* = Q_z \frac{X_{max}\,(Sr^{90})}{X_{max}\,(z)} = \frac{fF}{V_s} A_z \frac{X_{max}(Sr^{90})}{X_{max}\,(z)}$$

where Q_z^* is the source strength of isotope (z) expressed in the equivalent source strength of Sr^{90}. Let

$$Q' = \sum_z Q_z^* .$$

In this instance the X_{max} associated with Q' is that for Sr^{90}. This summation is permissible in examining effects on the same parts of the body. In the following calculations this summation is made for total body dose, dose to the bone, and the iodine dose to the thyroid. Using the summations, the stack height required in order not to exceed the maximum ground concentrations is determined as follows:

$$h^2 = \frac{2 \sum_z Q_z^*}{\pi e \bar{u}\, X_{max}(Sr^{90})}$$

---

[25] Meteorology and Atomic Energy, AECU-3066, Weather Bureau, Washington, D. C. (July, 1955).

$$= \frac{2\sum_z Q_z \frac{X_{max}(Sr^{90})}{X_{max}(z)}}{\pi e \bar{u} X_{max}(Sr^{90})}$$

$$= \frac{2\sum_z fA_z\left(\frac{F}{V_s}\right)\frac{X_{max}(Sr^{90})}{X_{max}(z)}}{\pi e \bar{u} X_{max}(Sr^{90})}$$

The equilibrium activity in the system for the case of H^3 is given by (see 13.4.1)

$$A = \frac{N\sigma\phi\lambda}{\lambda + \frac{\alpha}{T}}$$

where N is the number of atoms/cm^3 of He^3, σ is the cross section for He^3 $(n,p)H^3$ reaction (cm^2), ϕ is the thermal flux (neutrons/cm-sec), λ is the decay constant for H^3 (sec^{-1}), α is the fractional by-pass to filters, and T is the cycle time (sec). From previous calculations shown in 13.2, $A_{H^3} = 67.5$ curies.

The equilibrium activity for the case of fission products leaking into the system is given by:

$$A_z = \frac{2.1 \times 10^{19}\ Y}{(3.7 \times 10^{10})(5.6 \times 10^4)\lambda}\ \nu\left(\frac{\lambda}{\lambda + \frac{\alpha}{T}}\right)(1 - e^{-\lambda t})\left[1-e^{-(\lambda+\frac{\alpha}{T})t}\right]n$$

where Y is the fission yield, λ is the decay constant (sec^{-1}), α is the fractional by pass to filters, T is the cycle time (sec), ν is the escape rate coefficient (sec^{-1}), and n is the number of leaking fuel capsules. For t = 10 yr,

$$\left[1 - e^{-(\lambda + \frac{\alpha}{T})t}\right] = 1.0$$

regardless of λ since $\frac{\alpha}{T} = 2 \times 10^{-6}\ sec^{-1}$. Therefore, at ten years,

$$A_z = \frac{1.01 \times 10^4 Y\nu}{\lambda}\left(\frac{\lambda}{\lambda + \frac{\alpha}{T}}\right)(1 - e^{-\lambda t})n$$

TABLE 13.16. ACTIVITIES IN GAS STREAM IMPORTANT TO INTERNAL DOSE CALCULATIONS DOWNWIND FROM STACK DISCHARGE

Nuclide	Half Life	Decay Const., λ (sec^{-1})	Fission Yield, Y (%)	Escape Rate,* ν (fraction of atoms/sec)	$\frac{\lambda}{\lambda + \frac{\alpha}{T}}$ ($\alpha/T = 2 \times 10^{-6}$)	$(1 - e^{-\lambda t})$ ($t = 10$ yr)	A_z (curies)	X_{max}, Total Body** ($\mu c/cm^3$)	X_{max}, Critical Organ** ($\mu c/cm^3$)	
Cs^{137}	26.6y	8.27×10^{-10}	5.9	1×10^{-7}	4.13×10^{-4}	0.23	6.84 n***	2.2×10^{-8}	3.6×10^{-8}	Muscle
Sr^{90}	28y	7.85×10^{-10}	5.9	7×10^{-10}	3.92×10^{-4}	0.22	4.57×10^{-2} n	3.0×10^{-10}	4.4×10^{-11}	Bone
H^3	12.26y	1.795×10^{-9}			8.92×10^{-4}		67.5	7.4×10^{-6}	5×10^{-6}	Body water
Kr^{88}-Rb^{88}	2.8h	7.0×10^{-5}	3.8	1×10^{-7}	1	1	1.10 n	6.3×10^{-8}		
Xe^{135}	9.13h	2.11×10^{-5}	6.2	7×10^{-8}	1	1	2.08 n	2.5×10^{-6}		
I^{131}	8.05d	9.96×10^{-7}	2.9	4×10^{-8}	0.332	1	3.9 n	2.7×10^{-7}	4.4×10^{-9}	Thyroid
I^{133}	20.8h	9.25×10^{-6}	6.5	4×10^{-8}	0.822	1	2.34 n	1.2×10^{-6}	1.7×10^{-8}	Thyroid
Ba^{140}-La^{140}	12.8d	6.27×10^{-7}	6.3	6×10^{-10}	0.238	1	0.289 n	1.0×10^{-7}	2.0×10^{-8}	Bone
Ce^{144}-Pr^{144}	290d	2.76×10^{-8}	6.1	1×10^{-11}	0.0136	1	6.09×10^{-3} n	1.1×10^{-8}	3.3×10^{-9}	Bone
Y^{91}	58d	1.38×10^{-7}	5.9	2×10^{-12}	0.0645	1	5.56×10^{-4} n	7.9×10^{-8}	1.2×10^{-8}	Bone
Sr^{89}	54d	1.48×10^{-7}	4.8	7×10^{-10}	0.069	1	1.58×10^{-1} n	6.1×10^{-8}	4.7×10^{-7}	Bone

*These values from Sec. 13.2.10, "Leak Through Defect in Fuel Capsule Wall."

**Unpublished data currently believed to be better than data in Handbook 52, U.S. Department of Commerce.

***Where "n" is the number of leaking fuel elements.

An investigation of the activities to be expected from all the fission products, recoil activities, helium activation, and impurity activation was made and the nuclides tabulated in Table 13.16 were proven to be the important ones for the cases under study.

B. Total Body Dose. The total body dose is then obtained from the data in Table 13.15 by calculating the corresponding value of Q_z^* for each isotope and summing the results. Values of Q_z^* for each isotope are listed in Table 13.17 The summation is performed by grouping isotopes into the three cases of interest, H_2^3, fission product gases, and other fission products, as follows:

TABLE 13.17

STRENGTH OF SOURCE, Q_z^*, OF ACTIVITIES IMPORTANT TO TOTAL BODY DOSE

Nuclide[a]	A_z(curies)	Q_z^*(curies/sec)
Cs^{137}	6.84 n	9.34×10^{-2} fFn/V_s
Sr^{90}	4.57×10^{-2} n	4.57×10^{-2} fFn/V_s
H^3	67.5	2.74×10^{-3} F/V_s
Kr^{88}	1.10 n	5.24×10^{-3} Fn/V_s
Xe^{135}	2.08 n	2.5×10^{-4} nF/V_s
I^{131}	3.9 n	4.34×10^{-3} fFn/V_s
I^{133}	2.34 n	5.85×10^{-4} fFn/V_s
Ba^{140}-La^{140}	0.289 n	8.66×10^{-4} fFn/V_s
Ce^{144}-Pr^{144}	6.09×10^{-3} n	1.66×10^{-4} fFn/V_s
Y^{91}	5.56×10^{-4} n	2.12×10^{-6} fFn/V_s
Sr^{89}	0.158 n	7.75×10^{-4} fFn/V_s

[a] Nuclides taken from Table 13.16

where f is the fraction of isotope passing stack filter, A_z is the equilibrium activity in system (curies), F is the rate of gas release (cm^3/sec), and V_s is the volume of gas in system (cm^3).

$$Q' = \sum_z Q_z^* = 2.74 \times 10^{-3} F/V_s + 5.49 \times 10^{-3} \frac{nF}{V_s} + 1.458 \times 10^{-1} \frac{fFn}{V_s}$$

$$= 2.74 \times 10^{-3} \frac{F}{V_s} \left[53.4\ fn + 1 + 2n \right]$$

$$h^2 = \frac{2Q'}{\pi\, e\, \bar{u}\, X_{max}(Sr^{90})}$$

Let $X_{max}(Sr^{90}) = 10^{-10}$. This gives a safety factor of 3.

$V_s = 1.41 \times 10^{10}$ cm^3 at STP.

Therefore,

$$h^2 = \frac{(2)(2.74 \times 10^{-3})F}{\bar{u}(\pi e)(1.41 \times 10^{10})(10^{-10})} \left[53.4\ fn + 1 + 2n\right] \quad (\text{meters}^2)$$

$$= 4.71 \times 10^{-4} \frac{F}{\bar{u}} \left[53.4\ fn + 2.0 + 1\right] \quad (\text{meters}^2)$$

or

$$h = 7.11 \times 10^{-2} \sqrt{F \frac{(53.4\ fn + 2.0n + 1)}{\bar{u}}} \quad (\text{ft})$$

The formula shown above is for a continual release of activity. In Case 1, gas is released continually. In Case 2, gas is released only at infrequent intervals. Therefore the equation above is now written as:

$$h = 7.11 \times 10^{-2} \sqrt{\frac{F(53.4\ fn + 2.0n + 1)\gamma}{\bar{u}}}$$

where γ is the fraction of the time of gas release.

If no credit is taken for the filter in the stack, f will equal one. Where only gaseous fission products are assumed to escape, it is equivalent to f = 0. Assume the mean wind speed is four meters/sec.

<u>Case 1</u>

$F = 1.63 \times 10^3$

$n = 1$

$\gamma = 1$

$f = 0$ (Since only gaseous activity able to escape)

$h = 2.49$ ft

or with 150-ft stack, 5450 leaking capsules can be tolerated.

<u>Case 2</u>

$F = 1.31 \times 10^4$ cm^3/sec

$n = 1$

$\gamma = 0.10$

$f = 1$

$h = 9.65$ ft

or with 150-ft stack, 246 leaking capsules can be tolerated.

C. Dose to the Bone.

TABLE 13.18

STRENGTH OF SOURCE, Q_z^*, OF ACTIVITIES IMPORTANT TO DOSE TO THE BONE

Nuclide*	A_z (curies)	Q_z^* (curies/sec)
Sr^{90}	4.57×10^{-2} n	4.57×10^{-2} fFn/V_s
Ba^{140}-La^{140}	0.289 n	6.35×10^{-4} fFn/V_s
Ce^{144}-Pr^{144}	6.09×10^{-3} n	8.12×10^{-5} fFn/V_s
Y^{91}	5.56×10^{-4} n	2.04×10^{-6} fFn/V_s
Sr^{89}	0.158 n	1.48×10^{-3} fFn/V_s

*Refer to Table 13.17 for symbols.

$$Q' = \sum_z Q_z^* = 4.79 \times 10^{-2} \text{ fFn/}V_s$$

$$h^2 = \frac{(2)\ Q'}{\pi\ e\ \bar{u}\ X_{max}(Sr^{90})} = \frac{(2)\ (4.79 \times 10^{-2})\ \text{fFn}}{(1.41 \times 10^{10})\ \pi\ e\ \bar{u}\ (4.4 \times 10^{-11})}$$

$$= 1.8 \times 10^{-2}\ \text{fFn}/\bar{u}\ \text{meters}^2$$

or

$$h = 0.44 \sqrt{\frac{\text{fFn}}{\bar{u}}} \qquad \text{(ft)}$$

If $f = 1$, $\bar{u} = 4$

$$h = 0.22 \sqrt{\text{Fn}\gamma}$$

For Case 2, $\gamma = 0.10$, $F = 1.31 \times 10^4$, $h = 7.95$ ft. Or, with 150-ft stack, 355 leaking capsules can be tolerated.

D. Dose to the Thyroid.

TABLE 13.19

STRENGTH OF SOURCE, Q_z^*, OF ACTIVITIES IMPORTANT TO DOSE TO THE THYROID

Nuclide*	A_z (curies)	X_{max} ($\mu c/cm^3$)	Q_z^* (curies/sec)
I^{131}	3.9 n	4.4×10^{-9}	3.9 fFn/V_s
I^{133}	2.34 n	1.7×10^{-8}	0.605 fFn/V_s

*Refer to Table 13.17 for symbols.

$$Q' = 4.5 \frac{fFn}{V_s}$$

$$h^2 = \frac{(2)\ 4.5\ fFn}{\pi\ e\ \bar{u}\ V_s\ X_{max}(I^{131})}$$

$$= \frac{9\ fFn}{(\pi e)\ \bar{u}(1.4 \times 10^{10})(4.4 \times 10^{-9})} \quad \text{meters}^2$$

$$= 1.71 \times 10^{-2} \frac{fFn}{\bar{u}} \quad \text{meters}^2$$

If $f = 1$, $\bar{u} = 4$

$$h = 0.215 \sqrt{Fn\gamma\ ft}$$

For Case 2

$$h = 7.75\ ft$$

or, with 150-ft stack, 363 leaking capsules can be tolerated.

13.8.2 Emergency Discharge of Activity Up Stack (Case 3): It may be necessary to release all of the gas in the system up the stack. For this calculation it is assumed that all of the activity is instantaneously available at the top of the stack and since this would be an emergency, a dose of 2.5 rem is used.

The maximum integrated dosage (TID) at a point on the ground downwind of an instantaneous elevated source is given by:[26]

$$TID_{(max)} = \frac{2\ Q}{\pi\ e\ \bar{u}\ h^2} \quad \mu c\ sec/cm^3$$

where Q is the source strength (curies), $\bar{u}$ is the average wind speed (meter/sec), and h is the height of source (meters).

The maximum exposure to a part of the body may be expressed in the following form:

$$D\ (\frac{m\ rem}{\mu c}) \times TID_{max}\ (\frac{\mu c\text{-}sec}{cm^3}) \times BR(\frac{cm^3}{sec}) = E\ (rem) \times 10^3$$

[26] A Meterological Survey of Oak Ridge Area: Final Report (Covering the Period 1948-52), ORO-99, p. 538, Weather Bureau, Oak Ridge, Tennessee.

where E is the exposure to a part of the body (rem), BR is the breathing rate (cm^3/sec), $TID_{(max)}$ is the maximum total integrated dosage (μc-sec/cm^3), and D is the dose to a part of the body caused by 1 μc of activity, (m rem/μc).

If the breathing rate is taken as 30 liters/min, then,

$$D \times (TID)_{max} = \frac{E\ (rem)\ 10^3}{\frac{30,000}{60}}$$

Since

$$(TID)_{max} = \frac{2\ Q}{\pi\ e\ \bar{u}\ h^2}$$

then if

$$\bar{u} = 4 \text{ meter/sec}$$

and

$$D = \frac{2\ Q}{\pi\ e\ \bar{u}\ h^2} = \frac{E\ (rem)\ 10^3}{\frac{30,000}{60}}$$

the stack height is given by

$$h^2 = \frac{Q\ D}{E\ 4} \left[\frac{1}{\pi e}\right] \text{meters}^2$$

$$h = 0.66 \sqrt{\frac{Q\ D}{E}} \quad \text{ft}$$

Data for the following calculations are listed in Table 13.20. The values of Q and D are obtained from Tables 13.21, 13.22, and 13.23 for the isotopes (i) determining exposure to the bone, thyroid and total body, respectively, where[27]

$$D = 73.8\ f_a \left[\sum_i E_i\ (RBE)\ N\right] \quad T/M \text{ rem}/\mu c$$

E_i energy absorbed in the organ and is multiplied by factors which correct for the relative biological effective (RBE) of the isotope, and the effect of deposition N, M is the mass of the organ in grams, and T, the effective half-life in the body.

---

[27] T. J. Burnett, "Reactors, Hazard vs Power Level," Nuclear Science and Engineering, 2, No. 3 (May, 1957).

TABLE 13.20. FISSION PRODUCTS OF SIGNIFICANCE FOR INTERNAL EXPOSURE

Isotope	Fraction Reaching Critical Organ by Inhalation, f_a	Energy Absorbed, $\sum_i E_i$ (RBE) N (Mev)	Effective Half Life, T (days)	Mass of Critical Organ, M (gm)	Dose mrem/μc
		Bone			
Sr^{90}	0.28	5.5	6.4×10^3	7×10^3	104,000
Sr^{89}	0.28	2.8	50.4	7×10^3	416
Y^{91}	0.1875	2.9	57.8	7×10^3	332
Ba^{140}, La^{140}	0.1925	4.2	10.7	7×10^3	91.6
Ce^{144}, Pr^{144}	0.075	6.3	243	7×10^3	1210
		Thyroid			
I^{131}	0.15	0.23	7.6	20	966
I^{133}	0.15	0.54	0.87	20	260
		Total Body			
Sr^{89}	0.4	0.55	50.4	7×10^4	11.7
Sr^{90}	0.4	1.1	5701	7×10^4	2640
Y^{91}	0.25	0.59	57.8	7×10^4	9.0
H^3	0.0102	0.75	19	7×10^4	0.154
Cs^{137}	0.75	0.59	70	7×10^4	32.6
I^{131}	0.75	0.44	7.6	7×10^4	2.64
I^{133}	0.75	0.84	0.87	7×10^4	0.58
Ba^{140}, La^{140}	0.275	2.3	10.7	7×10^4	7.12
Ce^{144}, Pr^{144}	0.25	1.3	191	7×10^4	65.5

Note: Values of f_a, $\sum_i E_i$ (RBE)N, T, and M are as tabulated in unpublished data currently believed to be better than data in Handbook 52, U.S. Dept. of Commerce.

TABLE 13.21. VALUES OF Q AND D FOR DOSE TO THE BONE

Nuclide	Q-Curies	D, Exposure in mrem per μc of Isotope	% of Total Curies	D mrem/μc
Sr^{90}	4.57×10^{-2}	104,000	9.16	9526.4
Sr^{90}	1.58×10^{-1}	416	31.60	131.5
Y^{91}	5.56×10^{-4}	332	0.112	0.37
Ba^{140}, La^{140}	0.289	91.6	57.91	53.04
Ce^{144}, Pr^{144}	6.09×10^{-3}	1,210	1.22	14.76
Total	4.993×10^{-1}			9726.07

TABLE 13.22. VALUES OF Q AND D FOR DOSE TO THE THYROID

Nuclide	Q Curies	D, Exposure in mrem per μc of Isotope	% of Total Curies	D mrem/μc
I^{131}	3.9	966	62.5	603.75
I^{133}	2.34	260	37.5	97.5
Total	6.24			701.25

TABLE 13.23. VALUES OF Q AND D FOR DOSE TO THE TOTAL BODY

Nuclide	Q Curies	D, Exposure in mrem per μc of Isotope	Number of Leaking Fuel Capsules							
			n = 1		n = 10		$n = 10^2$		$n = 10^3$	
			% of Total Curies	D mrem/μc	% of Total Curies	D mrem/μc	% of Total Curies	D mrem/μc	% of Total Curies	D mrem/μc
Sr^{89}	1.58×10^{-1} n	11.7	1.95×10^{-1}	0.0228	0.777	0.0909	1.108	0.13	1.158	0.135
Sr^{90}	4.57×10^{-2} n	2640	5.64×10^{-2}	1.717	0.225	5.94	0.32	8.45	0.3349	8.841
Y^{91}	5.56×10^{-4} n	9.0	6.86×10^{-4}	6.17×10^{-5}	2.73×10^{-3}	2.46×10^{-4}	3.9×10^{-3}	3.5×10^{-4}	4.04×10^{-3}	3.63×10^{-4}
H^3	67.5	0.154	83.25	0.128	33.2	0.0511	4.73	0.007	4.94×10^{-1}	7.6×10^{-4}
Cs^{137}	6.84 n	32.6	8.44	2.75	33.6	10.95	47.98	15.64	50.12	16.339
I^{131}	3.9 n	2.64	4.81	0.127	19.18	0.506	27.36	0.722	28.58	0.755
I^{133}	2.34 n	0.58	2.89	0.0167	11.5	0.0667	16.42	0.095	17.14	0.0994
Ba^{140}, La^{140}	0.289 n	7.12	0.356	0.0253	1.42	0.101	2.03	0.144	2.12	0.151
Ce^{144}, Pr^{144}	6.09×10^{-3} n	65.5	7.5×10^{-3}	0.0049	0.0299	0.0196	0.0427	0.028	0.0446	0.0292
			100	D = 4.792	100	D = 17.725	100	D = 25.22	100	D = 26.35
				Q = 81.08		Q = 203.29		Q = 1425.4		Q = 13646.8

A. Dose to the Bone: If the maximum exposure to the bone is 25 rem, then for

$$E = (25 \text{ rem})\ 0.1 = 2.5 \text{ rem}$$

$$Q = 0.4993 \text{ curies per fuel element leaking}$$

$$D = 9726.07 \text{ mrem}/\mu c$$

the stack height is $h = 0.66 \sqrt{\frac{(0.4993\ n)(9726.07)}{2.5}} = 24.65 \sqrt{n}$

or, with a 150-ft-high stack, 36 leaking fuel capsules would give the allowable dose to the bone of 2.5 rem.

B. Dose to the Thyroid: If the maximum exposure to the thyroid is 50 rem, then for

$$E = (50 \text{ rem})\ 0.1 = 5 \text{ rem}$$

$$Q = 6.24 \text{ curies per fuel element leaking}$$

$$D = 701.25 \text{ mrem}/\mu c$$

the stack height is $h = 16.6 \sqrt{n}$

or, with a 150-ft-high stack, 82 leaking fuel capsules would give the allowable dose to the thyroid.

C. Dose to the Total Body: If the maximum exposure to the total body is 25 rem, then for

$$E = (25 \text{ rem})\ 0.1 = 2.5 \text{ rem}$$

and

$$n = 1$$

$$Q = 81.08$$

$$D = 4.792$$

the height is $h = 0.66 \sqrt{\frac{Q\ D}{E}} = 0.355 \sqrt{Q\ D}$

or, with a 150-ft-high stack, 492 leaking capsules can be tolerated.

13.8.3 Gas Leakage in the Reactor System: Leakage out of the pressure vessel will present a radiation hazard. In view of the fact that the system will be helium leak checked, any residual leakage might contain tritium or the noble gases, but not particulate activity as the latter would not escape through the capillary leaks. Previous calculations have shown that the gaseous activity leaking from the system is as follows:

Nuclide	A (curies)	Q (curies/sec)	$Q^*_z = Q \frac{X_{max}(H^3)}{X_{max}(Z)}$
H^3	67.5	$\frac{67.5\ F}{V_s}$	$\frac{67.5\ F}{V_s}$
Kr^{88}	1.1 n	$\frac{1.1\ nF}{V_s}$	$\frac{129\ nF}{V_s}$
Xe^{135}	2.08 n	$\frac{2.08\ nF}{V_s}$	$\frac{6.15\ nF}{V_s}$

where

$$Q' = \sum_z Q^*_z \left[135n + 67.5\right] \frac{F}{V_s}$$

and Q' is the activity released from the system by leakage (curies/sec), F is the leakage from the system (cm^3/sec), V_s is the total volume of system at STP (cm^3), and n is the number of fuel capsules leaking. Assuming n = 1

$$Q' = 1.44 \times 10^{-8}\ F \text{ curies/sec.}$$

If the air dilution is represented by F_A in cm^3/sec, the activity at a leak will be

$$A_L \approx \frac{1.44 \times 10^{-8}\ F}{F_A}$$

where A_L is the concentration of activity at a leak (curies/cm^3) and F_A is the air dilution, cm^3/sec.

Since the maximum permissible concentration of H^3 for continuous exposure is 7.4×10^{-6} $\mu c/cm^3$

$$F_A = \frac{1.44 \times 10^{-8}\ F\ (c/sec)}{7.4 \times 10^{-12}\ (c/cm^3)} = 1950\ F\ cm^3/sec$$

therefore, the rate of air dilution required is 1950 times the rate of leakage. This assumes only the tritium and fission product gases escape.

A. Leakage at the Pressure Vessel. The region between the pressure vessel and the shield is on the suction side of the shield cooling blower so that activity leaking there will be discharged up the stack. Assuming that all of the leakage occurs in this region, and assuming an upper limit on the leakage of 1.63×10^3 cm^3/sec (1%/day), the air dilution required

to limit the dose to usual tolerance levels is:

$$V_A = (1950)\ 1.63 \times 10^3 = 3.18 \times 10^6\ cm^3/sec = 6.75 \times 10^3\ cfm$$

Since the cooling air flow through the shield is 2.5×10^4 cfm, the gaseous activity inside the shield will be kept below the tolerance level, although this is not necessary since the region in question is not accessible to operating personnel.

B. Leakage at Bellows in Main Gas Pipes. The leakage at the bellows in the main gas pipes will be directed into the area inside the shield and will then be discharged to the stack. This area is operated at a negative pressure, thus preventing airborne activity from spreading into the operating plant area.

C. Leakage at a Steam Generator. Assuming that each steam generator has a leakage equal to 1/10 of the system leakage, the air dilution required to maintain tolerance levels would be 675 ft^3/min. Since the steam generators are located outside the main building, the H^3 would be able to diffuse into the atmosphere.

D. Leakage at Blowers, Valves, and other Equipment. Assuming 30% of all gaseous activity escaped into the building the air dilution required would be:

$$F_A = \frac{(0.30)(1.63 \times 10^3)(1950)(60)}{2.8 \times 10^4} = 2010\ ft^3/min$$

Since normal building air ventilation should exceed this value, leakage into the building atmosphere should present no hazard.

13.8.4 Activity in Building in Event of Pressure Vessel Rupture: Calculations indicate that in the event of a pressure-shell rupture, the gases in the system will escape into the area inside the shield, and might in the extreme limiting case blow off the top concrete slab (see 13.7.2). For such an extreme case, it is estimated that the time to reduce completely the pressure inside the shielded compartment to atmospheric pressure is less than 1 sec. Therefore, for this incident, it may be assumed that the source of activity is an instantaneous source. Since the previous calculation has shown the dose to the bone to be controlling, only the bone calculation is used here. The released activity was taken as 0.499 n curies, where n is the number of leaking fuel capsules. This is the activity of importance

in calculating "Dose to the Bone" in the preceding analysis of 13.8.2.

$$E(\text{rem}) = D\left(\frac{\text{m rem}}{\text{c}}\right) \text{BR} \left(\frac{\text{cm}^3}{\text{sec}}\right) \quad Q\left(\frac{\mu\text{c}}{\text{cm}^3}\right) t(\text{sec})\ 10^{-3}$$

where $D = \frac{\text{m rem}}{\mu\text{c}}$ is taken from Table 13.20, BR is the breathing rate (30 liters/min), Q is the source strength ($\mu c/cm^3$), and t is the length of time a man breaths 30 liters/min (sec). Then

$$E(\text{rem}) = (9726.07)\left(\frac{30{,}000}{60}\right) \frac{0.499\ n\ 10^6}{V_B}\ t \times 10^{-3}$$

where V_B is the building volume (cm^3) and n is the number of fuel capsules leaking fission products; therefore,

$$t = \frac{(60)}{(9.73 \times 10^3)(30 \times 10^3)\ 0.499 \times 10^6 \times 10^{-3}} \quad \frac{E\ V_B}{n}$$

If the maximum dose to the bone is 25 rem, and if the building volume is assumed to be:

$$V_B = (60\ \text{ft})(90\ \text{ft})(105\ \text{ft}) = 5.67 \times 10^5\ \text{ft}^3 = 1.61 \times 10^{10}\ \text{cm}^3$$

the time that a man might breathe the contaminated atmosphere in the building is:

$$t = \frac{(4.2 \times 10^{-10})(25)(1.61 \times 10^{10})}{n} = \frac{184}{n}\ \text{sec.}$$

In the event that this extreme situation of a pressure vessel rupture, occurs, the top shield plug would rise to a considerable height. If this happened with no outer containment vessel, most of the gases escaping would be released to the atmosphere and would not remain in the building. Therefore, the concentration of activity would be greatly reduced in the building, allowing a greater time than that indicated above.

13.8.5 Dose From Cold Cloud Following Pressure Vessel Rupture: The dose to the bone at some point downwind from the building following a rupture of the pressure vessel may be expressed as:

$$E = (TID)(BR)(D) \times 10^{-3}$$

where E is the dose in rem, TID is the total integrated dose at a point on the ground downwind of an elevated source (μ curies sec/cm^3), BR is the breathing rate (cm^3/sec), and D is the dose in the bone due to one μc(m rem/μc). Also,[28]

$$TID = \frac{2\,Q}{\pi\, C^2\, \bar{u}\, (\bar{u}T)^{2-N}} \exp\left[\frac{-\,h^2}{C^2\,(\bar{u}t)^{2-N}}\right]$$

where Q is the source (curies), C is the diffusion coefficient, N is a non-dimensional parameter associated with the stability, $\bar{u}$ is the average wind speed (meters/sec), ($\bar{u}$t) is distance (meters), and h is the effective height (meters). For the case under consideration, the following values may be used:

BR = 30 liters/min = 500 cm^3/sec

D = 9726.07 (from Table 13.20)

Q = 0.499 n curies (from Table 13.20)

h = 100 ft = 30.48 meters

n = number of fuel capsules releasing fission products

therefore,

$$\frac{E}{(500)(9726)\,10^{-3}} = \frac{(2)(0.499)\,n}{\pi\, C^2\, \bar{u}\, (\bar{u}t)^{2-N}} \exp\left[\frac{-\,(30.48)^2}{C^2(\bar{u}t)^{2-N}}\right]$$

$$E = \frac{1390\,n}{\bar{u}\, C^2(\bar{u}t)^{2-N}} \exp\left[\frac{-\,928}{C^2(\bar{u}t)^{2-N}}\right]$$

During the day[29]

N = 0.23

C = 0.30

$\bar{u}$ = 8 m/sec

---

[28] A Meterological Survey of Oak Ridge Area: Final Report (Covering the Period 1948-52), ORO-99, p. 537, Weather Bureau, Oak Ridge, Tennessee.

[29] Ibid.

During the night[30]

$$N = 0.35$$

$$C = 0.105$$

$$\bar{u} = 5 \text{ m/sec}$$

Therefore, in the daytime,

$$E(\text{rem}) = \frac{1390\ n}{8(0.3)^2(\bar{u}t)^{2-0.23}} \exp\left[\frac{-\ 928}{(0.3)^2(\bar{u}t)^{2-0.23}}\right]$$

$$= \frac{1.935n \times 10^3}{(\bar{u}t)^{1.73}} \exp\left[\frac{-\ 10311}{(ut)^{1.73}}\right]$$

During the night

$$E(\text{rem}) = \frac{1390\ n}{5(0.105)^2(\bar{u}t)^{2-0.35}} \exp\left[\frac{-\ 928}{(0.105)^2(\bar{u}t)^{2-0.35}}\right]$$

$$= \frac{2.526n \times 10^4}{(\bar{u}t)^{1.65}} \exp\left[\frac{-\ 8.43 \times 10^4}{(\bar{u}t)^{1.65}}\right]$$

The distance of the maximum dose is given by,

$$(\bar{u}t) = \left[\frac{h^2}{C^2}\right]^{\frac{1}{2-N}}$$

For the daytime

$$(\bar{u}t) = \left[\frac{(30.48)^2}{(0.3)^2}\right]^{\frac{1}{2\ -\ 0.23}} = 210 \text{ meters}$$

For the night time

$$(\bar{u}t) = \left[\frac{(30.48)^2}{(0.105)^2}\right]^{\frac{1}{2\ -\ 0.35}} = 955 \text{ meters}$$

The dose downwind during either the day or the night is shown in Fig. 13.19.

13.9 Potential Energy of the Graphite

As was previously noted in 13.7, the containment afforded by the fuel cladding and the pressurized helium system is believed to be adequate if fuel capsule melting does occur. Consideration of the temperature transients in the

[30] Ibid.

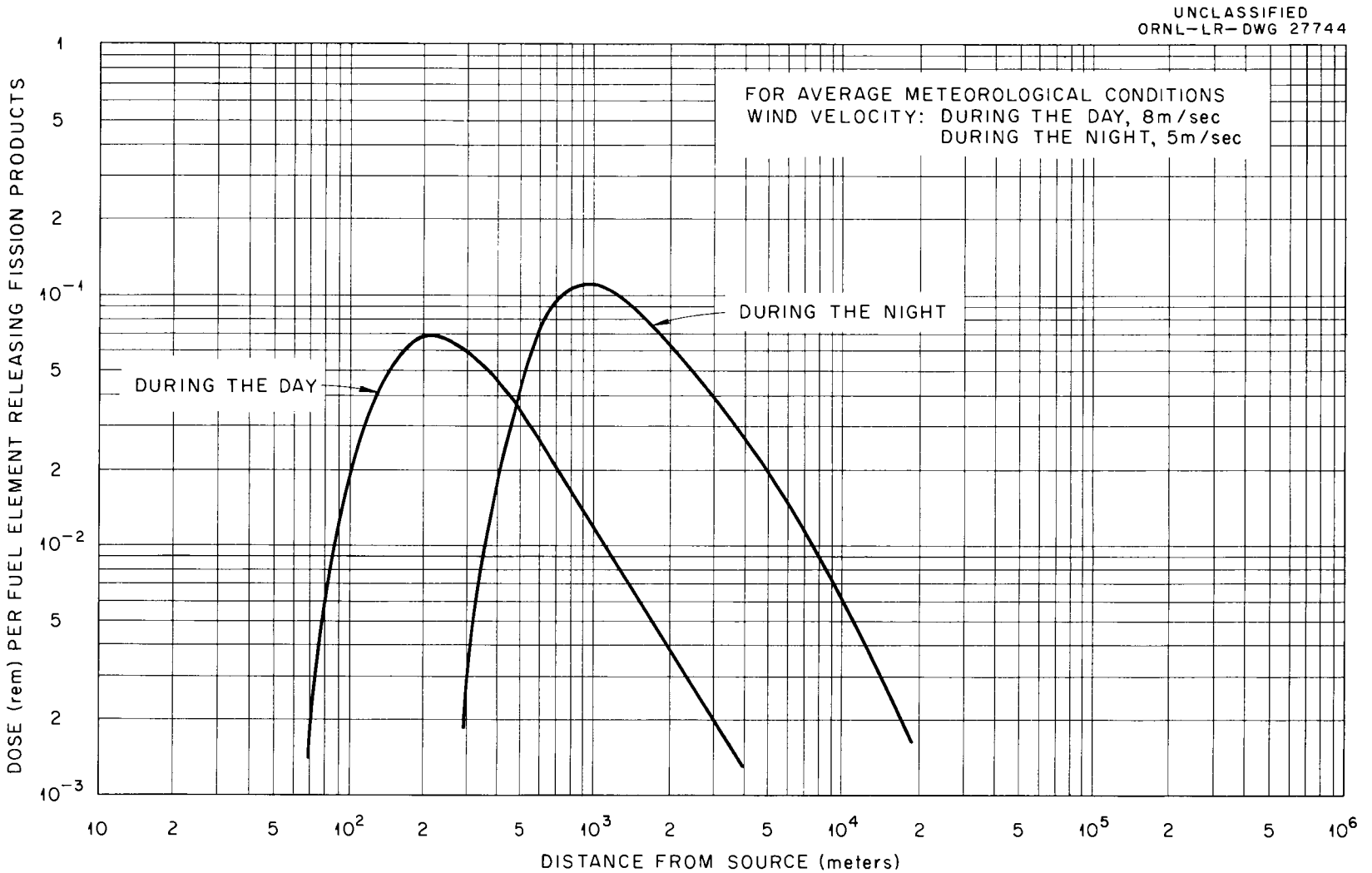

Fig. 13.19. Dose Downwind from Reactor Incident.

fuel with the afterheat removed by radiation alone has shown that the fuel element temperature does not exceed the graphite temperature by more than 100°F after the initial transient. It is of interest, therefore, to examine circumstances under which graphite temperature might reach a high level during these transients as this would then result in still higher fuel temperatures. Only two mechanisms appear to be available: oxidation of the graphite and release of irradiation energy stored in the graphite. Both of these cases are discussed below and neither appears capable of causing significant temperature overshoots.

13.9.1 Oxidation of the Graphite: In the event of a major system failure, either air or steam (or both) enter the helium system. Convective flow of the heated gases in the reactor channels would expose the graphite to an oxidizing atmosphere. Three oxidizing reactions are possible:

$$C + H_2O = CO + H_2$$

$$C + CO_2 = 2CO$$

$$2C + O_2 = 2CO$$

Of these, however, the first two are endothermic and would result in a temperature reduction should the reactions occur. This immediately rules out a steam leak as a serious hazard, since there would be no positive heat of reaction and the small increase in reactivity would be overridden by the automatic rod insertion, described in 13.6. Some oxidation of the fuel elements would occur but this could not seriously damage them in the time span involved.

The reaction between graphite and oxygen is exothermic and, therefore, presents a potential hazard. However, the oxidation reaction, which becomes significant at temperatures[31] above 840°F, does not ignite the graphite but is evident as a weight loss as the gaseous reaction products (CO and possibly CO_2) are removed. These reaction rates are so slow that graphite is employed for crucibles and electrodes in air at temperatures well above 1000°F. While it may, therefore, be inferred that the reactor graphite would not support combustion even in the event of a pressure-vessel rupture which would admit air to the graphite, an attempt has been made to estimate the effect of the oxidizing atmosphere on the graphite temperature based upon a simplified model of the

---

[31] J. A. Slyh, "Graphite," The Reactor Handbook, 3, Section 1, 152 (March, 1955).

system. A test program designed to simulate these conditions is underway at Brookhaven.

The reaction rate of graphite and oxygen is temperature dependent. It is very small at low temperatures, and increases with temperature. If a "threshold oxidation temperature" is defined as the temperature at which a sample loses 1% of its weight in 24 hr, pure graphite has a threshold oxidation temperature of 965 – 1040°F. This effect can be seen from Table 13.24 in which the oxidation rates for typical specimens of pure graphite are shown as a function of temperature.

TABLE 13.24

OXIDATION RATES FOR PURE GRAPHITE IN STAGNANT AIR

Oxidation Temperature	Time for 1% Weight Loss (hr)
930°F	200
1110°F	7
1290°F	0.6

In the GCR-2 reactor, the effect of oxidation was checked for a "worst case" condition in which it assumed that the graphite shape and the oxygen supply were such that the above oxidation rate would apply. The heat liberated by the $C + O_2 = CO_2$ reaction was assumed to be absorbed completely by the graphite. The results are shown in Fig. 13.20 in which the rate of temperature rise of the graphite mass is plotted against the graphite reaction temperature.

These values are reassuring in that the graphite temperature would hardly exceed 1100°F and thermal convection would be available to remove heat. The reaction rates at the surface would probably be greater than those shown here because of the convective flow of air, but the rates at the interior would probably be much less than those shown. It is believed that the combined effects would lead to temperatures well below those shown here.

13.9.2 Irradiation Effects on the Graphite: The irradiation of graphite is known to affect many of the physical properties of the graphite including heat capacity, electrical resistivity, thermal conductivity, physical dimensions, crystal lattice spacing,and crystallite size. Moreover, the magnitude of the

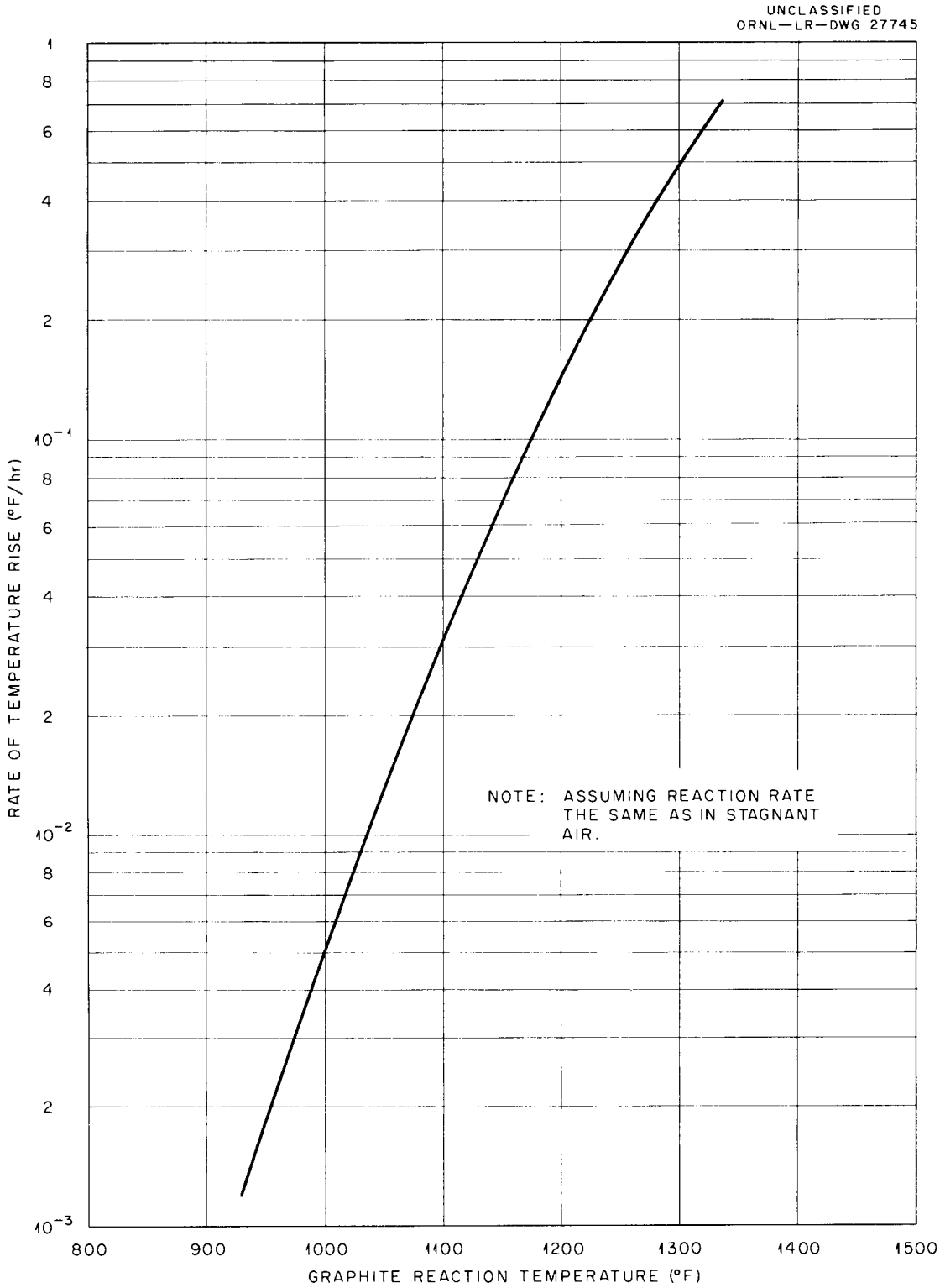

Fig. 13.20. Rate of Graphite Temperature Rise If Heat of Reaction with Air Is Totally Absorbed.

effect on each of these properties is a function of both irradiation time and irradiation temperature, and furthermore, the effect may be annealed by one of several mechanisms including heat, irradiation, and shock. Of special interest to the GCR-2 is the information on the stored energy, thermal conductivity, and dimension changes in irradiated graphite; these effects have been examined and do not appear to pose a serious problem for the GCR-2.